

24653902



MICHIGAN STATE UNIVERSITY LIBRARIES

3 1293 00609 6659

This is to certify that the

dissertation entitled

The Determination of Attenuation-Velocity Products in a Layered Homogeneous Medium

presented by

Joseph Nodar

has been accepted towards fulfillment of the requirements for

Doctoral degree in Electrical Engineering

Major professor

Date <u>October 27, 1989</u>

MSU is an Affirmative Action/Equal Opportunity Institution

0-12771

PLACE IN RETURN BOX to remove this checkout from your record. TO AVOID FINES return on or before date due.

•	DATE DUE	DATE DUE
JUN 1 5 1992 Tul. 3 1, 1992		
200 1 0 1 1 1 1 1 1 1 1 1 1 1 1 1 1 1 1		

MSU Is An Affirmative Action/Equal Opportunity Institution

THE DETERMINATION

OF

ATTENUATION-VELOCITY PRODUCTS

IN A

LAYERED HOMOGENEOUS MEDIUM

By

Joseph Nodar

A DISSERTATION

Submitted to
Michigan State University
in partial fulfillment of the requirements
for the degree of

DOCTOR OF PHILOSOPHY

Department of Electrical Engineering

1989

ABSTRACT

THE DETERMINATION OF ATTENUATION-VELOCITY PRODUCTS IN A LAYERED HOMOGENEOUS MEDIUM

By

Joseph Nodar

In the field of acoustic imaging, many techniques have been forwarded to permit the creation of images by means of the attenuation properties of the object under study. Each of these has its own advantages and drawbacks. In this thesis, a new method of accomplishing this type of amplitude-based imaging is proposed, using attenuation-velocity products as an imaging index. It is shown that this choice has the advantage of providing high contrast between various media, which can allow the identification of the inner materials comprising an object to be performed remotely.

Using a bidirectional interrogation of a one-dimensional object model, it is shown that the solution of the N-layer object problem can be found uniquely, and that separation of the effects of reflection coefficient and attenuation can always be made. No assumptions are necessary concerning the values of the various parameters, with the exception of the need to know the loss factors of the two outermost layers. An algorithm is presented that has successfully eliminated the deleterious effects of multiple reflections on the solution, and it also solves for the number of layers within

the object, often an unknown quantity, when given just the experimental data acquired during the bidirectional interrogation of the object, i.e. the left echoes, the left-right transmission, the right echoes, and the right-left transmission. It is demonstrated that only this set of signals provides for such a solution. Rationale is given for the apparent uniqueness of this solution even in the presence of the extraneous multiple reflection signals. Also, a detailed consideration of the components required to implement such a measurement system is made, with appropriate error analyses performed. Preliminary experimental results are presented, and the reasonable errors that have been achieved are compared with the standard published values for the materials utilized. Finally, suggestions for certain future work to extend the results are outlined.

Copyright by JOSEPH NODAR 1989

This thesis is dedicated to my family.

ACKNOWLEDGMENTS

The author would like to thank Dr. Bong Ho, Department of Electrical Engineering, for his support and discussions during the work on this thesis, Dr. Pavol Meravy, Department of Mathematics, for his considerable help and sincere interest, and Drs. Mani Azimi, Donnie K. Reinhard, and H. Roland Zapp, Department of Electrical Engineering, for their valuable constructive criticism of this work. Special thanks are also in order to Gayle J. Sears, for his assistance above and beyond the call of duty.

TABLE OF CONTENTS

LIST	r of '	CABLES	5	page ix
LIST	r of i	FIGURE	S	x
I.	INTE	RODUC	TION	1
II.	BAC	KGROU	JND	10
	2.1		Acoustic and Mechanical Properties and Wave Behavior	
	2.2	Genera	al Acoustic Imaging	16
	2.3	The Ta	arget	17
Ш.	ATT	ENUAT	TON IMAGING	24
	3.1	Attenu	ation	24
	3.2	Attenu	ation Imaging	27
	3.3	Attenu	nation-Velocity Products	32
IV.	DET	ERMIN	ATION OF ATTENUATION-VELOCITY PRODUCTS	34
	4.1	Basic	Goals of This Section	35
	4.2		m Statement and Definition of Terminology	
	4.3		ptions to Solve the One-Dimensional Model	
	4.4		nknown Quantities	
	4.5		on of The Problem	
		4.5.1	Case 1: Single-Sided Purely Reflective Interrogation	40
		4.5.2	Case 2: Pure Transmission Interrogation	
		4.5.3	Case 3: Bidirectional Interrogation	44
	4.6	Findin	g the Attenuation-Velocity Products of the N-Layer Object	52
	4.7		ole Reflection Elimination and Finding the Number of Layers	
		4.7.1	Finding N, the Number of Layers	54

		4.7.2	Finding the Primary Data Set in the Presence of	
			Multiple Reflections	55
V.	SYS	TEM A	NALYSIS AND ERRORS	61
	5.1	Introdu	uction	61
	5.2		est Object	
	5.3	The Tr	ransducer	64
	5.4	The Tr	ransmitter and Receiver	72
	5.5	Signal	Acquisition	75
	5.6	Signal	Processing	82
	5.7	Sensiti	ivity of Equations (4.20) and (4.21)	
		to Erro	ors in the Amplitudes of the Primary Data	90
	5.8	Additi	onal System Requirements	95
	5.9	Conclu	usions	97
VI.	SIM	ULATIO	ONS AND EXPERIMENTAL RESULTS	98
	6.1	Simula	ations and Results	98
	6.2	Experi	imental Results	103
VII.	REC	OMME	NDATIONS AND CONCLUSIONS	120
	7.1	Recom	nmendations for Future Investigation	121
		7.1.1	Extension to Higher Dimensional Objects	121
		7.1.2	Extension of the Alpha-V Method to Transmission	
			Tomography	123
		7.1.3	Extension to Electromagnetic (and General Wave) Situations	126
			Situations	120
	7.2	Conclu	usions	127
APF	PEND	X A	Program: TWOSIDE	131
APF	PEND	ХВ	Program: ALPHA-V	136
APF	END	X C	Program: TWOCHANNEL	140
BIB	LIOG	RAPHY	7	145

LIST OF TABLES

Table 3.1	Attenuation-velocity products of various media at a 1 MHz transducer frequencypage 33
Table 6.1	The results of program TWOSIDE on the example of Figure 6.1 101
Table 6.2	Physical constants for some materials, at 2.25 MHz
Table 6.3	Summary of the experimental results for the single layer plexiglass sample
Table 6.4	The experimental results for the aluminum sample
Table 6.5	Summary of the results for the five layer object
Table 6.6	(a) The experimental data, and (b) the calculated results for the liver sample

LIST OF FIGURES

Figure 1.1	An example layout of an ultrasound imaging systempage	4
Figure 1.2	The driving characteristics of a piezoelectric transducer	6
Figure 2.1	Wave behavior at an impedance discontinuity 1	14
Figure 2.2	The pulse-echo imaging technique	17
Figure 2.3	An example test object, and its one-dimensional model	18
Figure 2.4	An example steplike impedance profile for an isotropic one-dimensional object bounded by discontinuities	21
Figure 2.5	Example of multiple imaging artifacts in an object	23
Figure 4.1	The object model to be studied and the notation conventions used in the derivation of the equations in this chapter	37
Figure 4.2	Example of left side echo data	40
Figure 4.3	The definition of R _i with respect to L _i	45
Figure 4.4	Example of right side input echo returns	46
Figure 4.5	The algorithm described in this section that finds the set {N, k, r, t} and eliminates multiple reflections	56
Figure 4.6	Illustration of the difference between the boundary properties when viewed from opposite sides	58

Figure 5.1	Detailed block diagram of the components of the attenuation-velocity product measurement system to be analyzed in this chapter	62
	cnapter	. 02
Figure 5.2	The geometry for finding the effective receiver area when the beam illuminates an angular planar reflector	. 65
Figure 5.3	Plot of Equation (5.2), the effective receiver area	. 67
Figure 5.4	The geometry used to determine the transducer beam pattern and beam width	. 68
Figure 5.5	Plot of Equation (5.3), the transducer receiving beam pattern	. 70
Figure 5.6	An electrical equivalent circuit for a piezoelectric transducer	. 71
Figure 5.7	The use of a time/gain amplifier to boost the lower level echo amplitudes for increased accuracy and dynamic range	. 74
Figure 5.8	The spectrum of the function of Equation (5.10)	. 76
Figure 5.9	Plot of Equation (5.16), the quantization error	. 81
Figure 5.10	The software preprocessing for the algorithm of Figure 4.5	. 83
Figure 5.11	The window detector in action	. 84
Figure 5.12	The windowing algorithm used to produce Figure 5.11	. 84
Figure 5.13	The effect of sampling nearly at the Nyquist limit on the accuracy of peak amplitude determination	. 86
Figure 5.14	Plot of the effects of cubic splines on the peak amplitude approximation	. 89
Figure 5.15	The various sensitivity relations derived in Section 5.7	. 92
Figure 6.1	The example object to be considered, with N=4	100
Figure 6.2	The results of program Alpha-V using the data shown in Table 6.1	102

Figure 6.3	The layout of the experimental system
Figure 6.4	The example setup to illustrate the experimental procedure
Figure 6.5	(a) The experimental time signals, and (b) the set {L, T _{LR} , R, T _{RL} } _{experimental} for Figure 6.4
Figure 6.6	The experimental setup for the aluminum sample
Figure 6.7	The experimental data for the aluminum sample
Figure 6.8	The configuration of the five layer object
Figure 6.9	(a) The experimental time signals, and (b) the echo data for the five layer object of Figure 6.8
Figure 6.10	The experimental setup for the liver sample
Figure 7.1	The type of object proposed in Section 7.1.2

CHAPTER I

INTRODUCTION

In many circumstances, there exists a requirement for non-invasive and non-destructive probing of the internal characteristics of an object under study. Such objects range from the living tissue structures that are encountered in a medical setting, to manufactured industrial products that need verification of their internal or compositional soundness prior to shipping from the factory. In each of these instances, it is undesirable or impossible to disassemble or damage the object in question in any manner, yet some means must be found to acquire information regarding the internal structures, and in some cases to even identify the actual material from which a particular part is constructed. In the clinical setting, this problem is further exacerbated since no prior knowledge of the exact makeup or dimensions of any internal form is possible, in contrast with the industrial situation wherein any manufactured component is usually thoroughly designed beforehand and is therefore precisely defined in comparison.

Several techniques have come to the forefront of this very basic problem, namely X-ray tomography, nuclear magnetic resonance imaging (MRI), and ultrasound. Each has certain advantages, and each presents its own problems, both technical and practical. For example, both X-ray tomography and MRI imaging systems

are capable of producing excellent pictures of a widely diverse class of test objects, and in some cases can even be used to give a three-dimensional reconstruction of these objects. Also, an excellent clarity of the boundaries separating the internal parts is the norm, which is invaluable in medical diagnostic tests, particularly in delicate areas where exploratory surgery is not feasible or possible without patient risk. Commercial systems are rather well developed, with many features available, and are quite widespread, currently in operation at many sites worldwide. There are, however, certain problems with these systems, for example the extremely high cost, which can usually exceed several million dollars, and the admittedly unknown health risks posed by exposure to the high intensity energy emissions used to interrogate the object being probed.

In contrast with the above technologies, ultrasound is relatively underdeveloped. The acoustic measurement and imaging systems that are presently available commercially are rather expensive when one considers their somewhat more limited capabilities in comparison with X-ray tomographic and MRI imagers; the typical acoustic system can cost over two hundred thousand dollars (1989) and cannot as yet deliver images that stand up to even an offhand judgement against the other methods. This situation has resulted in ultrasound being relegated to a somewhat less significant position among the various imaging technologies; yet ultrasound possesses features that the other methods will always lack, namely comparatively lower cost and a greater potential for safety in operation. The latter is evident because while both X-ray tomography and MRI imaging rely on narrow duration high intensity

electromagnetic energy emissions to penetrate the object--resulting in the aforementioned short- and long-term safety risks--ultrasound uses only high frequency mechanical wave propagation and interaction with the object to form conclusions about the internal structure. This type of energy intromission has the possibility of being safer to apply since peak and average power levels can be kept significantly lower than the amounts employed in the other imaging schemes.

The standard ultrasound system is comprised of several key components and units:

(1) some form of energy emitting transmitter, which originates the high frequency mechanical waves used to interrogate the object under study, (2) some form of receiving device that is used to recapture the emitted wave energy after it has passed into and/or through the object, (3) some means of saving the information contained in this received signal, and (4) some scheme of processing and presenting the signal/data for display and information dissemination to the system operators.

Depending upon the final intent of the application, it is usually advantageous for the basic components to take various forms, particularly with respect to how the transmitter and receiver are defined and oriented in relation to the object. Figure 1.1 shows a common way to set up such a system.

In many ultrasound systems, it is common for the transmitter and receiver functions to be combined into one device. Typically, a piezoelectric effect device is employed in this position, since this physical phenomenon directly relates electrical and mechanical stimuli and responses in a bilateral manner--i.e. a single unit can be electrically

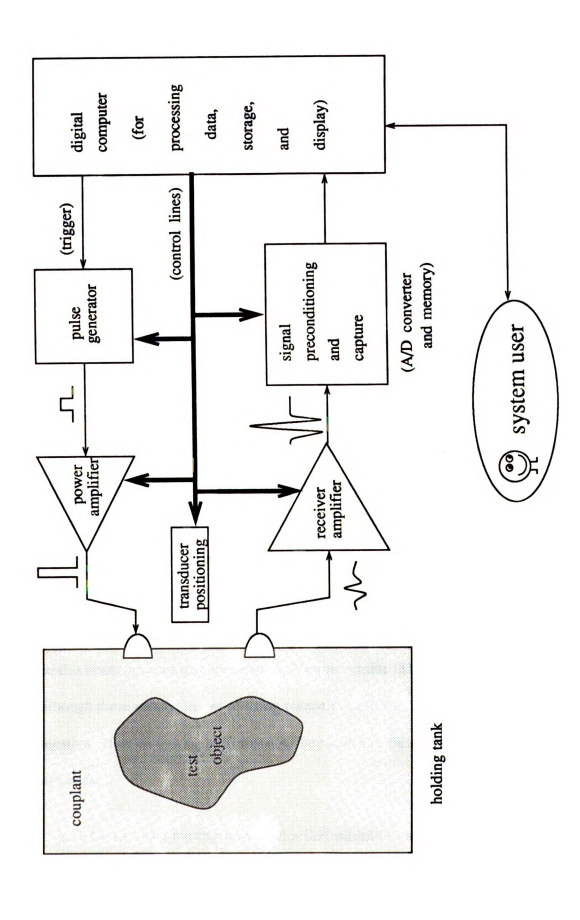


Figure 1.1 An example layout of an ultrasound imaging system.

excited in an appropriate manner and thereby emit mechanical vibrations, and likewise the same device can perform the conjugate function of transforming the subsequently received mechanical waves into corresponding electrical signals. This conciseness usually allows the electromechanical portion of the system to be compact in form, possibly handheld, and precludes the potentially nasty problems of alignment and the matching/calibration that is necessary in the case of a separate transmitter and receiver. The fact that these piezoelectric devices are electrically and mechanically coupled gives rise to another prominent characteristic, that of narrow frequency bandwidth operation. This is due to the resonant nature of the physical structure and materials from which the unit is constructed, commonly a thin crystalline material such as quartz. The implications of this are several: (1) the unit has a limited frequency response, (2) the unit will tend to resonate at its own natural frequency when stimulated, from both electrical and mechanical sources, (3) the fact that the bandwidth is narrow tends to lower the received noise, (4) it is difficult to produce very narrow transmitted pulses, which are usually necessary for high resolution imaging, and (5) the narrowly tuned nature of these devices makes matching among several of them difficult in systems that use multiple units, and causes arrays of transducers to exhibit beam patterns that are somewhat unpredictable [8]. It should be noted that although these consequences of using piezoelectric devices will sometimes have a negative effect on system performance, they also may be used to advantage in other instances.

In order to create the requisite mechanical waves that are the foundation of any

acoustic measurement, some form of electrical stimulation is commonly used. Most often, a high amplitude voltage pulse of extremely narrow time duration is applied to the transmitting transducer, the result being that such a driving signal "shock excites" the transducer unit into natural resonance, thus beginning the generation of mechanical output waves as a consequence of the piezoelectric effect. Figure 1.2 shows a typical transducer natural response to such a driving signal. After these vibrations are created, they begin to propagate away from the transducer, and usually first encounter some type of coupling medium that (1) serves as an impedance match, (2) has well known acoustic properties, and (3) fills all the "bumps and lumps" (even microscopic) that comprise the outer surface of the the object. Water is popular—being inexpensive, readily available and relatively safe—and it surrounds the test object under its own volition, always a convenience. This ensures that the mechanical waves will reach the object intact (air usually presents problems



Figure 1.2 The driving characteristics of a piezoelectric transducer.

for ultrasound propagation since it is highly attenuative at the frequencies commonly needed for clear imaging). After initial wave impingement upon the surface of the object, interaction in a mechanical sense then occurs internally, i.e. reflection, transmission, and absorption of the acoustic energy, with the eventual return of some portion of the initially transmitted pulse energy to the receiver of the system. This signal is then converted back into electrical signals and is processed by the remaining system components, eventually destined for presentation to the system user. It is important to realize that this sequence of events will ultimately comprise only a single position or point of view with regard to the object being imaged; in order to obtain a two- or three- dimensional image, the transducer must be moved or scanned to various positions about the object, and the entire sequence repeated each time.

Performing this operation repeated will enable a complete multi-dimensional reconstruction to be created.

With only minor variations, the above description of the operation of an ultrasound imaging system would suffice for most examples in use today. Typically, thicknesses on the order of a millimeter or less can be distinguished, but lateral resolution can vary greatly, being dependent on transducer size, beamwidth, and the interval over which the scanning motion is conducted; also, the object geometry has an influence on the lower bound of this parameter. Limitations on the performance of acoustic imaging systems arise from many sources, and will be discussed in some detail in the next section, but many systems self-impose restrictions on their own abilities by virtue of simply not using most of the information contained in the received signals.

The data that can be extracted is rich with information concerning the acoustic properties of the object interior, since the sound has passed through this region and has therefore been affected by its mechanical and physical qualities. In particular, the amplitude information of the received signals is commonly ignored by many systems, even though [48] this is a source of much more quantitative information than is available from only a consideration of the time data, and has hidden within a record of the acoustic impedances, reflection coefficients, and attenuations encountered during its time of flight. In the past, electronic technology was not sophisticated enough to permit the older ultrasound systems to capture for processing the returning signals in a form from which this data could be gleaned; today, however, it is possible to record these signals very accurately using high-speed analog-digital conversion and fast, large semiconductor memories, placing the entire waveform at the disposal of a digital computer for processing. This allows possibilities of data processing, interpretation, and display that simply were not feasible a short while ago, all at very affordable costs and with reasonable operational speeds. The question reduces to one of how to process these captured signals in a useful manner, and it is to this end that this thesis work has been addressed.

As previously mentioned, it is extremely desirable to not only identify whether a boundary is internally present or not in an object, but also to be able to determine what sort of material is between those boundaries, and to eventually be able to identify the material that comprise the regions within the object. Examples of applications that might use such a capability are numerous and obvious. For many years, a safe

and reliable method of tumor detection/identification has been sought by the medical community, and a capable ultrasound system that is equipped with the sophistication necessary to allow material identification would certainly fill this need [43]. Other medical uses include instrument positioning during delicate surgical procedures, and location of foreign objects in a wound site. In the industrial sector, ultrasound has been extensively explored for use in testing manufactured products, such as composite materials, which are commonly formed of layers of woven cloths such as carbon fiber and embedded in some type of resin for binding and rigidity. These materials are hoped to eventually be used in place of metals in many applications since they can be lighter and stronger, but in order for this to be true, the layered structure of the composite must be intact. Delamination of the layers of cloth is at present difficult to detect by any means, particularly in shaped composites installed permanently. A simple method of commercially useful testing is needed before these materials can be placed into practical service [12]. An ultrasound imaging system with the capability to detect and identify nonuniformities or the existence of foreign substances inside an object would definitely be of immense value in these and other such applications that require the safer operation and lower cost possible by acoustic methods.

In Chapter 2, we examine some preliminary acoustic phenomena and background information, then discuss acoustic imaging in general, reserving attenuation to be the focus of Chapter 3.

CHAPTER II

BACKGROUND

In order to discuss the research undertaken in this thesis, it will be necessary to momentarily digress to review certain preliminary concepts of acoustic imaging. We first describe some basic properties of acoustic interaction in a material, including boundary behavior, finally covering in some detail the more complicated properties that frequently are considered non-idealities, such as scattering, in the context of the broader considerations of acoustic imaging in general.

2.1 Basic Acoustic and Mechanical Quantities and Wave Behavior

When mechanical waves propagate through a material medium, certain properties are always of interest; we now describe these as they relate to the imaging problem.

Normally for the purposes of imaging, we desire the acoustic energy to propagate in a single direction exclusively, usually in the manner of longitudinal vibration, i.e. all the mechanical motion is confined to the path of propagation. Due to the net motion of energy, the particles from which the medium is composed are displaced from their rest locations, and this disturbance moves through the medium. Such motion is naturally resisted by the elastic binding forces that hold the medium together as an entity,

and this results in the exchange of potential and kinetic energy along the direction of energy propagation. Since we expect a controlled wave motion in our medium, we normally consider the wavefront to consist of a series of plane pressure waves of infinite extent, for the purposes of a mathematical description. If we define a particle of medium as simply a unit of matter that is small enough so that any physical and mechanical quantities of interest are constant along its extent, and allow for monochromatic (single frequency) periodic medium excitation, then the particle displacement about its mean location in the lattice is given by

$$x(t) = x_0 + A_1 \sin(2\pi f_{wave} t)$$
 (2.1)

where x(t) is the particle displacement, x_0 is the particle rest position, A_1 is the amplitude of the oscillation, and f_{wave} is the wave oscillation frequency. In order to find the particle velocity and acceleration about its rest position, we simply differentiate Equation (2.1). Of more interest to us is the velocity of the wave, which may be considered to be a constitutive parameter of the medium in which propagation is occurring; this quantity is contained in the function

$$u(x,t) = u_0 + A_2 \sin[2 \pi f_{wave} (t - x / v_{wave})]$$
 (2.2)

which describes the plane wave both in vibration and translation, where u(x,t), u_0 , A_2 , and f_{wave} are defined in a manner similar to the particle, x is the wave positional location at a particular time t, and v_{wave} is the velocity of wave translation.

It is pertinent to realize that since we have assumed unidimensional wave propagation, any distance we may compute from the experimental data resulting from any measurement will be assumed to lie along this same line of motion. Usually, we use the common simple relation

$$x = v_{\text{wave}} t_{\text{measured}}$$
 (2.3)

--where x is a distance, v_{wave} is again the wave velocity, and $t_{measured}$ is any time that we may have measured in a given experimental situation--to calculate a distance, at least when we know the wave velocity beforehand. Alternatively, we may find a value for v_{wave} when we have no such prior knowledge.

The velocity of wave propagation represented by our quantity $\mathbf{v}_{\mathbf{wave}}$ is governed by such physical quantities as temperature, medium density and stiffness, and the frequency of wave oscillation. For normal use, we consider a region made from a single type of material to be isothermal, so in this case $\mathbf{v}_{\mathbf{wave}}$ is given by

$$v_{\text{wave}} = \sqrt{k/\rho}$$
 (2.4)

where k is the material stiffness (elastic constant) and ρ is the material density in units of inverse cubic distance, for the one dimensional model that we have defined. This relation could be made much more complex by including other factors such as temperature, large signal constitutive parameters (which can be required under the

high amplitude drive conditions present in e.g. ultrasonic welding), and coupling of wave energy into other vibration modes.

Another quantity of importance is λ , the wavelength of the wave in the medium, which of course depends on the wave frequency and velocity as

$$\lambda = v_{\text{wave}} / f_{\text{wave}}$$
 (2.5)

This quantity is of great importance when choosing a frequency for which to use in imaging, since (1) the transducer, being piezoelectric in action, must be resonant at this frequency, and (2) the resolution of the image will depend inversely on λ [49]. We will consider this later when we discuss acoustic imaging.

The intensity of an acoustic wave may be attenuated by several loss mechanisms as the wave propagates through a medium, such as heating loss, lateral beam spreading, and partial scattering, but these are not of sufficient interest to discuss in detail here. In the next chapter, we will describe the present state of the attenuation literature, and some mention will be made about these types of problems. For our purposes though, the total effects of these loss actions may be combined into a single parameter α with the units of inverse distance [13].

Another quantity that is commonly defined in conjunction with a particular material is the characteristic acoustic impedance, which is analogous to the same quantity that is defined in the case of distributed electrical networks, and is given by

$$Z_{\text{characteristic}} = \rho v_{\text{wave}}$$
 (2.6)

where the quantities ρ and v_{wave} are as defined before. The characteristic impedance of a medium arises from the dual-quantity nature of the pressure and velocity in mechanical systems, again analogous to electrical voltage and current.

By means of the concept embodied in Equation (2.6), we can now investigate the action of a wave at a boundary of two media, particularly ones with differing characteristic impedances. Using Snell's Law and the continuity of both pressure and velocity at a boundary [2], we can write for Figure 2.1 that

$$v_{i} \sin \theta_{i} - v_{r} \sin \theta_{r} = v_{t} \sin \theta_{t}$$

$$\vdots$$

$$p_{i} + p_{r} = p_{t}$$
(2.7)

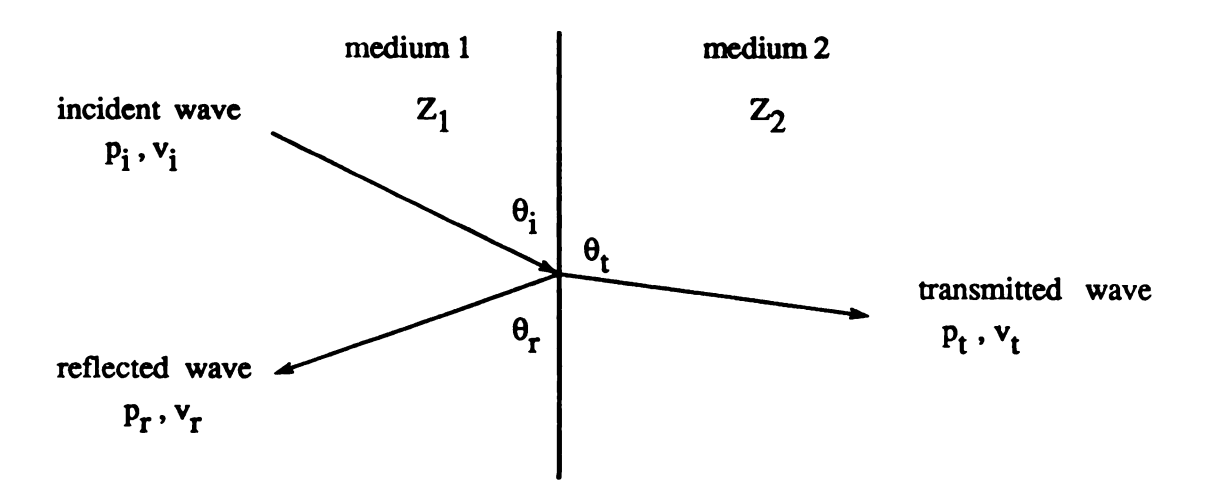


Figure 2.1 Wave behavior at an impedance discontinuity.

where the subscripts i, r, and t stand for "incident", "reflected", and "transmitted" respectively, p is the wave pressure, v is the wave velocity, and Z is the characteristic impedance of the medium. From the dualistic nature of pressure p and velocity v, we know that the relationship

$$v = Z_{characteristic} p$$
 (2.8)

must hold, again in a manner similar to electrical networks. By substitution of Equation (2.8) into the lower Equation (2.7), and then solving the system in Equation (2.7) simultaneously, we arrive at the following ratios as the pertinent solution:

$$\frac{p_{\mathbf{r}}}{p_{\mathbf{i}}} = \frac{Z_{2} \sin \theta_{\mathbf{i}} - Z_{1} \sin \theta_{\mathbf{t}}}{Z_{2} \sin \theta_{\mathbf{i}} + Z_{1} \sin \theta_{\mathbf{t}}}$$

$$\frac{p_{\mathbf{t}}}{p_{\mathbf{i}}} = \frac{2 Z_{2} \sin \theta_{\mathbf{i}}}{Z_{2} \sin \theta_{\mathbf{i}} + Z_{1} \sin \theta_{\mathbf{t}}}$$
(2.9)

where we have used the fact that $\theta_i = \theta_T$ to simplify the equations. Usually, the equations given in (2.9) are called the reflection and transmission coefficients, respectively—that is, we define the reflection coefficient to be

$$r = p_r/p_i \tag{2.10}$$

and the transmission coefficient to be

$$t = p_t / p_i \tag{2.11}$$

We note in passing, by inspection of Equation (2.9), the interesting fact that

$$t = 1 + r \tag{2.12}$$

a fact that we will use often later. Also, in the case of *normal* incidence, where $\theta_i = \theta_r = \theta_t = 90^{\circ}$, the definitions of the reflection and transmission coefficients reduce to the more commonly known

$$r = \frac{Z_2 - Z_1}{Z_2 + Z_1}$$

$$t = \frac{2 Z_2}{Z_2 + Z_1}$$
(2.13)

where Equation (2.12) naturally holds as well.

2.2 General Acoustic Imaging

In its most basic form, the method of acoustic imaging is rather similar to the operating principle of a radar system--signals are transmitted from the source into a medium which might have objects embedded within that must be detected, and the presence or absence of such an object is indicated by the existence or lack of an echo return, or reflection, from the target. This idea for medium imaging is usually called pulse-echo imaging, and is illustrated in Figure 2.2. The distance of the object from the transmitter is computed in a simple manner, by

object distance =
$$(propagation \ velocity)(time \ of \ flight) / 2$$
 (2.14)

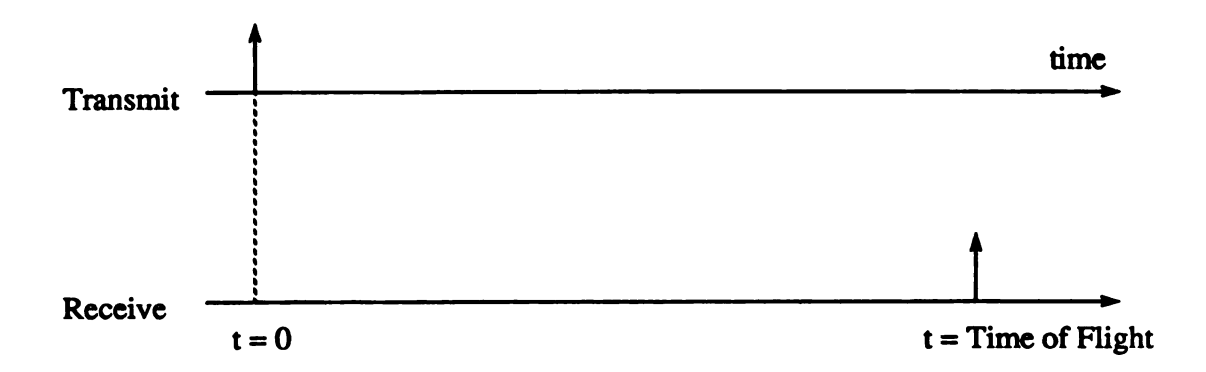


Figure 2.2 The pulse-echo imaging technique.

and naturally this definition of displacement requires the prior knowledge of the velocity of propagation in the medium being interrogated.

Another significant fact about the pulse-echo imaging technique is that in order to image a volume, as opposed to the one-dimensional interrogation performed in Figure 2.2, the transmitter must be scanned or positioned so as to allow data to be taken in different measurement directions, as mentioned in Chapter 1, and then this information must subsequently combined into an appropriate picture after suitable processing. We will discuss this processing in more detail in later chapters, but it now suffices to say that the time and amplitude information present in the echo are usually handled independently from each other, and both are strongly dependent upon the wave characteristics of the objects from which the echoes were reflected.

2.3 The Target

As we mentioned earlier, some assumptions are usually necessary to be made

concerning the physical structure of an object under test, in order to simplify the analysis of the internal acoustic wave behavior and potential sources of problems with the accuracy of the resulting image. We will now discuss these in limited detail.

The test object is usually considered to be composed of regions of different media as shown in Figure 2.3. In a particular measurement direction, the object is thought

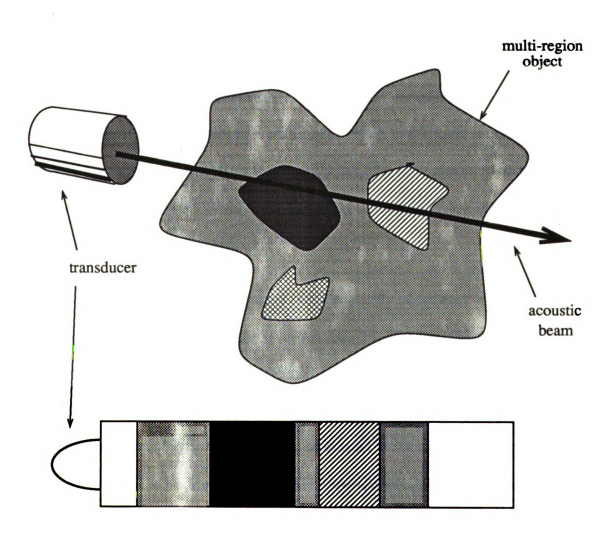


Figure 2.3 An example test object, and its one-dimensional model.

of as a series of layers arranged in one dimension, as shown at the bottom of Figure 2.3, where the different layers have been shaded in accordance with the upper part of the figure. Usually, we desire that the boundaries of such a test object be rather smooth, and also be perpendicular to the acoustic beam. There are several reasons for this, one being obvious from Figure 2.1, we showed that any such incident angle other than 90° will cause both the reflected and transmitted waves to leave the path of the transducer line of sight; in the expanded case of multiple layers and angular incidence, we can be almost completely sure that the beam will be lost to the receiver, unless it is positioned at a different angle than the transmitter with respect to the transmitter line of sight. In order to reconstruct an image in this case, we must scan both the transmitter and the receiver individually and over all angles so as to capture both the entire object and all of the returning energy reflected at every angle. This is discussed in greater detail in Chapter 7.

The planar layer assumption discussed above is usually considered valid when lateral spatial changes in object features are gradual, this being judged with respect to the transducer wavelength in the incident medium. Naturally, this situation does not always happen, e.g. at sharp corners in a boundary. Additionally, we cannot expect that all the inner boundary surfaces are flat and normal; in fact, by examining Figure 2.3 one can see that as the scanning angle of the transducer is changed around the example object in the figure, the apparent number of layers will change in each of the one-dimensional models resulting from each position, and we can expect that at some angles the acoustic beam will encounter a steeply curved boundary surface.

At such locations, diffraction and angular scattering must occur, and unless a separate receiver is employed at a different angle to intercept this energy, the imaging system will usually present erroneous data at this location. There has been some research to done with regard to this problem, but not much success has been achieved, primarily because of uncertainties in the profile of the acoustic beam emitted from the transmitter. This is discussed further in Chapter 5, but we can mention here that this profile is not a column of uniform intensity and phase, as usually assumed, but rather a complex variation of width (due to focusing and radial pressure divergence), and amplitude and phase (which both depend on the coupling medium and the transducer design). This profile can vary widely from transducers from even the same production lot, making fixed specification of the beam shape difficult to perform. The end result of this problem is that a great uncertainty exists concerning exactly what occurs acoustically inside a sample when it is being interrogated. For the purposes of this thesis, however, we will not address this problem further, other than to discuss the implications of its effects on the attenuation-velocity product technique.

The example object of Figure 2.3 is composed of layers of differing media, but we usually cannot expect these layers to be isotropic in their acoustic properties. For example, the attenuation of in-vitro tissue can vary significantly from the center of an organ toward the outer boundary [35], and we would like in principle to be able to observe this information non-invasively as well as the discontinuities of the boundary surfaces. Some research has been done to investigate the problem of reconstructing such an arbitrary spatial variation of acoustic properties [e.g. 23, 25, 29, 30, and 40],

but only in the case of internally boundaryless objects. In Chapter 7, we discuss the possibility of extending the work in Chapters 4, 5, and 6 to handle the cases of objects with spatial property variations, even with multiple regions bounded by discontinuities of, for example, acoustic impedance, but for the main purposes of the work done here, we will consider only the case of isotropic object regions bounded by discontinuities. In such objects, the one-dimensional model we construct in each measurement direction is then presumed to be made of layers of uniform media bounded by discontinuous impedance transitions, implying that the acoustic constitutive parameters of the object, when plotted versus distance within the object, form a steplike profile like that shown in Figure 2.4. This assumption can also be made in cases of spatial parameter variation, in which case it will result in a calculation of a sort of average value for the parameter between its bounding discontinuities.

Another problem that arises in a target object is that the acoustic parameters defined for the boundaries and layers, such as reflection coefficients and attenuations,

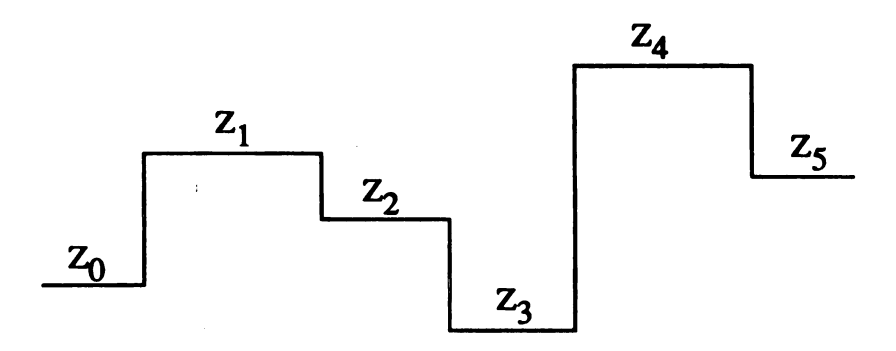


Figure 2.4 An example steplike impedance profile for an isotropic one-dimensional object bounded by discontinuities.

are functions of the frequency of the acoustic signal propagating in the medium, and therefore these parameters depend on the transducer frequency as well. For example, acoustic attenuation occurs in direct proportion to frequency (to a power greater than unity) in many materials, thus limiting the upper range of useful operating frequencies [17]. As we mentioned earlier, the resolution of an imaging system is a direct function of this frequency, so consequently the smallest detectable vertical distance is limited to some fraction of the wavelength given by Equation (2.5). Some work has been done to improve this resolution limit, including methods such as the deconvolution of the echo return signals [19], but the problem still stands as a fundamental limit.

Possibly the most perplexing difficulty of acoustic imaging is the problem of multiple reflections and transmissions. This phenomena is a consequence of the boundary behavior of an incident wave that we investigated in the derivation of Equation (2.9) in relation to Figure 2.1. Put simply, we must expect that any wave travelling inside an object will see an impedance discontinuity as a boundary whether it is incident from the left or the right. This is of immense importance to pulse-echo imaging in cases where a test object is constructed of several layers, like in our Figure 2.3, since echoes that return to the receiver from the deeper layers will encounter the outer boundaries on their right on their return trip, and will be re-reflected back into the object, as illustrated by Figure 2.5. This situation will occur repeatedly, and in theory continues indefinitely, which makes the phenomenon difficult to analyze in a formal manner. The end result is that instead of a single echo returning from each boundary, there will be a cavalcade of superfluous signals that will only cause great

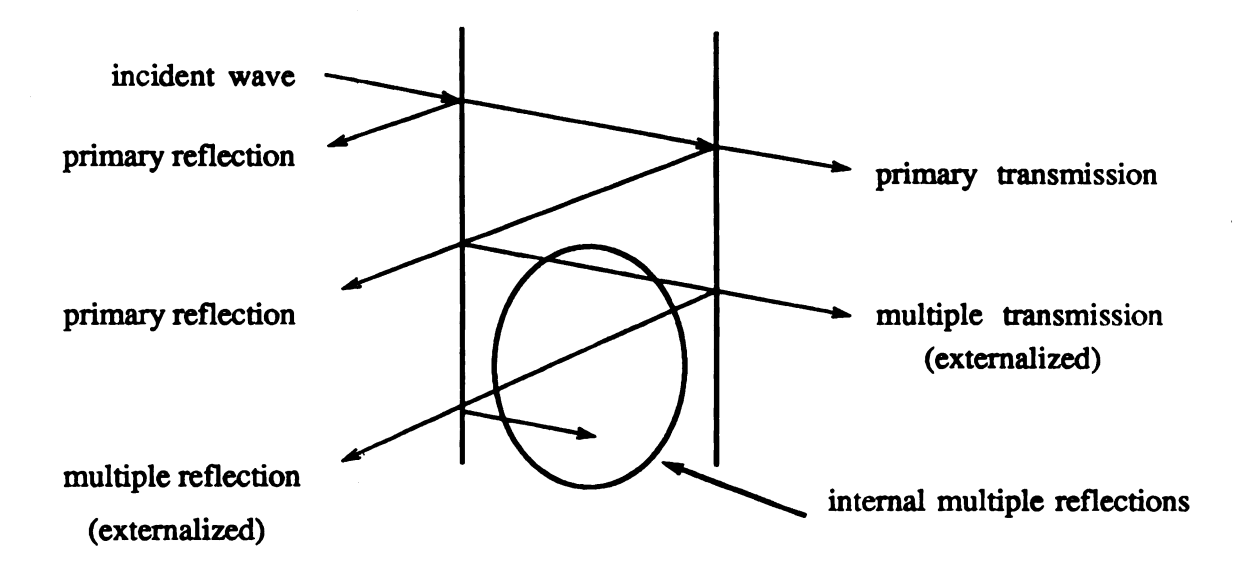


Figure 2.5 Example of multiple imaging artifacts in an object.

confusion about which echoes are real and which are artifacts, at best, or at worst will obscure the real echoes so that the ultrasound system cannot detect them at all. In the latter case, there is little that can be done at present but to accept the data as received and present it as best as possible, but in the former case, presumably, we can perform some sort of filtering operation to reduce or eliminate these obfuscating effects on the imaging quality [16]. We consider this further in Chapter 4, where an algorithm is presented that has been rather successful at performing this filtering operation.

One final property of interest in target objects is attenuation, but we reserve this discussion for Chapter 3.

CHAPTER III

ATTENUATION IMAGING

In the previous chapter, we considered the basic physical phenomena that influence acoustic energy, particularly for the conditions surrounding acoustic imaging, with the exception of loss mechanisms. We now briefly discuss the considerable subject of mechanical wave loss mechanisms in solids and liquids, and take a look at previous efforts to apply these phenomena to the imaging problem.

3.1 Attenuation

As a mechanical wave propagates through a transmission medium, the intensity of the wavefront maxima will reduce as a function of distance travelled; this result can be brought about from various sources, but the total effect is usually spoken of generally as "attenuation". We must distinguish this particular type of diminution of wave amplitude from other sources of such, for example, transmission through an impedance discontinuity, as mentioned in Section 2.1 and Figure 2.1, where the amplitude of the incident wave is modified by the boundary behavior that was therein discussed. Loss of amplitude of this type is *not* attenuation in the sense we have defined above,

and in practice, the influence of this behavior complicates accurate identification of the portion of the amplitude loss due to actual attenuation. We will discuss the separation of the effects of wave reflection at discontinuities and actual attenuation in the following chapter, where we will show that these two phenomena can in fact be decoupled even in a multi-layered measurement situation (i.e. one with many such boundaries). The discussion that follows is based on those given in Wells [2], and Herzfeld and Litovitz [14].

One mechanism of attenuation that results from beam nonuniformities is the change in apparent energy per unit beam area that is a consequence of the deviation of the beam from parallel [49]. Recall we mentioned earlier that typically the beam is assumed to consist of plane wavefronts (or at least constant intensity over each beam cross section); in effect, we thus also have presumed that the beam does not converge on (focusing) or diverge from (spreading, or defocusing) the line of sight. Attenuation from this mechanism may be computed by simple calculation [36], under the assumption that the phase fronts were initially constant.

A second class of acoustic absorption can be delineated from energy conversion phenomena, such as viscosity and hysteresis losses, and heat conduction. These mechanisms have been thoroughly considered in the literature, and so will not be covered here (see, e.g., Stumpf [13]). In addition to these phenomena can be added losses due to wave oscillation mode conversion [52], lattice/particle vibration resonances [51 and 53], and relaxation absorption [50 and 54]. With the exception of

mode conversion, which can be considered a macroscopic phenomenon, these are microscopic properties of solids and liquids, and all may share the energy present in a vibrating mechanical system. Loss occurs when the stored energy is returned out of phase with the desired dominant propagation mode, in our case longitudinal.

We note that the total loss observed in a particular sample medium may in fact be a combination of some of these individual effects. For the purposes of our work here, we can lump the separate mechanisms together and define as in [13]

$$\alpha = loss per unit distance (in units of inverse distance)$$
 (3.1)

to be a quantity that relates the "lossiness" of a particular material to the general imaging problem. Using the above definition of attenuation, we can also define a factor, as in [14],

$$\mathbf{k} = \exp\left[-\alpha \mathbf{x}\right] \tag{3.2}$$

to be a "loss factor (or parameter)" that is of interest for a specific object, where α is the attenuation per unit distance as defined in Equation 3.1, and x is the distance travelled during the propagation of the wave. Note that $k \in (0, 1]$, a fact that we will use later in Chapter 4.

One last concept that is of experimental importance is that attenuation is a frequency-dependent quantity; by this, we mean that the measurable loss of a particular material is different for different acoustic wave oscillation frequencies. For

example, biological materials, such as liver and muscle, exhibit an inverse dependence of loss with increasing frequency (see e.g. Bamber and Hill [39]). Other inorganic media exhibit a proportional dependence of attenuation with frequency for a wide range, then behave differently outside of that band [14]. These sorts of dependencies make measurement of attenuation difficult, since many of the techniques available to accomplish this employ pulsed ultrasound to interrogate a sample; in fact, a standard set of data for common materials has yet to be decided upon. In this thesis, we will not tangle directly with this problem, but consideration of the worries of gathering accurate experimental data in Chapter 5 will touch upon it again.

3.2 Attenuation Imaging

The literature involving imaging and related problems by means of loss parameters is varied, both in application and extent. Here we endeavor to give the reader a glimpse of the more salient aspects of this past work. In the process, a view of the current state of acoustic imaging will be forthcoming, and the chapter will conclude with some comments on the motivation of the work undertaken in this thesis in this regard.

Acoustic attenuation has been a topic of interest from the beginnings of research in the field of sound. For example, Fry (1952) [46] discussed in analytical detail the mechanisms that cause attenuation to occur in tissue structures; his early work was the basis for many of the later papers on such phenomena. The industrial uses of ultrasound also attracted researchers to investigate how lossy materials might be

processed by acoustic means; such applications are amply discussed in older textbooks such as Blitz (1967) [1], and new uses are constantly being forwarded, many related to materials processing and manufacture.

The imaging problem has long been acknowledged in medical and industrial research, but using attenuation to accomplish this is a relatively recent endeavor, primarily because of the reducing cost of computer equipment. Among the more prominent of the earliest work is that of Greenleaf et al. in [24, 25, 29, and 30], where' various techniques are described to accomplish acoustical computed tomography in a manner similar to that of X-ray diagnostic equipment. The work centered on the soft tissues of the human breast, with an intention to find a means of early tumor detection. Other researchers, for example Clement at al. in [56], were involved in applying arrays of transducers to similar uses. The promise of arrays is still unfulfilled, but as techniques of integrating more sophisticated acoustoelectric materials on a common substrate become more financially possible, perhaps these methods will be more widely investigated. Addison et al. in [55] describe an interesting alternative to electronically scanned arrays of physical transducers, using an optical laser to generate thermal stress on the target surface and induce mechanical waves. In the above work, examples of a noncontact system are given, and mention is made of the possibilities of simulating arrays of point sources in complex configurations. This work has yet to see a more widespread acceptance however, and it certainly will be some time before the complex and delicate optics required to perform the requisite signal reception are of sufficient durability to satisfy non-research applications.

Typical of the attenuation measurement systems reported is that of Klepper et al. in [28]. Their intention is to find points of in-vitro tissue pathology, specifically for cardiac infarction. Their experimental set up is much like we have already described, utilizing a pair of diametrically opposed transducers that are computer controlled in rotational position about the object. The transducers they employ are of acoustoelectric nature, which gives the receiver the property of being somewhat phase insensitive with respect to the incoming signal [23]. Reconstruction of the object is done by means of one of several imaging parameters, including attenuation and time-offlight. In the above paper, a mathematical model is formed along straight lines that pierce the object in the various measurement directions, thus ignoring possible angular scattering. The results indicate a reasonably good quality of image for the object model used, and the authors report that they were able to detect the tissue abnormality in most of the cases they investigated. Additional experiments performed by imaging with the attenuation slope between two neighboring frequencies seems to have given even more accurate images. The authors concluded that such effort had potential for in-vivo mammography, although no experiments have appeared subsequently to substantiate this opinion.

Glover and Sharp [7] reported an imaging system based on time-of-flight projections along straight lines through the object, again using a pair of rotatable transducers and the transmission tomography technique. The interest in this work is centered about the clarity of the images obtained and their marked similarity to the actual physical object. The conclusions the authors arrive at is that transmission

signals are far less affected by the amplitude distorting effects we will consider in Chapter 5, and that these signals are of prime importance to an imaging system that will investigate varied objects.

Other methods intended to pursue this goal abound. Farrell [48] proposes an iterative filtering technique to combat the image distortions associated with speckle, a by-product of the transducer position scanning that is necessary in the pulse-echo technique. Kuc et al. [32] exploited the approximate linear relation between the transducer frequency and the acoustic absorption to form imaging parameters based on the frequency slope of the attenuation. Data in this work is taken at several distinct operating frequencies, as opposed to using Fourier analysis; they propose that certain statistical measures be used for best advantage of the interpretation of any results that such a technique might yield. Parker and Waag [42] forwarded results of experiments they performed to process backscattered ultrasound signals from tissue boundaries to determine the medium loss as a function of frequency. They describe in detail the steps necessary to compensate for the distortion introduced by employing a time-gain compensator (see Chapter 5), and proceed to compute the attenuation within a selected portion of the structure, which they suggest would be useful for diagnostic clinical situations. Dameron [40] discusses the case of continuous media, and discusses the enhancement of attenuation images by means of correction of the distortion introduced from a nonuniform propagation velocity within the sample. Greenleaf et al. in [43] consider the effects of digital signal processing kernels on the results obtained from electronically scanned arrays, in order to obtain

synthetic focusing of the transducer beam. Studies were presented that indicated a greatly increased lateral resolvability for their system, and mention is made of the compensation for beam diffraction in limited instances, primarily in simulated tests. Further work in this vein was reported in Greenleaf et al. in [26] and [30], where specific attempts to apply attenuation imaging to production of human mammograms was undertaken in-vivo. Methods were described for the solution of various acoustic parameters of interest, with some results forwarded indicating that automated identification of tumor structures is conceivable.

Much of the reported research has emphasized the engineering aspects of building such systems, so it is only natural that some assumptions have been made in pursuit of the goal of a practical and affordable system. Often, the authors are not explicit when discussing the application of their theories, and the means by which they acquired their experimental results are often unclear. For example, as we demonstrate in the following chapters, simply using the amplitudes of the echo returns or transmission signals is not theoretically adequate to determine the attenuation of a medium under a wide range of circumstances, since other mechanisms can influence the amplitude data. Most papers neglect to mention how such influences are removed from necessity of consideration, which limits the usefulness of these works to others. The work in the following chapters attempts to clearly list the assumptions and limitations, as well as the implications, of each item, tedious as this might be for the reader and writer.

3.3 Attenuation-Velocity Products

In an effort to reevaluate the existing methods of attenuation imaging, the author arrived at the conclusion that in general it is impossible to determine the value of α in an experimental situation where nothing is known about the object internal makeup beforehand. We will see this clearly in Section 4.6, where we show that the velocity and attenuation of a material are inseparably bound together when using the pulse-echo imaging technique. It was therefore convenient to speak in terms of the product of these quantities as being a desirable unknown. Further investigation led to the discovery that the range of values for αv is very large, as shown in Table 3.1, and this wide spread permits a high degree of contrast between different media. In fact, such a wide difference would permit material identification to be made, given a predefined table of values for various media, perhaps in conjunction with the reflection coefficient information calculated by the solution method of Chapter 4. This would be extremely useful for many of the imaging situations that we have previously discussed.

In Chapter 4, we begin discussion of the theoretical specifics to determine the quantity αv in a general one-dimensional object. In following chapters, a more pragmatic viewpoint is taken, and application methodology and error sources are more closely evaluated.

Material	α (dB/cm)	v (m/sec)	αν (dB/sec)
water	0.0022	1480	325.60
aluminum	0.018	6400	11,520.0
plexiglass	2.00	2680	536,000.0
air	12.00	331	39 7,2 00.0
castor oil	0.950	1500	142,500.0
mercury	0.00048	1450	69.60
polyethylene	4.70	2000	9.4 x 10 ⁶
fat	0.630	1450	91,350.0
brain	0.850	1541	130,985.0
liver	0. 940	1549	145,606.0
blood	0.180	1570	28,260.0
skull bone	20.00	4080	8.19 x 10 ⁶
muscle	1.30	1585	206,050.0
kidney	1.00	1561	156,100.0
lens of eye	2.00	1620	324,000.0

Table 3.1 Attenuation-Velocity Products of various media at a 1 MHz transducer frequency (based on Wells [2]).

CHAPTER IV

DETERMINATION OF ATTENUATION-VELOCITY PRODUCTS

Up to this point in this thesis, we have considered both the principles and problems that are involved in acoustic measurements, and have also discussed the available literature in the field of attenuation-type acoustic imaging. As we have seen, there have been many attempts, both theoretical and practical, to address this difficult application of ultrasound, and there have been varying degrees of success in achieving this goal. After reviewing this literature, the author is of the opinion that different concepts about what constitutes attenuation imaging seem to exist, and no real formalization of this technique has yet become accepted by the research community at large. This is unfortunate, since applications and non-specialist users will only be suspicious and remain unconvinced that what they themselves expect in their diagnostic tool is what is really being done inside the "black box".

One of the basic motivations of undertaking the research delineated in this thesis simply was to investigate this very same inconsistency in attenuation imaging and perhaps help to create a more formal approach to visualizing the conditions of the problem. In particular, it was intended to examine the importance of each aspect of an ultrasound system as related to computing the attenuation of the regions in a

test object, with an awareness of the need for identification of solvable and insoluble difficulties, and to reflect on possible compromises to these problems. One item that becomes apparent upon perusal of the literature is a tendency to neglect rigorous and thorough listing of the assumptions made and the exact techniques employed to create the results and images that are presented, and the end result of this oversight can only be that the usefulness of this work is limited to other researchers. No significant progress can be made in any field without the cooperation and precise interaction of many people, and in a subject such as acoustics, with such a broad base of phenomena and applications, each demanding individual expertise, this need for clear interfacing between researchers and others is even further crucial. The intention here is to clearly identify the assumptions and their effect on the generality of the results.

The discussion that follows in this and subsequent chapters will take the a progressive outline, in the interest of presenting the new material earliest so that later examination of the impact of other difficulties on the concepts will be feasible; with this in mind, we start at the beginning...

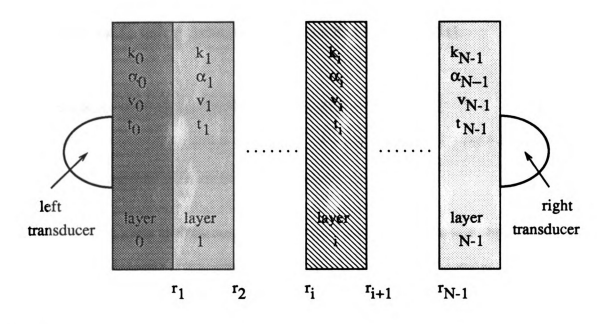
4.1 Basic Goals of This Section

Our primary intention is to investigate the experimental data that is necessary to allow computation of a quantity related to acoustic attenuation in a layered test object, while keeping in mind the assumptions and efficacy of any method/computations we propose to achieve this goal. For example, in practice we are not likely to know beforehand the number of layers that comprise the test object in a particular direction,

so any technique we devise should solve for this number, as well as any other such unknown quantities. Additionally, we ask what importance the reflection coefficients of each boundary may have on the computation of the attenuation in the object layers.

4.2 Problem Statement and Definition of Terminology

We set up the situation shown in Figure 4.1. This is a simple one-dimensional model that is intended to represent the internal layout of our test object in a particular direction. Note that there are N layers of up to N distinct materials comprising the object, and that we have allowed for the possibility of two transducers (the maximum number possible in a one-dimensional situation) being used in our measurement. Since our goal is to accomplish attenuation-like imaging, by inspecting Figure 4.1 we see that we are then required to determine the N values of k that represent the loss present in each layer. We should point out that each k; may in fact be a continuous function of position, i.e. $k_i(x)$ where x is a position within the layer, but any discontinuities are not permissible within the layer boundaries since, as we have noted in the derivation of Equation (2.9) and in Figure 2.1, any discontinuity of impedance (or any other constitutive parameter, for that matter) will cause an impinging wavefront to exhibit the type of boundary behavior we described at that time in Chapter 2. Also, any precipitous values of the derivative(s) in the constitutive parameters, when compared with a wavelength of the wavefront at the transducer operating frequency, are disallowed, since such a occurrence can cause behavior not unlike that of a discontinuity (in fact, this latter can be considered to be a definition



where

N = the number of object layers.

k; = the loss parameter of the i-th layer.

=
$$\exp \left[-\alpha_i v_i t_i \right]$$

 α_i = the attenuation in layer i in units of (distance)⁻¹.

v; = the propagation velocity in layer i in units of (distance/time).

t_i = the propagation time delay in layer i in units of (time).

r; = the reflection coefficient between boundaries i-1 and i.

Figure 4.1 The object model to be studied and the notation conventions used in the derivation of the equations in this chapter.

of a discontinuity, for somewhat inexact but practical purposes) [51].

4.3 Assumptions to Solve the One-Dimensional N-layer Object

In order to successfully attack the N-layer problem, we will make the following assumptions, and then later examine their implications:

- (1) We will use the pulse-echo type of measurement to probe the object; this will allow us to rather easily measure the amplitude of each echo in the signal, by e.g. a local peak detector.
- (2) Unidimensional wave propagation is the only mode allowed, in order to remain consistent with our one dimensional model. This precludes angular scattering.
- (3) Homogeneous layer composition, or simply that $k_i(x) = k_i$, in order simplify the variables to constants. We must first ask whether this case can be solved, before tackling the more difficult spatial variation problem.
- (4) Coplanar layers and boundaries are necessary in order to remain consistent with Assumption (2) above; implicit in this is the added condition that the boundaries be perpendicular to the line of sight along the beam path of the transducers.
- (5) No multiple reflections are present in the data we will manipulate to solve for the loss parameters k. This is not unreasonable since we will later discuss an algorithm to accomplish this very feat.

(6) The number of layers, N, is a known quantity; although this too appears to be unreasonable, it will be shown later, as in Assumption (5), that this can in fact be done before processing the data.

The assumptions above are not inconsistent with our one-dimensional object model, and yet do not strongly limit the generality of possible values for the constitutive parameters, within reasonable limits. For example, extreme attenuation in a particular layer, even under the best circumstances, will most likely cause difficulty in observing underlying layers, perhaps to the point of total obfuscation. With such cases suitably discounted beforehand, we can now begin to investigate the solution of the N-layer problem.

4.4 The Unknown Ouantities

By examining Figure 4.1 and considering the assumptions given above, we arrive at the following list of unknown quantities pertaining to the N-layer object:

- (1) The N values of k_i , the loss parameters of the layers.
- (2) The N-1 values of r_i, the reflection coefficients of the boundaries.
- (3) The N values of t_i, the propagation time delays in the layers.

Taken as a whole, we can represent the object as a set $\{N, k, r, t\}$, where N is the number of object layers in this direction, k is an N-vector that is comprised of the loss parameters of the layers, r is an (N-1)-vector with as its elements the N-1 reflection

coefficients of the boundaries, and t is an N-vector that is comprised of the time delays t_i of the layers. We note that by specifying the set $\{N, k, r, t\}$ we completely and uniquely describe the object in this direction, and thus to find a unique solution to the posed N-layer problem we must find all the elements in this set.

4.5 Solution of the Problem

We now undertake to consider several arrangements of experimental data that the configuration given in Figure 4.1 can provide to us, subject to our stated assumptions. The possibilities and problems inherent in each will be explored.

4.5.1 Case 1: Single-Sided Purely Reflective Interrogation

In most ultrasound imaging systems, only a single transducer is used to probe the test object, and this is done only from a single side during the entire measurement procedure, even when the transducer is used in B and C scans. For example, consider the "left" transducer of Figure 4.1 (noting that we may use a like discussion for the "right" side, if we so desired). In this situation, with the assumptions above in mind, we derive a series of echoes, one from each boundary, as shown in Figure 4.2.

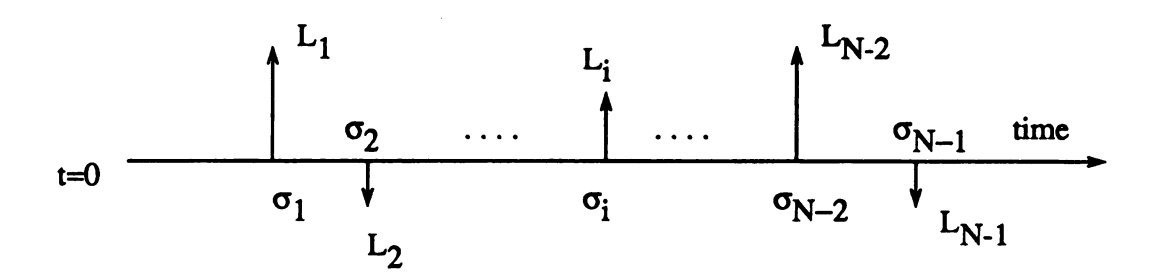


Figure 4.2. Example of left side echo data.

In Figure 4.2, we see that what we measure is a series of N-1 echoes L_i which each reflect from a boundary, specifically the i-th, and return to the receiving transducer at times σ_i , where we allow i to range from 1 to N-1. As we have assumed, we know the value of N, the number of layers in the object, beforehand, from prior consideration by means of our yet to be discussed algorithm.

In order to compute t_i, the propagation time delay in the i-th layer, and thus find the N-vector t, we simply can do the following:

$$t_i = (\sigma_i - \sigma_{i-1}) / 2$$
 (4.1)

if we will define $\sigma_0 = 0$ and allow i = 1 to N-1. We note in passing that if we had known what the acoustic velocity in each layer was, we could then compute the physical thicknesses of the layers, or vice versa, using also these values of t_i , but since these quantities are unavailable, we cannot do this.

It can be rather easily verified, by ray tracing and use of Equation (2.13) (recall that we have assumed normal incidence here), that the equation describing the amplitudes of the N-1 left echoes is

$$L_i(\mathbf{k}, \mathbf{r}) = A_{\text{input/left}} k_0^2 r_i (1 - r_1^2) k_1^2 \dots (1 - r_{i-1}^2) k_{i-1}^2$$
 (4.2)

where i=1 to N-1 and A_{input/left} is the initial left-input pulse amplitude sent out. Also

time
$$(L_i) = 2(t_0 + t_1 + ... + t_i)$$
 (4.3)

where i=1 to N-1, is the time delay of the left echo, where we have used the definition of t_i given in Equation (4.1). We note, by inspection of Equation (4.2), that

$$sign(r_i) = sign(L_i)$$
 (4.4)

where i=1 to N-1, which is an important fact that we will use later.

We are thus presented with a problem that we cannot solve, since we only have the N-1 equations given in Equation (4.2) and the N-1 experimental values of L_i that are illustrated in Figure 4.2, but have many more unknowns to find, specifically the values of $A_{input/left}$, k_0 , ..., N_{-1} , r_1 , ..., N_{-1} , which total to 2N unknown quantities. We should note that we actually need only find the magnitudes of r_i since the signs of the reflection coefficients are already known, by Equation (4.4). In some cases, the value of $A_{input/left}$ might be known, but this is generally not possible in practice since the initial pulse amplitude is a function of temperature, damping, etc., all of which are quantities that are difficult to hold fixed even under laboratory conditions. We naturally would prefer to not deal with this value at all, and later we show how it is possible to eliminate it from consideration completely.

From the above discussion, we can only decide that attenuation imaging is impossible to achieve from a single direction and merely single sided data echoes. The best that we can do is to compromise on strictness and speak only in terms of quantities that are vaguely proportional to attenuation, such as rk products. Even this is not acceptable, since the value of the rk product for a specific material will change

in different measurement configurations, e.g. different adjacent materials. This is due to the fact that r is dependent on two adjacent layers and not only on a single layer's characteristics; therefore this is not a good choice for an imaging index.

4.5.2 Case 2: Pure Transmission Interrogation

In the manner of Greenleaf et al. [43], we now investigate the situation of transmission imaging. The discussion here is limited to consideration of the effects of r and k on an single measurement line (direction), one of the many used to construct an image in the paper above. It can be shown, in like manner as in Equation (4.2), that the left-to-right transmission pulse amplitude is given by

$$T_{LR}(\mathbf{k}, \mathbf{r}) = A_{\text{input/left}} k_0 (1 + r_1) k_1 \dots (1 + r_{N-1}) k_{N-1}$$
 (4.5)

and that the time delay of this single pulse is given by

time
$$(T_{I,R}) = t_0 + t_1 + \dots + t_{N-1}$$
 (4.6)

where the quantities are as defined for Case 1 above. It is significant to realize that in this instance, multiple reflections are never a problem since we are only interested in this single pulse, and it is the first to arrive at the receiver. Note that this experimental situation requires that we use both the left and right transducers in Figure 4.1, oppositely aligned and either matched or calibrated to be so. Also, from an argument similar to that taken in Case 1, we know immediately that this single Equation (4.5) is woefully inadequate to solve for the same 2N unknowns we listed in Case 1. In the

work of Greenleaf et al., this difficulty is circumvented by two means: (1) the reflection coefficients are assumed to be negligibly small (when compared to unity), and (2) defining the object in a different manner than we have, as a continuous variation of impedance and attenuation. The latter is advantageous in their case since they intend to make a series of measurements from many vantage points around the object, and then synthesize an attenuation map of the inside by means of a CT scanner-like solution of a large linear system. We can, by inspection of Equation (4.5), see the negative effect of the reflection coefficients on the results of their calculations, which in the present author's experience can be considerable at times. Assuming that the reflection coefficients are negligibly small severely limits the scope of their ranges, as well as the classes of permissible objects. In the next chapter, we briefly discuss how to extend the method presented in this thesis to include the work of Greenleaf et al. and allow loss-like imaging in objects with both spatial variation of attenuation and non-negligible reflection coefficients.

4.5.3 Case 3: Bidirectional Interrogation

With the set up of Figure 4.1, having two oppositely placed transducers, we can generate additional data by probing the object from both the left and the right sides (sequentially, not simultaneously), and since the data from these measurements arises from like physical situations, we can use all of it simultaneously to solve for r and k. By an argument similar for Equations (4.2) and (4.3), we find that the right side echo return amplitudes due to an independent right side input pulse are given by the equation

$$R_{i}(\mathbf{k},\mathbf{r}) = A_{input/right} k_{i}^{2} (-r_{i}) (1 - r_{i+1}^{2}) k_{i+1}^{2} \dots (1 - r_{N-1}^{2}) k_{N-1}^{2}$$
(4.7)

and that the time delays of these echoes are given by

time
$$(R_i) = 2(t_i + t_{i+1} + \dots + t_{N-1})$$
 (4.8)

where we have defined R_i to be the right-input echo that bounces off of boundary i, using the numbering given in Figure 4.1, in correspondence with L_i as shown in Figure 4.3, and where $A_{input/right}$ is the amplitude of the initial right input pulse and i=1 to N-1. In general, we cannot expect that $A_{input/left}$ and $A_{input/right}$ are identical quantities, for the same reasons given in Case 1 regarding the impracticality of knowing $A_{input/left}$. One consequence of the numbering scheme we chose in Figure 4.1 and Equation (4.7) is that the right-input echoes come out in the reverse indexed order than do the left-input echoes given in Figure 4.2; this is illustrated by

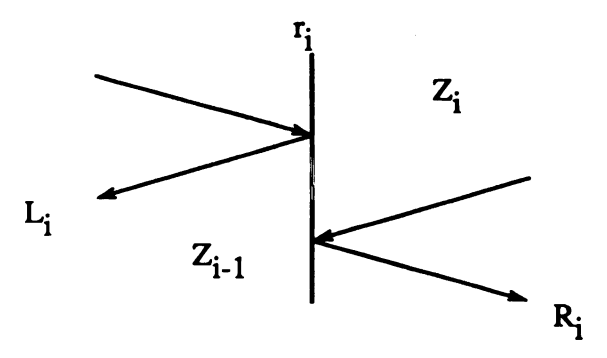


Figure 4.3 The definition of R_i with respect to L_i .

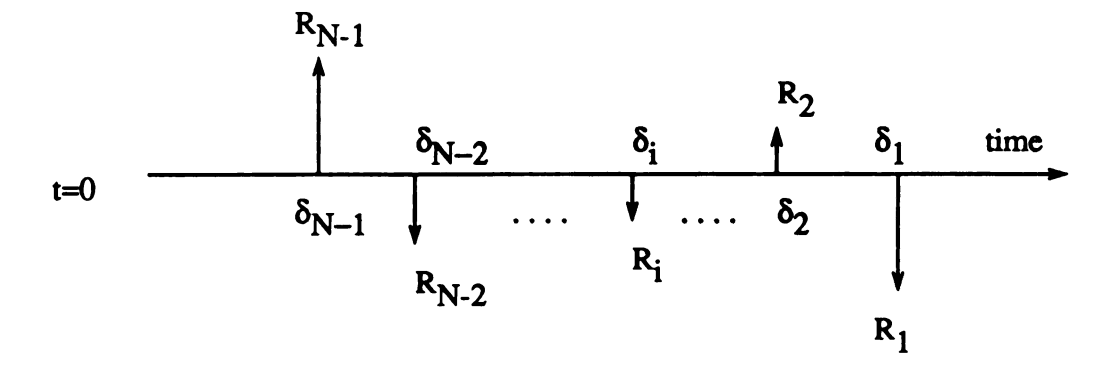


Figure 4.4 Example of right side input echo returns.

Figure 4.4, which shows an example compatible with Figure 4.2, the left side input echo example.

Note that we can use Equation (4.1) to derive the time delays of the layers t, but for completeness we note that by using the right side echo arrival times shown in Figure (4.4), that

$$t_i = (\delta_{N-i-1} - \delta_{N-i}) / 2$$
 (4.9)

where δ_i is as indicated in Figure 4.4, i=1 to N-1, and we must define $\delta_N=0$.

In a manner similar to Equation (4.4), we see that by inspection of Equation (4.7) that

$$sign(r_i) = - sign(R_i)$$
 (4.10)

and using Equation (4.4) we arrive at a simple but important fact we will make use use of later also, that

$$sign(L_i) = -sign(R_i)$$
 (4.11)

The negative sign in Equations (4.10) and (4.11) arises from the fact that a reflection coefficient viewed from the right has the opposite sign of the same viewed from the left side; one may see this readily from either Equations (2.9) or (2.13).

As we stated before, the 2N-2 left and right echoes that give us the 2N-2 values of experimental data L; and R; are derived from similar physical situations in the object and thus we may use these data simultaneously in our solution.. There now exist 2N+1 unknowns (now including A_{input/right}), so we see that the problem is still underspecified to allow a solution. In order to accomplish this, we must either (1) reduce the number of unknowns, or (2) increase the number of equations/experimental data pairs. Certainly from a practical standpoint the values of k_0 and k_{N-1} are usually known to us (or are measurable independently) beforehand, since these layers are almost always water or some other type of acoustic couplant, and therefore are identified materials with accessible properties (e.g. by tables). In order to solve this dilemma of not enough equations/data, we will use the latter fact, along with the added information available from the transducer opposite to the transmitter, i.e. the transmission data as well, namely Equations (4.5) and (4.6) for T_{LR} and, for the right-to-left transmission pulse, that

$$T_{RL}(k,r) = A_{input/right} k_0 (1 - r_1) k_1 ... (1 - r_{N-1}) k_{N-1}$$
 (4.12)

and

time
$$(T_{RL}) = t_0 + t_1 + \dots + t_{N-1}$$
 (4.13)
= time (T_{LR})

It is interesting to note that Equations (4.5) and (4.12) are not identical; once again, these differing signs are the results of the left and right viewpoints of the reflection coefficients. The implication of this distinction in the two equations is that the amplitude of the left-right and the right-left transmission pulses are different in value, a fact which seems non-intuitive. To understand this, however, one need simply to look at a single boundary, as in Figure 2.1, and examine Equations (2.10) and (2.11); it becomes readily apparent that even in the single boundary case of Figure 2.1, the transmission coefficient is different when looking from either the left or right side. We expect then that the N-layer case will behave similarly, and our conclusions about Equations (4.5) and (4.12) are valid. Additionally, this left and right difference has been substantiated in laboratory experiments.

With the addition of the two extra transmission equations, we now have 2N pairs of equations/data to use in solving the N-layer problem. We will denote this set by {L, T_{LR}, R, T_{RL}}_{primary}, where we intend the subscript "primary" to distinguish this set of data without multiple reflections from {L, T_{LR}, R, T_{RL}}_{experimental}, which is the set of all the data that we derive from the object, including any multiple reflections that occur. The primary data is then a "filtered" version of the experimental data, and the algorithm we present later is expected to accomplish this filtering before we perform any solution. The number of unknowns has been reduced to 2N-1, since

we have assumed that we know k_0 and k_{N-1} , but if we inspect Equations (4.2), (4.5) (4.7), and (4.12), we will see that it is not possible to solve for either $A_{input/left}$ or $A_{input/right}$, and we must deal with this, or else we cannot solve the problem at all. We can approach this as follows:

Form the ratios

$$H_{i}(\mathbf{k},\mathbf{r}) = \frac{L_{i+1}(\mathbf{k},\mathbf{r})}{L_{i}(\mathbf{k},\mathbf{r})}$$

$$H_{N+i-2}(\mathbf{k},\mathbf{r}) = \frac{R_{i}(\mathbf{k},\mathbf{r})}{R_{i+1}(\mathbf{k},\mathbf{r})}$$
(4.14)

where i = 1 to N-2. Importantly, we note that the above equations do not involve either $A_{input/left}$ or $A_{input/right}$. If we define new equations to solve, i.e.

$$G_{i}(\mathbf{k},\mathbf{r}) = H_{i}(\mathbf{k},\mathbf{r}) - \frac{L_{i+1}(\text{experimental})}{L_{i}(\text{experimental})}$$

$$G_{N+i-2}(\mathbf{k},\mathbf{r}) = H_{N+i-2}(\mathbf{k},\mathbf{r}) - \frac{R_{i}(\text{experimental})}{L_{i+1}(\text{experimental})}$$
(4.15)

where again i = 1 to N-2, thus forming a system of 2N-4 equations. We notice that the definition given in Equation (4.15) is made so as to force the solution of the

problem when we set G(k,r) = 0. Substitution of Equations (4.2) and (4.7) into Equation (4.15) yields

$$G_{i}(\mathbf{k},\mathbf{r}) = k_{i}^{2} (1 - r_{i}^{2}) \frac{r_{i+1}}{r_{i}} - \frac{L_{i+1}(\text{experimental})}{L_{i}(\text{experimental})}$$

$$G_{N+i-2}(\mathbf{k},\mathbf{r}) = k_{i}^{2} (1 - r_{i+1}^{2}) \frac{r_{i}}{r_{i+1}} - \frac{R_{i}(\text{experimental})}{R_{i+1}(\text{experimental})}$$

$$(4.16)$$

where i = 1 to N-2. This is a fascinating result, since it clearly shows that the uniqueness of the solution depends only on the values of r and not at all on those of k; in effect, we have successfully decoupled the single problem into two smaller ones, and the problem of solving for k is simply a matter of setting G(k,r) = 0, once we have the values of r. We should also note that our solution has the implicit assumption that the values of k_0 and k_{N-1} are known, as we discussed before. Additionally, it seems that the uniqueness of the solution depends only on the magnitudes of the values of r, since we have the signs of r by either of Equations (4.4) or (4.10). In order to find the values of r, we perform the following steps:

Using Equations (4.7) and (4.12), form the product

$$T_{LR}(\mathbf{k},\mathbf{r}) T_{RL}(\mathbf{k},\mathbf{r}) =$$
 (4.17)
 $A_{\text{input/left }} A_{\text{input/right }} k_0^2 (1 - r_1^2) k_1^2 \dots (1 - r_{N-1}^2) k_{N-1}^2$

We note the similarity between this product and the echo equations. Also form

$$L_{i}(\mathbf{k},\mathbf{r}) R_{i}(\mathbf{k},\mathbf{r}) = \tag{4.18}$$

$$A_{input/left} A_{input/right} k_{0}^{2} k_{i}^{2} (-r_{i}^{2}) (1-r_{1}^{2}) k_{1}^{2} \dots$$

$$\dots (1-r_{i-1}^{2}) k_{i-1}^{2} (1-r_{i+1}^{2}) k_{i+1}^{2} \dots (1-r_{N-1}^{2}) k_{N-1}^{2}$$

where i = 1 to N-1. Comparison of Equations (4.17) and (4.18) allows us to write that

$$L_{i}(\mathbf{k},\mathbf{r}) R_{i}(\mathbf{k},\mathbf{r}) = T_{LR}(\mathbf{k},\mathbf{r}) T_{RL}(\mathbf{k},\mathbf{r}) \left[\frac{-r_{i}^{2}}{1-r_{i}^{2}} \right]$$
 (4.19)

where i = 1 to N-1. Using the experimental values for L and R, we can solve the above equations for the values of r_i

$$r_i = sign(r_i) \sqrt{\frac{-R_i L_i}{T_{LR} T_{RL} - R_i L_i}}$$
 (4.20)

11.77-

where i =1 to N-1. This is the result that we desired, and it is unexpectedly simple, involving only the echoes from the i-th boundary and the transmission amplitudes. Recall that we can find the signs of r by use of either Equations (4.4) or (4.10). It is worth noting that the roots in Equation (4.20) always exist, since the radicand is always positive, which is easy to see by Equation (4.11), and the fact that both T_{LR} and T_{RL} are always positive as well, by inspection of Equations (4.5) and (4.12). We

can now solve for the vales of $k_1, \ldots, N-2$ (recall that we assumed that we know the values of k_0 and k_{N-1}) by using either of Equation (4.16); i.e.

$$k_i = \sqrt{\frac{L_{i+1} r_i}{L_i r_{i+1} (1 - r_i^2)}}$$
 (4.21a)

or the similar result involving the right echo amplitudes

$$k_i = \sqrt{\frac{R_i r_{i+1}}{R_{i+1} r_i (1 - r_{i+1}^2)}}$$
 (4.21b)

where for both Equations (4.21a) and (4.21b) we allow i = 1 to N-2. The combination of Equations (4.20) and (4.21) is the solution to the N-layer problem we desired.

4.6 Finding the Attenuation-Velocity Products of the N-layer Object

The solution that we derived in the previous section for the one-dimensional N-layer problem is completely general in use, since we have assumed no restrictions on the range of values that may be taken by any r or k in the object. After conducting a pair of left and right input measurements, yielding the experimental data set that we have called $\{L, T_{LR}, R, T_{RL}\}_{experimental}$ which may include multiple reflections, we then apply the algorithm which is described in the following section which provides the filtering of this experimental set into the set $\{L, T_{LR}, R, T_{RL}\}_{primary}$ which does

not contain multiple reflections, and has implicitly contained in it the value of N, the number of layers in the object in this particular direction (this value is easily found from the primary data set by simply counting the number of echoes in either L or R, and adding one). Application of Equations (4.1), (4.4), (4.10), (4.20), and (4.21) will then provide the solution to the posed N-layer object, in the form of set {N, k, r, t}, which as we have stated earlier is sufficient to uniquely define the object model in the measurement direction we have chosen.

Once having acquired the proper set {N, k, r, t}, we then would proceed to compute the imaging parameters that we would use for output and/or graphic display. For example, it is possible to use the time delays t in the layers as a parameter for this purpose. Perhaps of more interest would be a display of the reflection coefficients, or even a display of the characteristic impedances of the layers. We can accomplish this easily because of our knowledge of the impedances of layers 0 and N-1 (or we might simply normalize these values to unity for convenience), and by making use of a rearranged version of Equation (2.13a), i.e.

$$Z_{i} = Z_{i-1} \frac{1 + r_{i}}{1 - r_{i}}$$
 (4.22)

where i = 1 to N-2 and we know Z_0 and Z_{N-1} already. This can be used in impediography, as first suggested by Jones [41], only the calculations here will be more accurate than in the above paper since we decoupled the effects of k and r on the echo amplitudes.

As the title of this thesis suggests, we are primarily concerned with finding the attenuation-velocity products of the layers for use as imaging parameters, so we now describe this computation. As shown in Figure 4.1, the definition of k_i contains the product of α_i and v_i , which are thus inseparable since, even though we know t_i , we are not aware of the layer thicknesses and thus cannot compute v_i separately. However, if we would rather use the attenuation-velocity products, we can solve for them simply by rearrangement of the definition of k_i , i.e.

$$\alpha_i v_i = -t_i^{-1} \ln k_i \tag{4.23}$$

where i =0 to N-1. We then possess the quantities we originally sought, and can proceed to image, perhaps with a gray-scale or color graphics display to enhance the different regions of the object.

4.7 Multiple Reflection Elimination and Finding the Number of Layers

The final issues left to consider in this chapter are: (1) the determination of N, the number of object layers in the measurement direction, and (2) the elimination of the multiple reflection artifacts in $\{L, T_{LR}, R, T_{RL}\}_{experimental}$ to get the set of main echoes $\{L, T_{LR}, R, T_{RL}\}_{primary}$, which is lacking in these artifacts.

4.7.1 Finding N, the Number of Object Layers

In the case where there are no multiple reflections in the experimental data, this task is just limited to counting the number of echoes in either L or R and adding one.

However, when these artifacts are present, and experience seems to dictate that they are present in experimental data derived from even the simplest target objects, finding the value of N becomes more complex; in fact, it is inseparably tied together with the problem of filtering out the multiple reflections from the experimental data set.

4.7.2 Finding the Primary Data Set in the Presence of Multiple Reflections

Initially, this problems appears to be insoluble, but an algorithm was developed in conjunction with the solution given by Equations (4.20) and (4.21) that has been successful in choosing the primary data set from the experimental data, even in the presence of severe multiple reflections (e.g. if the number of multiple reflections is comparable to the number of primary echoes present in the data). This algorithm is diagrammed in Figure 4.5. Inspecting this, we see that the upper bound on the value of N to which the trial value N_{trial} is set is taken from the larger of the number of echoes in either L_{experimental} or R_{experimental}. This will result in one of the following three conditions being true: (1) N_{trial} is identical with N_{actual} (i.e. is the right value, since it is the same as the actual number of layers in the object), (2) the value of N_{trial} is larger than N_{actual} (which will occur in the presence of multiple reflections in either or both L_{experimental} and R_{experimental}), or (3) the value of N_{trial} is less than the value of N_{actual} (which can occur when deep-lying echoes from layers remote in the object are so diminished in amplitude that they are overlooked by the echo detection apparatus that precedes the algorithm). The latter case has a solution. which is discussed in more detail in Chapter 5, where we consider the effects of the

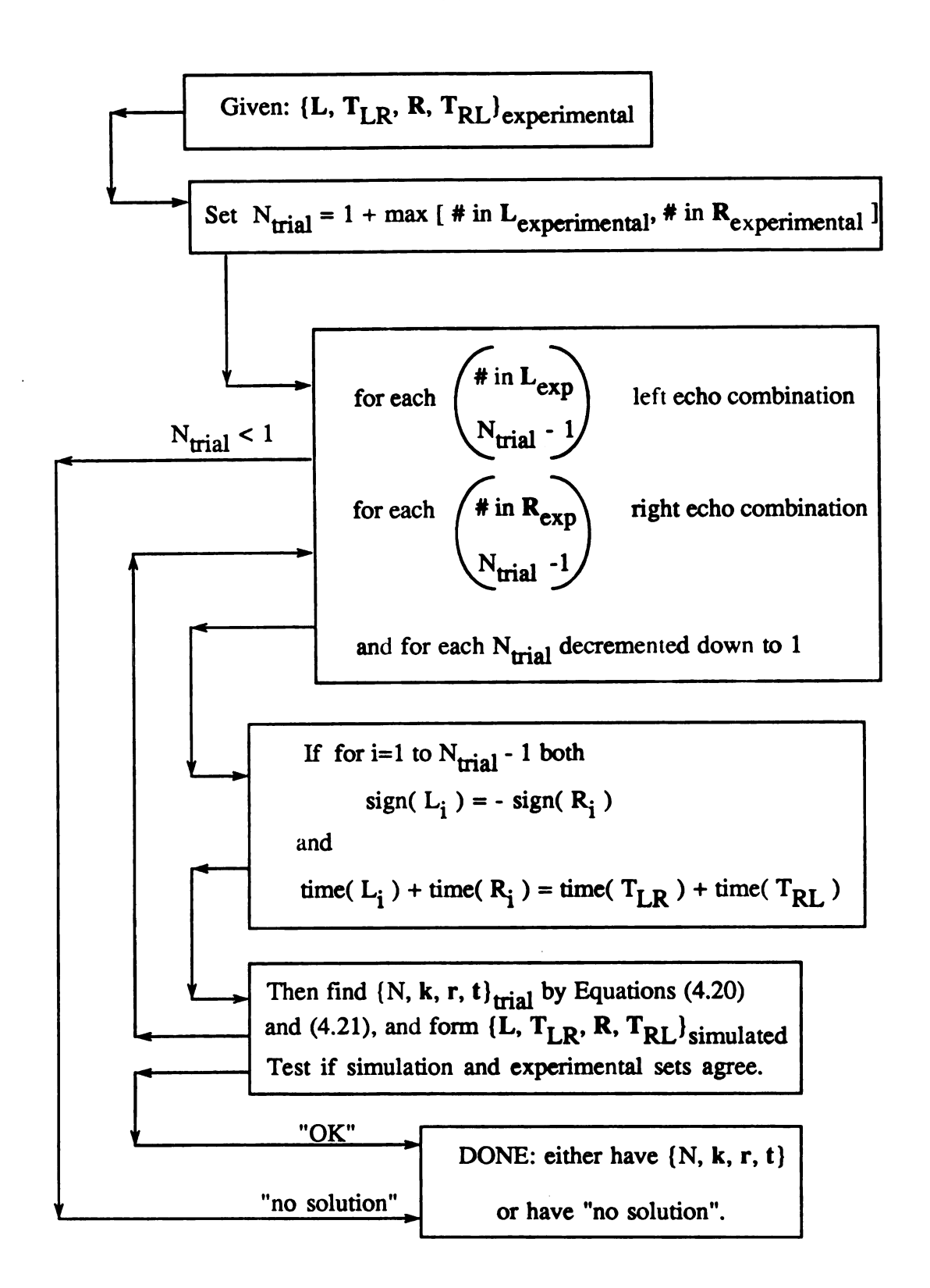


Figure 4.5 The algorithm described in this section that finds the set {N, k, r, t} and eliminates multiple reflections.

system components on the performance of the attenuation-velocity method.

In each of the three cases listed above, the algorithm of Figure 4.5 has been successful in either finding the correct primary echoes and set of {N, k, r, t}, or has correctly reported that no solution exists for the given experimental data set, e.g. in case 3, where some of the primary echoes are missing from the experimental data. What has proven to be particularly fascinating is that for even very complicated targets, with large N, only a single (correct) solution appears to exist for {N, k, r, t}, even in the presence of many multiple reflections! This surprising result leads to the optimistic speculation that perhaps the corrupting effects of these artifacts can be eliminated, or at least reduced in number, in the more useful (and difficult) three-dimensional object measurement situation, at some future date. The possibility of extending the attenuation-velocity product method to higher dimensions will be considered briefly in Chapter 7.

As a final note on the algorithm in Figure 4.5, we should comment on the method of simulating the trial model of the object. This is not difficult to perform, and the use of Equation (2.13) is necessary, along with the fact that the reflection coefficient of a boundary is opposite in sign, and a transmission coefficient is (1 - r) instead of (1 + r), if viewed from the opposite direction than they were originally defined. This concept is illustrated in Figure 4.6, and may be verified by consideration of Figure 2.1 and the derivation following that figure. In order to produce the simulated data set $\{L, T_{LR}, R, T_{RL}\}_{\text{simulated}}$, which is a set that is intended to correspond with the set of actual experimental data $\{L, T_{LR}, R, T_{RL}\}_{\text{experimental}}$, the following steps

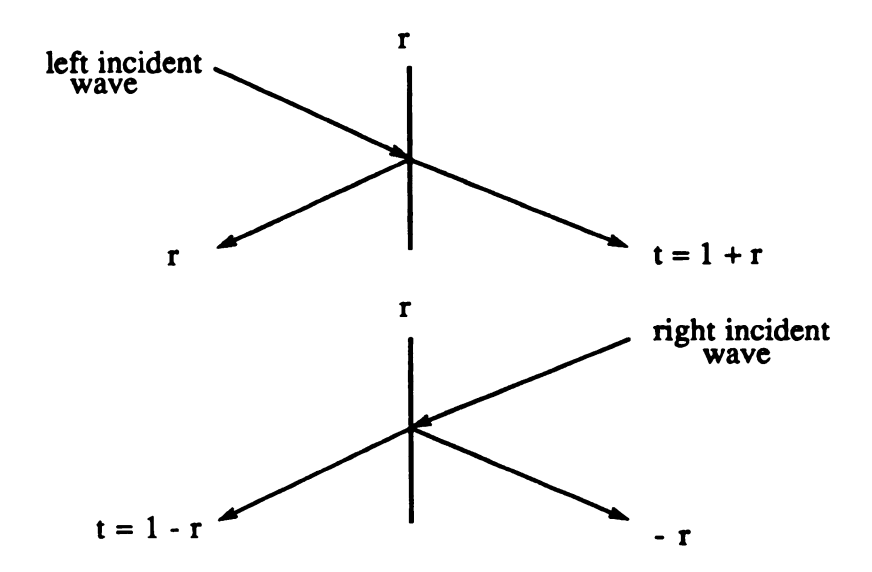


Figure 4.6 Illustration of the difference between the boundary properties when viewed from opposite sides.

are performed:

- (0) Given: {N, k, r, t}_{trial}
- (1) Select the minimum amplitude % tolerance to allow in the simulation by taking the minimum of

(2) Select the maximum simulated echo time by finding maximum [time($T_{L,R}$ (experimental)),

time(T_{RL} (experimental))]

- defined by {N, k, r, t}_{trial}. Follow this pulse from boundary to boundary, creating a reflected and a transmitted wave at each boundary encountered, using Figure 4.6 as a guide. Follow all these pulses likewise, modifying their amplitudes and times according to the values in {N, k, r, t}_{trial}. When either the minimum amplitude or maximum time limits are exceeded by a pulse, then eliminate it from further consideration. Eventually, pulses will reach the left side (boundary 0) and are considered to be left echoes and are put into L_{simulated} and eliminated, or reach the right side (boundary N) and be considered left-to-right transmissions and are put into T_{LR}(simulated) and eliminated. After a time depending on the tolerances and N_{trial}, all the pulses will have been eliminated.
- (4) Repeat (3) for a right input pulse at boundary N and forR(simulated), T_{RL}(simulated), etc.
- (5) Sort the pulses in $\{L, T_{LR}, R, T_{RL}\}_{simulated}$ into time order.
- (6) Scale each pulse in L_{simulated} and T_{LR}(simulated) by the factor

and scale each echo in $R_{simulated}$ and T_{RL} (simulated) by the like factor involving R_1 (experimental) and R_1 (simulated).

After performing these steps, we will have the set $\{L, T_{LR}, R, T_{RL}\}_{simulated}$, which is just a simulated version of $\{L, T_{LR}, R, T_{RL}\}_{experimental}$ that has used $\{N, k, r, t\}_{trial}$ instead of $\{N, k, r, t\}_{actual}$.

Finally, the trickiest part of applying the algorithm in Figure 4.5 is in making the comparison between the simulated and experimental data sets to determine if a good set {N, k, r, t}_{trial} has been determined. This is not as easy as it first appears, since what constitutes a good fit between the two sets is difficult to define, particularly since the dimensions of the vectors L, T_{LR}, R, and T_{RL} in either set may be of a different order (different dimensions, or number of echoes). In the trials done for this thesis, a simple requirement was employed that expected a fixed percentage of the non-primary echoes to be within a certain tolerance in amplitude and time. Naturally, more sophisticated methods of comparison could be used, such as pattern recognition.

In the next chapter, we investigate in more detail the requirements that implementing the attenuation-velocity product method would impose on a ultrasound system, and explore in some detail the sources of error that we can expect from each of the components in such a system. Also, some of the techniques that could be used to preprocess the experimental data before using the algorithm of Figure 4.5 will be discussed.

CHAPTER V

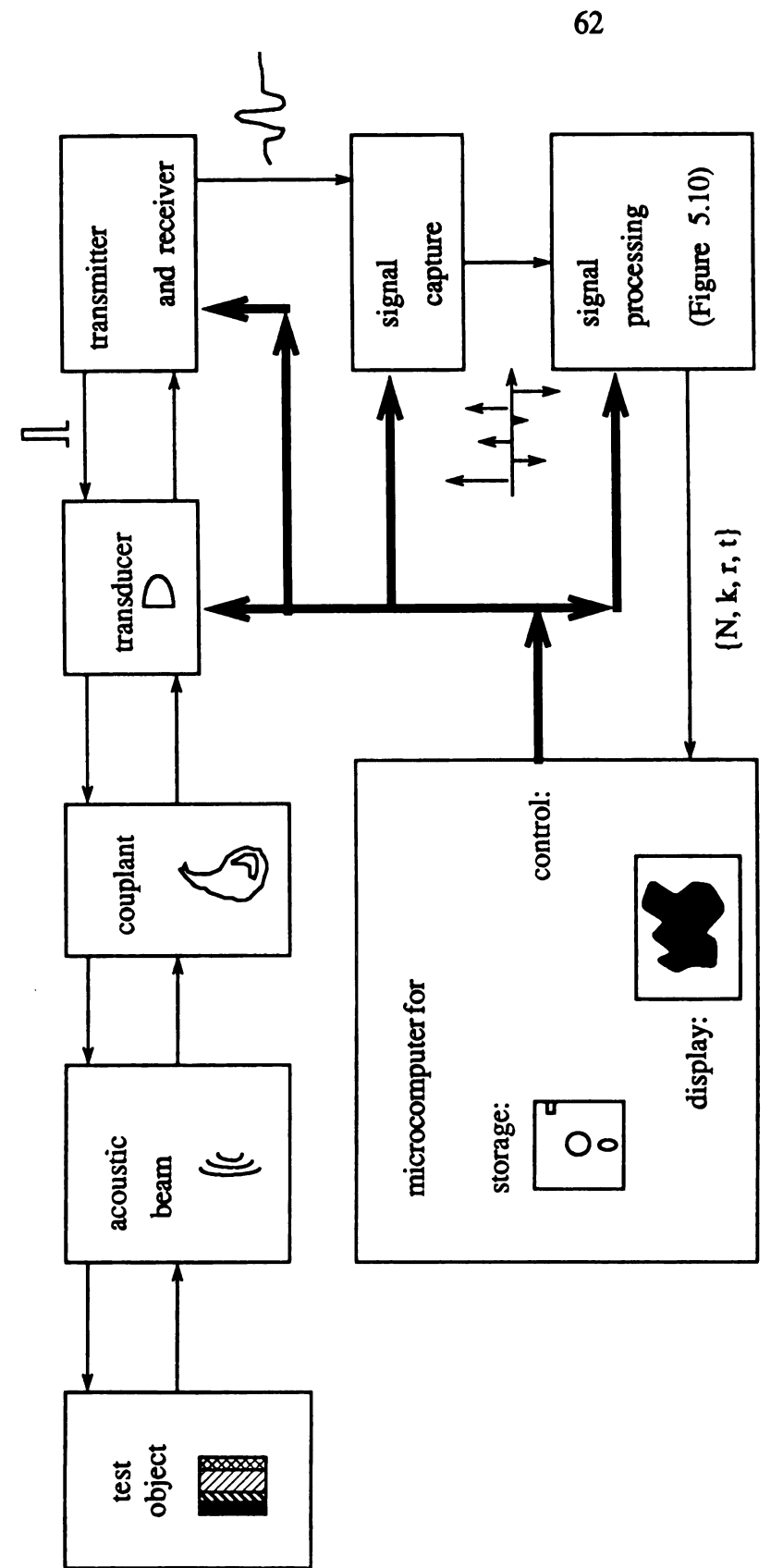
SYSTEM ANALYSIS AND ERRORS

5.1 Introduction

In the previous chapters, we have investigated the concepts and possibilities that the method of attenuation-velocity product imaging possesses; now we will turn to the more practical problems presented to one who would implement such a system. In particular, we are interested in what types of hardware and software components might be required, what features these must possess, and how the errors that each section and functional block introduce affect the accuracy of an acoustical measurement performed with such a system. For the purposes of our analysis, we will use the configuration diagrammed in Figure 5.1; the components indicated will be common in many ultrasound systems, and our queries will be enlightening even for the cases where a particular system might not follow this diagram literally. We will center our discussion on the issues that would confront an attenuation measurement system.

5.2 The Test Object

In Chapter 2, we approached the nature of acoustic wave behavior in a propagation medium from two points of view. First, we began with the mechanical wave and



Detailed block diagram of the components of the attenuation-velocity product measurement system to be analyzed in this chapter. Figure 5.1

discussed from its point of view how certain object conditions affect its dynamics, e.g.. the behavior at an impedance discontinuity. This allowed us to devise basic equations to use in further developments, which we approached in the second half of the chapter. From the transducer point of view, we considered the implications of certain object features and forwarded some assumptions that are usually introduced in order to simplify the analysis of the performance of a system. In this section, we will reconsider these and other items as they specifically relate to an attenuation measurement system.

We have already discussed the particular effects of the basic mechanical properties of acoustic waves on the amplitude of the received signals in Chapter 2, but in the discussion on scattering, we intentionally omitted a complication that can cause difficulties in imaging objects that are on the order of the beam width of the transducer. Normally, for objects that are large in this respect, the scattering takes the form of specular, or mirrorlike, reflection; i.e. the shape and spatial coherence of the incoming wavefronts are maintained by the scattering body (surface). However, for small objects, the acoustic beam is split into many smaller beams that travel in many separate directions, i.e. diffuse scattering [20]. Obviously, this situation is a problem for an imaging system, since the separate angular directions of scattering can be (mis)interpreted as separate scattering sources, and at present the resolution of this is unclear.

We also previously considered the effects of angular planar reflectors on the one-dimensional acoustic beam, and here we mention the interaction of this with

the echoes that return to the receiver from deeper lying layers. It is apparent that the reflection coefficients will be in error, as given by Equations (2.9) and (2.10), but less obvious is that the values of the loss factors k are adversely influenced as well, simply because the beam path length is increased due to the angular propagation. This will add to the error in the calculation of the attenuation-velocity products in Equation (4.23), of course. We mention once more that this angular propagation of the beam is more likely to send the deeper echoes in angled directions that are outside the beam pattern of the transducer, which we consider in the next section.

5.3 The Transducer

As we have mentioned in our previous discussion on the typical assumptions that are made in acoustical imaging, we usually consider the beam of mechanical vibrations that are emitted from the transmitting transducer to be a column of uniform sound in phase and amplitude, both axially and longitudinally. This of course is not the case, and most manufacturers of transducers provide some form of information with regard to this deviation. Analysis of this problem is pursued in the literature, and will not be considered further here, except to note that this nonuniformity of the beam profile will cause the efficiency of the mechanical to electrical signal transforming action of the receiving transducer to vary with different target distances, even for infinite planar planar targets. This problem is difficult to compensate, since the beam pattern can vary significantly between electrically-similar transducers and therefore the measurements necessary to learn the shape of the beam profile are not simple [6].

Another factor governing the efficiency and accuracy of the transforming action of a receiving transducer is the amount of received beam energy that actually intercepts the full receiver cross sectional area, e.g. in cases of reflectors that are not exactly perpendicular to the direction of propagation. To investigate this phenomenon, we will use the geometry of Figure 5.2, where we allow a uniform column beam to bounce off

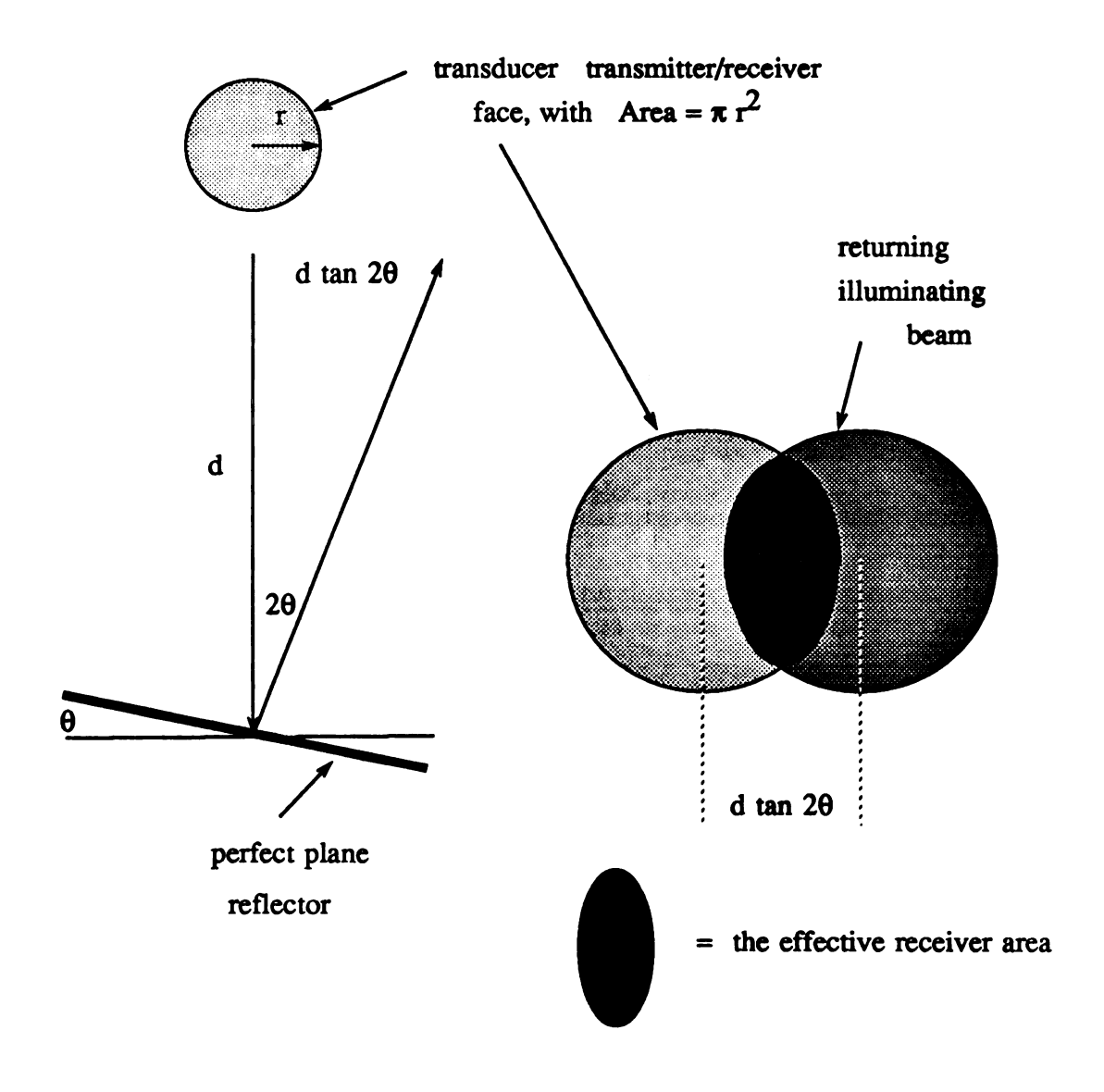


Figure 5.2 The geometry for finding the effective receiver area when the beam illuminates an angled planar reflector.

a perfectly reflective plane surface, which is positioned at an angle θ to the path of beam propagation. Note also that the transducer is located a distance d from the plane reflector, and has a radius r (usually transducers are round in shape), which gives us a maximum receiver area of π r². By simple trigonometric relations, we can find that the lateral displacement of the reflected beam which arrives at the transducer is d tan 2 θ , where we have used $\theta_i = \theta_r$ to determine the angle of reflection.

By integrating the effective receiver area, we find that

Effective receiver area = (5.1)

$$\pi r^{2} - 4 d \tan 2\theta \left[r^{2} - \frac{d^{2}}{4} \tan^{2} 2\theta \right]^{1/2}$$

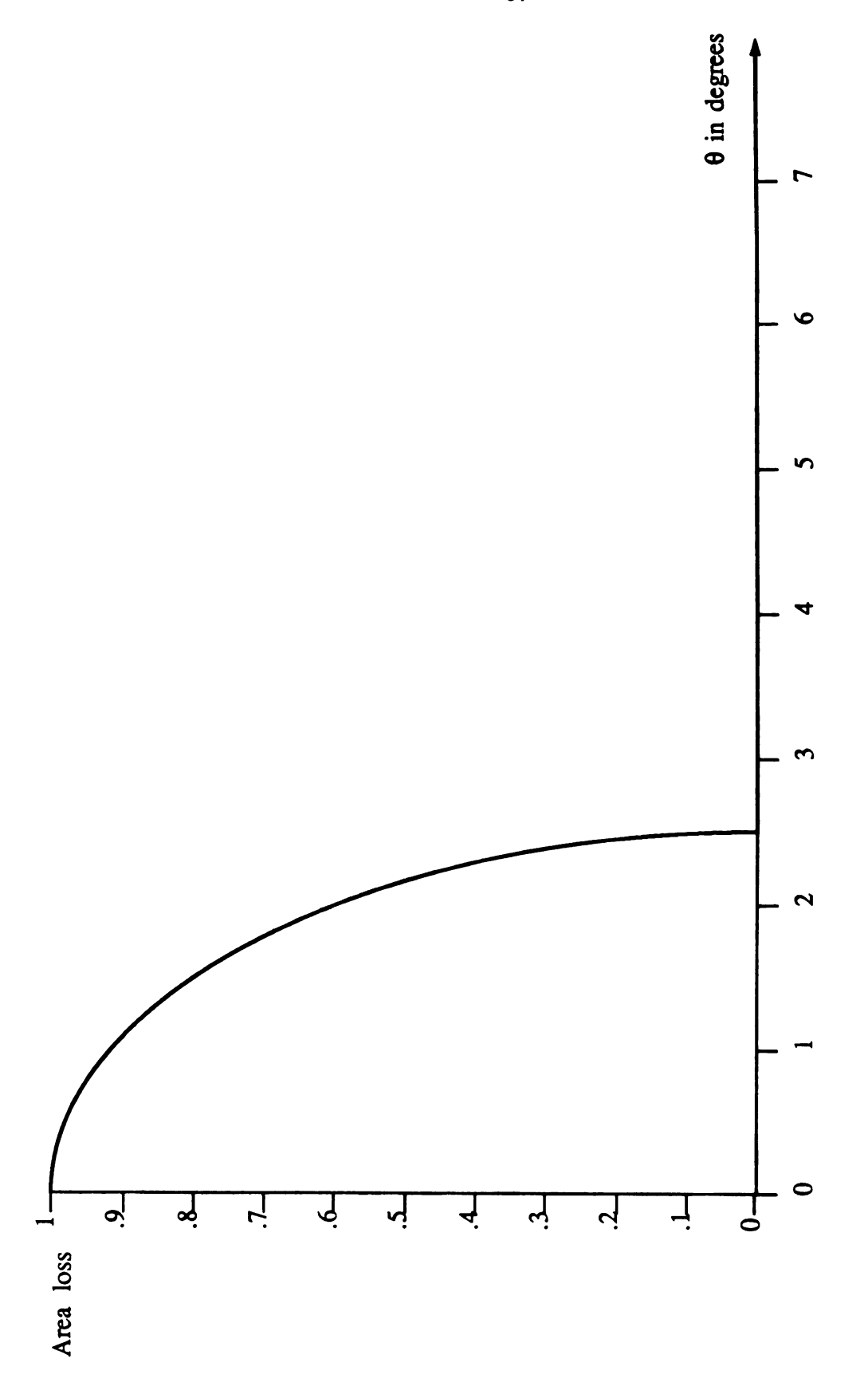
$$- 8 r^{2} \sin^{-1} \left[\frac{d \tan 2\theta}{2 r} \right]$$

we can define a percentage of area lost by the angled return beam, i.e.

% area loss = 1 -
$$\frac{\text{Effective receiver area}}{\text{Actual receiver area}}$$
 (5.2)

and this is plotted in Figure 5.3. We see that the influence of the angled reflector has a very significant effect on the accuracy of the amplitude information in a received signal, and thus is a major source of error when imaging nonideal objects.

Another important effect that the transducer exhibits is caused by the interaction of the materials from which it is constructed with the coupling medium. Typically the piezoelectric crystal that is the heart of the transducer is embedded in an epoxy



Plot of the angular sensitivity of a receiving transducer versus target angle, for d=10 cm, r=.5 cm, given by Equation (5.2). Figure 5.3

that is necessary for protection of the fragile crystal, but has a characteristic impedance that is several times larger than the couplant medium (e.g. water), which results in the appearance of a rather large reflection coefficient at the interface between the transducer active surface and the couplant [6]. By means of Equation (2.9), we can determine the effect of this on the receiving gain of such a transducer, as shown in Figure 5.4, where we allow a uniform beam to illuminate the transducer surface at an incident angle θ , with both being identical in cross sectional area. The coupling medium has a characteristic impedance Z_1 , and the transducer has an impedance of Z_2 , which as we have said is usually several times greater than that of the couplant. If we neglect the influence of the transmitted angle (i.e. set $\theta_t = 90^0$) in Equation (2.9), we can arrive at an expression for the transmission coefficient into the transducer that

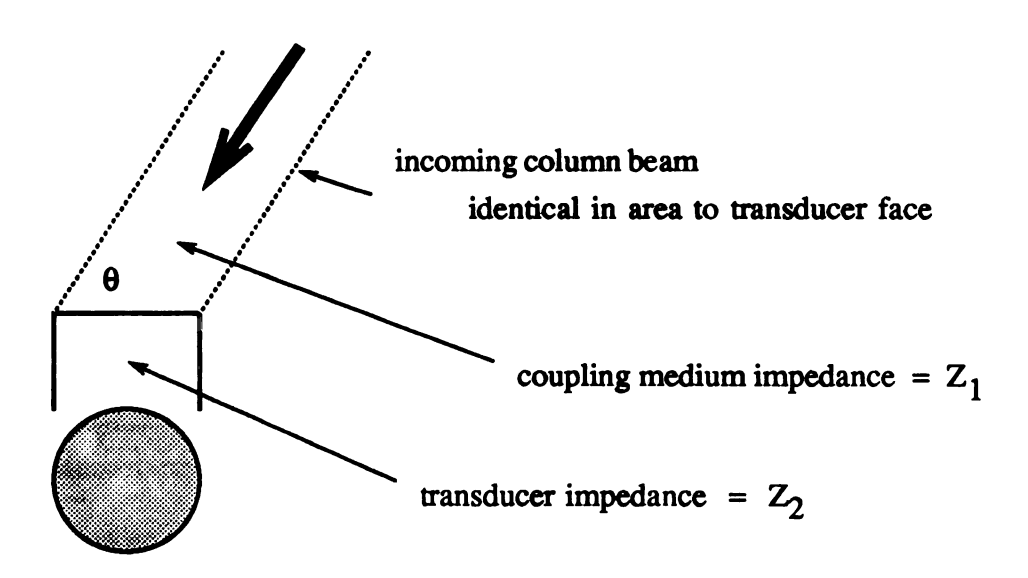


Figure 5.4 The geometry used to determine the transducer beam pattern and beam width.

involves just the incident angle, i.e.

$$t = \frac{2\sin\theta}{\sin\theta + Z_1/Z_2} \tag{5.3}$$

Note that this has been slightly rearranged to show the ratio of Z_1 and Z_2 , which is usually much less than one, and that this function is plotted in Figure 5.5. We see that the largest value of transducer receiving gain is

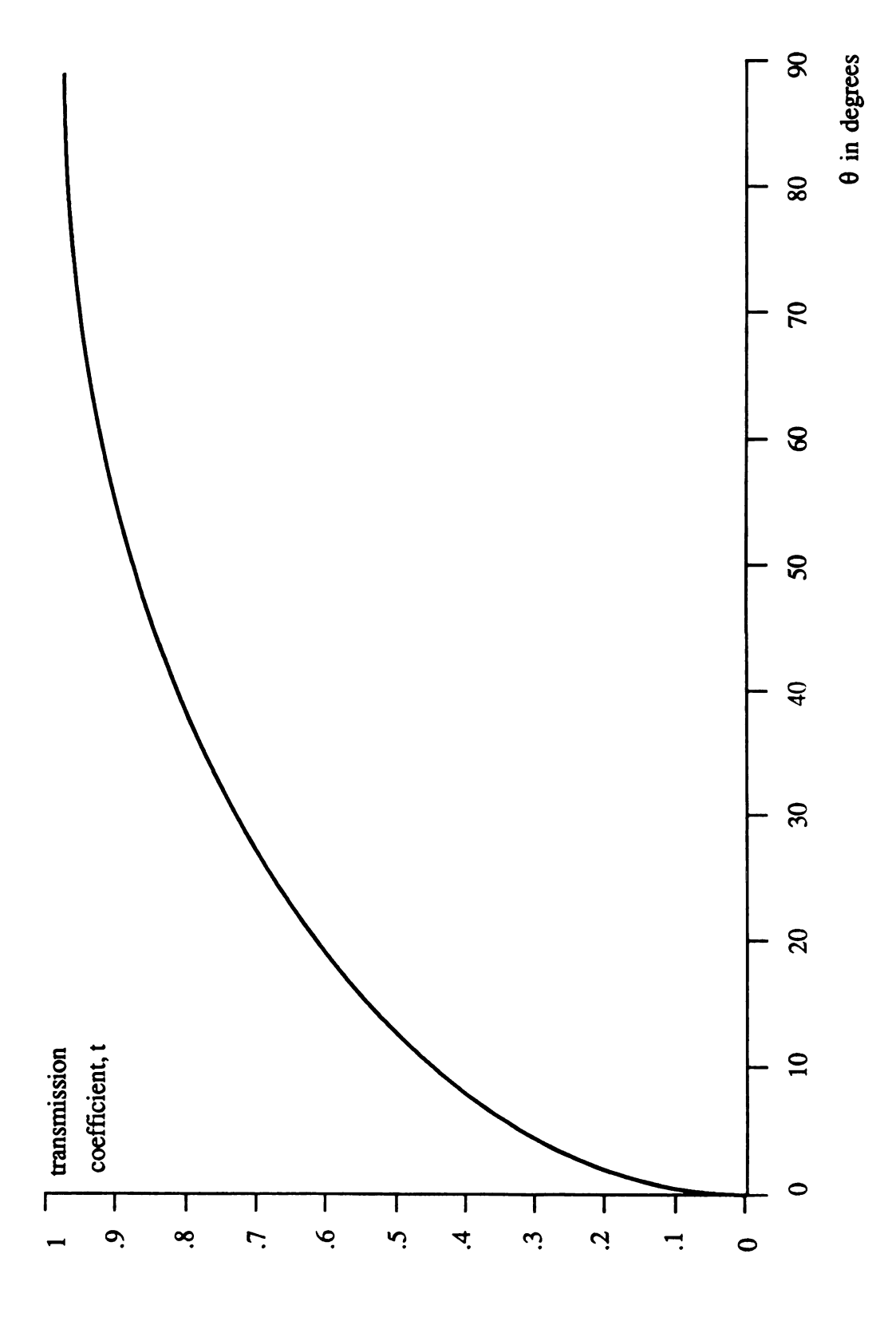
maximum receiver gain =
$$\frac{2}{1 + Z_1/Z_2}$$
 (5.4)

which occurs at normal incidence, and that the pattern half-beamwidth, found by setting Equation (5.3) to -3 dB or .707 of Equation (5.4), is given by

$$\theta \cong 90 - \sin^{-1} \left[\frac{.707 \, Z_1 / Z_2}{.293 + Z_1 / Z_2} \right] \tag{5.5}$$

which for the case of Figure 5.5 is approximately 79°, which is quite a broad receiving angle, but we have assumed no inherent beam pattern, which is only idealized.

As we mentioned in the introduction in Chapter 1, the transducer of many acoustic systems is piezoelectric in nature, which results in a rather specific natural resonant frequency being present in its characteristics. The exact value of this resonant frequency depends mainly on the physical geometry of the crystalline material used as the active element in the transducer, although the crystals lattice properties are also



Plot of the transducer receiving beam pattern, accounting only for reflection at the surface interface. Figure 5.5

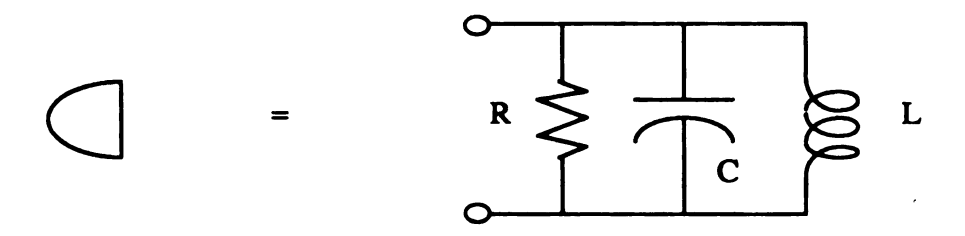


Figure 5.6 An electrical equivalent circuit for a piezoelectric transducer [6].

important. Electrically, the input port of this type of device appears to be a resonant tank, which can be modeled as shown in Figure 5.6. From electric circuit theory [4], we know that the resonant frequency of this network is given by

$$\omega_0 = \sqrt{\frac{1}{LC}} \tag{5.6}$$

which is identical with the transducer frequency, and the bandwidth is

$$\beta = \frac{1}{RC} \tag{5.7}$$

and the Q is

$$Q = 2\pi \frac{\text{maximum energy stored}}{\text{energy lost per period of oscillation}}$$

$$= \frac{\omega_0}{\beta} = R \sqrt{\frac{C}{L}}$$
(5.8)

The significance of Q is that a larger value of this parameter implies that the circuit will ring longer for the same input energy; by looking at Equation (5.8) above we see then that the value of R must be fairly small to limit the amount of ringing, and thus R can act as a damping control. Normally, this is made a variable resistor and provided as a front panel control for just this purpose, and usually the damping is made large to reduce the pulse width (by limiting the number of ringing cycles). If necessary, we can modify the transducer input impedance at resonance by adjusting R [4].

5.4 The Transmitter and Receiver

In commercial systems, the transmitter and receiver are usually combined into a single unit which has controls available to the user for making various adjustments. As was mentioned earlier, the transmitter is required to output a narrow high-voltage pulse to the transducer, in order to initiate the output mechanical wave. From the derivations done in Chapter 4, we know that some means of controlling the peak amplitude of this output pulse is necessary in order to avoid having the situation where any of the echo amplitudes are either too large for the receiving circuitry or too small for the level of noise present in the system. Again, we emphasize that the exact value of $A_{input/right}$ and $A_{input/right}$ are not important, as long as the receiver will not be overtaxed, so the controls that determine these values need not have fine resolution.

Another control on the transmitter/receiver that is important to system operation is the damping adjustment that is needed since the transducers are "tuned" devices; i.e. they will ring after the transmitter applies the output pulse to the electrical input port. The length of time that the ringing lasts will affect resolution of the echo detector, discussed later, and may be long enough to cause overlapping of subsequent echoes. Also, if the transducer damping is insufficient, the amplitude of the transducer ringing may be very large, since the Q of the resonant nature of the transducer is consequently large, and this may affect the receiver adversely. We see then that the amplitude and damping controls interact with each other, and therefore it is recommended that the damping be set first in such a manner to allow only one peak half-cycle of ringing to occur, at an amplitude that does not overdrive the receiver.

The receiver is usually a simple linear amplifier with some form of calibrated gain adjustment provided to allow setting the echo amplitudes to a reasonable value. Typically gains from 0-1000 are necessary, at a bandwidth exceeding the transducer resonant frequency, and with reasonably low noise to allow detection of low level echoes. One useful feature of a receiver amplifier is the ability to vary the receiving gain during the measurement cycle, particularly in the case of deep-lying echoes that are usually small in amplitude, perhaps sufficiently so to evade detection or cause introduction of error due to quantization, which we discuss in the next section. The effect of a Time-Gain amplifier is illustrated in Figure 5.7. The difficulty of using such an amplifier in attenuation computation systems is the need to know the exact gain variation with time during the measurement, which if not undone with accuracy can be a source of significant error in the values of echo amplitudes.

In the interest of completeness we should mention the impact of dynamic range

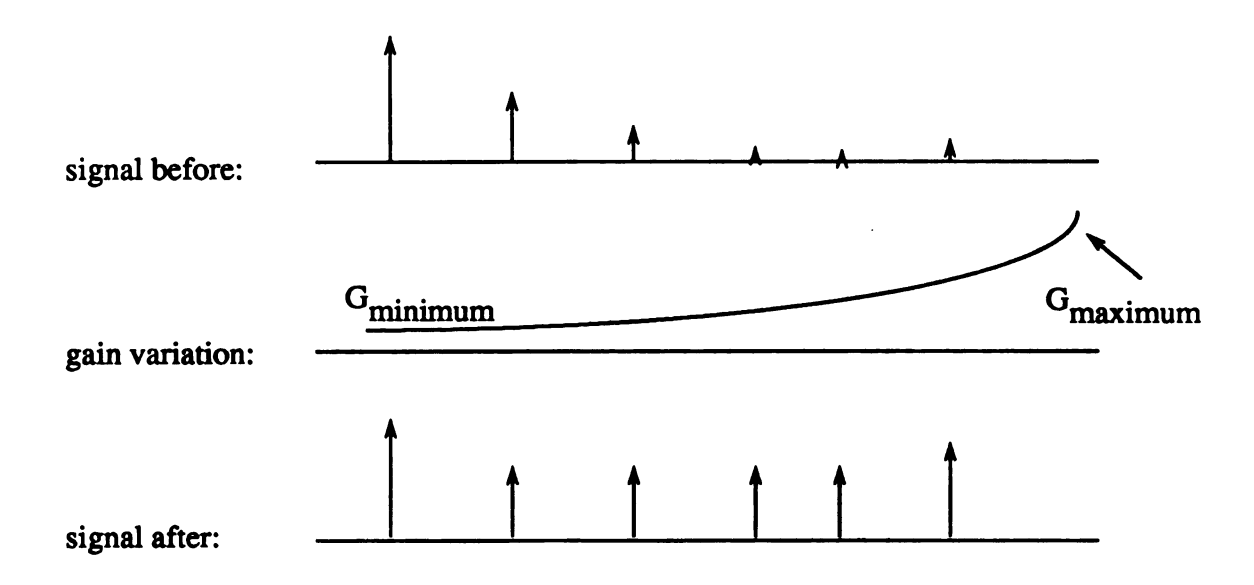


Figure 5.7 The use of a time/gain amplifier to boost the lower level echo amplitudes for increased accuracy and dynamic range.

on the system performance. We define the dynamic range as [3]

$$dynamic range (dB) = \frac{largest allowed signal (before distortion)}{smallest detectable signal (above noise)}$$
(5.9)

Usually in linear systems the noise floor determines the minimum detectable signal level, but our system is not completely linear, since as we discuss in the next section the effect of quantization is both nonlinear and extremely disruptive to the dynamic range, thereby reducing the sensitivity of our receiving system significantly. However, the influence of the receiving amplifier on this performance figure should be considered as being of similar significance. In the next section, we will consider this matter in more detail, particularly as to how it relates to the type of signal acquisition unit that is based upon an analog to digital conversion scheme.

5.5 Signal Acquisition

In a modern ultrasound system, it is most common to find some combination of high speed analog-to-digital (A/D) converter(s) and fast semiconductor memory arrays that are used to form a time-domain waveform capture unit. The features and costs of such units can vary quite extensively (take, for example, the many expensive multiple channel digital storage oscilloscopes with built in computational features that are now on the market from many manufacturers), but for the purpose of conducting acoustic measurements, our requirements are less demanding, particularly since we intend to accompany the signal acquisition unit by a microcomputer; in fact, we can reduce these needs to four: (1) the A/D sampling rate must be greater than the Nyquist rate for the transducer signal and bandwidth, (2) the size of the storage memory should be sufficient to ensure that the length of consecutive time that can be acquired is long enough to save the particular signals of interest, at the A/D clock rate, (3) the number of bits (quantization levels) in the output word of the A/D converter is sufficient to guarantee a useful value of system dynamic range, and (4) the triggering capability of the signal acquisition unit is accurate. One additional feature that might be useful is multiple channel (simultaneous) acquisition; sometimes this can be replaced by an analog multiplexing scheme that precedes the receiver of the system, e.g. in the case of large transducer arrays, where the sheer number of channels required prohibits the resulting cost and system size from implementing the receivers and signal acquisition in a separate manner.

In order to select the sampling rate for the signal acquisition system, we must

naturally first consider the nature of the signals that we are likely to be capturing.

As we already know from our previous discussions, the echo signals of the pulseecho method are comprised mostly of emptiness, and only a relatively small fraction
of the total time is filled with echo signals. As we showed in Figure 1.2, these echoes
are similar in form to a sinusoid at the transducer frequency amplitude modulated by a
gaussian pulse envelope; for simplicity, we can model this type of signal by [31]

$$s(t) = \frac{A \sin (2\pi f_{transducer} t)}{2\pi f_{transducer} t}$$
 (5.10)

which is shown in the frequency domain in Figure 5.8 [3].

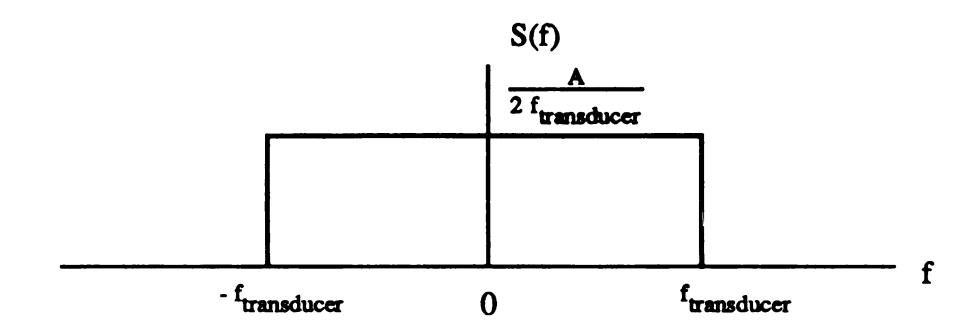


Figure 5.8 The spectrum of the function of Equation (5.10).

For this function, it is obvious by looking at the spectral characteristics that it is bandlimited to a frequency of f_{transducer}, and in order to satisfy the Nyquist criterion we would need to sample this signal at least 2 f_{transducer}. In practice however, the spectral characteristics of the transducer signal are not ideally bandlimited, and it is

common practice to oversample by several times the Nyquist limit in order to guarantee an accurate representation of the time signal in the sample memory. In the next section, we will consider this issue further in regard to the measurement of the peak value of the echo.

The memory capacity in words of the storage unit will directly influence the length of time that we can capture at once; for a single channel unit, this length of time is given by

time captured =
$$\frac{\text{# of memory words}}{f_{\text{sample rate}}}$$
 (5.11)

where f_{sample rate} is the sampling frequency. For example, a single channel system with a memory size of 16k (i.e., 16384) words, used at a sampling rate of 20MHz (or 20 million samples taken per second, i.e. "20MSPS"), will hold a time waveform of 819.2 microseconds in duration. As a final comment on this issue, we should note that some A/D units only are able to capture repetitive (periodic) signals at a high sampling rate, and this type of acquisition method is not very convenient for the more unpredictable type of signals usually encountered in acoustic measurements. Generally, this sort of unit is not used for this purpose.

The number of bits in the output word of the A/D converter used in the signal storage unit of a system will influence both the required memory word width (in number of bits needed per word), and also the accuracy of the recorded waveform amplitude information. In a binary output A/D converter with n bits in the output word,

the number of quantization levels is given by

quantization levels =
$$2^n$$
 (5.12)

for the full positive to negative input range allowed. Normally, for the signals we encounter in acoustics, we are concerned with only the time varying (AC) component of a signal, and the average (DC) value is not important. In this case, we require that the A/D converter be able to quantize both the positive and negative going portions of an echo pulse, and this will force us to offset the zero level to the midrange of the allowable input voltage, which causes us to have only one half of the number of levels given by Equation (5.12) to be available for both the positive or negative peaks, i.e.

bipolar quantization levels =
$$2^{n-1}$$
 (5.13)

For example, an 8 bit output word gives 127 quantization levels (from 0 to the maximum positive or negative value allowed. Note also that we must expect that the input signal to the A/D converter does not exceed these maximum values, causing an overrange condition that will lessen the accuracy of the captured data. If this occurs, we must reduce the amplitude of the input signal by reducing the receiver gain or by lowering the output level of the transmitter unit).

Another signal acquisition issue of importance to attenuation measurements is the system dynamic range, as we discussed in an earlier section in this chapter. In the A/D unit, we define the dynamic range similarly as in Equation (5.9), and we find, for the linear scale n bit binary output converter, that

A/D dynamic range in (dB) =
$$20 \log_{10} 2^{n-1}$$
 (5.14)

$$\approx 6 (n-1)$$

For the 8 bit example, this gives a dynamic range of about +42 dB, which is not very large (only about 120 to 1), and by itself is usually insufficient for attenuation measurements. As we discussed in the receiver section, a time/gain compensator (TGC) may be used to increase the dynamic range, provided that the amplitude distorting effects of this unit are undone prior to subsequent processing. Another method of increasing the dynamic range, which is more limited in usefulness than a TGC, is to average repetitive measurements performed in the same position on a sample-by-sample basis [10], using floating point arithmetic (note this action will also tend to reduce the uncorrelated noise that arises from measurement to measurement in the system, thus making echo identification easier). If we average 2⁸ times, then

effective dynamic range (dB) =
$$20 \log_{10} 2^{n+a-1}$$
 (5.15)
 $\approx 6 (n + a - 1)$

causing the system to appear to have an A/D converter with 2^{n+a} total quantization levels. One problem with this technique is that it is necessary to align the individual time waveforms with each other before averaging them together, otherwise distortion will invariably occur. By this we mean that the exact position of the echoes in each signal will vary somewhat due to uncertainties in the time of transmit pulse output, and unless steps are taken to correct this, we will cause more trouble than

we are remedying. Even with such alignment being done, the fact that we are sampling at almost the Nyquist in many situations can cause the additional problem of introducing phase distortion into the averaged version of the time signal, since the sample data is sparsely distributed over each cycle (at the transducer frequency) of the signal (this effect is considered in more detail in the next section). We can conclude therefore that this type averaging is rather difficult to perform in such cases, unless special care is taken, possibly interpolating values between the actual samples for use in computing the average time signal.

One problem of quantizing the input signal in an attenuation (amplitude) measurement system is that the error in the echo amplitudes measured will depend upon the the magnitude of those echoes. This of course is a consequence of the limited resolution that is available for small input signals. The percentage error introduced by quantizing an input signal with amplitude A with an n-bit linear span A/D converter that has a maximum voltage limit V_{max} is

% quantization error =
$$\frac{\frac{V_{max}}{2^n} \text{ integer } [2^n \frac{A}{V_{max}}] - A}{A}$$

$$= \frac{V_{\text{max}}}{2^n \text{ A}} \text{ integer } \left[\frac{2^n \text{ A}}{V_{\text{max}}} \right] - 1 \qquad (5.16)$$

which is plotted for our 8 bit example with $V_{max} = 1$ volt in Figure 5.9.

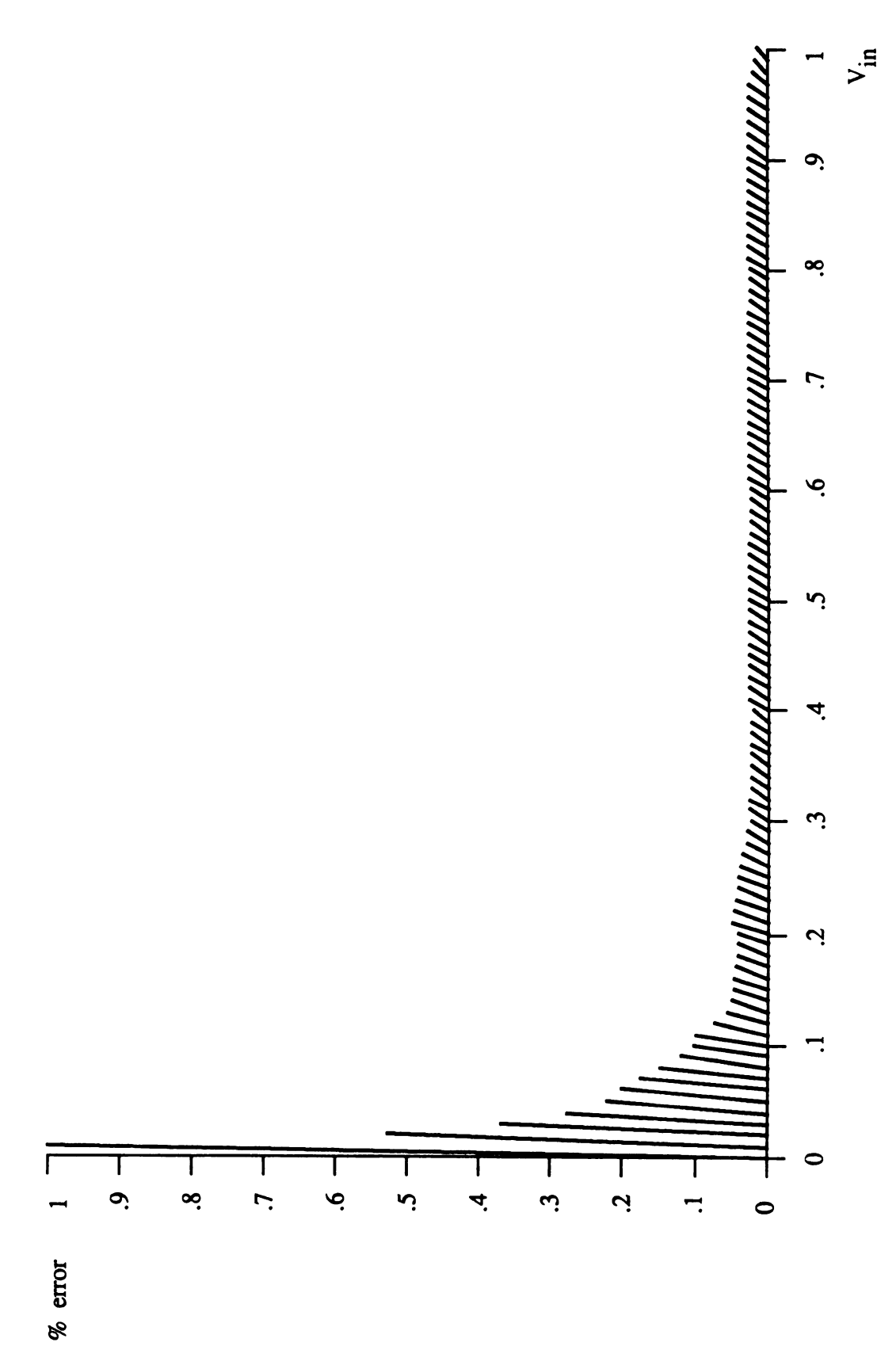


Figure 5.9 Quantization error for an 8 bit bipolar A/D converter, from Equation (5.16).

We can clearly see that the error introduced is much more pronounced for smaller values of A, which means that more error is introduced for these smaller values of echo amplitudes when they are quantized by the A/D converter.

The fourth and final consideration for the signal capture unit is the need for stable and reliable triggering of the storage action, particularly if signal averaging is being contemplated. If this requirement is not met, then it will be difficult to measure absolute time delays of the echoes, although relative time will be unaffected, and it will be impossible to accurately find the value of transmission pulse time delay, e.g.. time (T_{LR}) in Equation (4.6). In most commercial A/D systems, this triggering is a parameter well specified by the manufacturer, and usually then the acoustic system designer need only be aware of the problem, so that the system user can be assured of the time measurement accuracy.

5.6 Signal Processing

After the transient waveform has been digitized and captured, it is usually made available to a digital computer for processing prior to storage and display. Normally, some form of computations are performed before storage of the information in the signal, since saving the actual samples can require excessive memory or disk space, especially for the many distinct measurements that must be done in order to create a multidimensional image. Figure 5.10 indicates a possible block diagram of the necessary software to process the signals prior to application of the attenuation-velocity product algorithm of Figure 4.5; i.e., the routine that creates the set

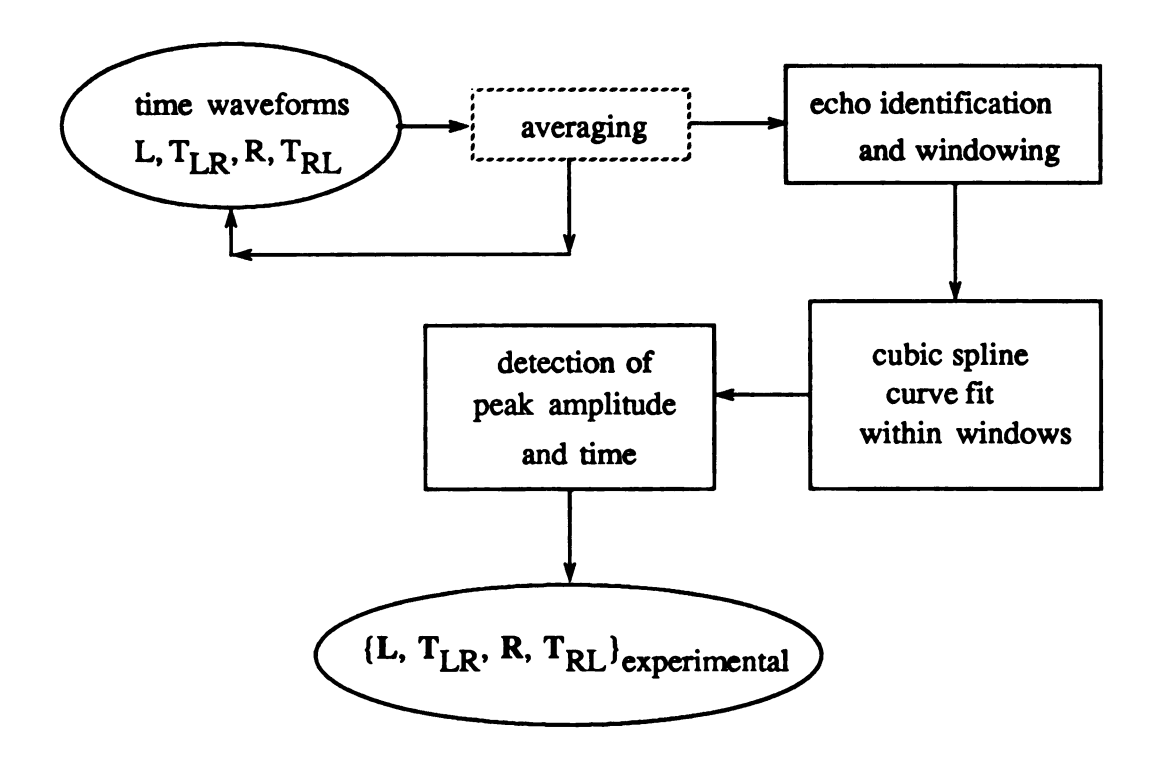


Figure 5.10 The software preprocessing for the algorithm of Figure 4.5.

 $\{L, T_{LR}, R, T_{RL}\}_{experimental}$ from the various time waveforms.

We have already considered the problems involved in signal averaging in the previous section, so here we will not discuss it directly; however, as we mentioned before, in order to do this operation properly without introducing distortion, it is necessary to interpolate between the sampling points given and align the peak values of the echoes. The theory and use of cubic splines will be discussed shortly, for the purpose of improving the accuracy of the reported peak echo amplitudes, and the discussion given there can naturally be adapted for the signal averaging technique.

The first task of the preprocessing software is to identify the location of pulses in

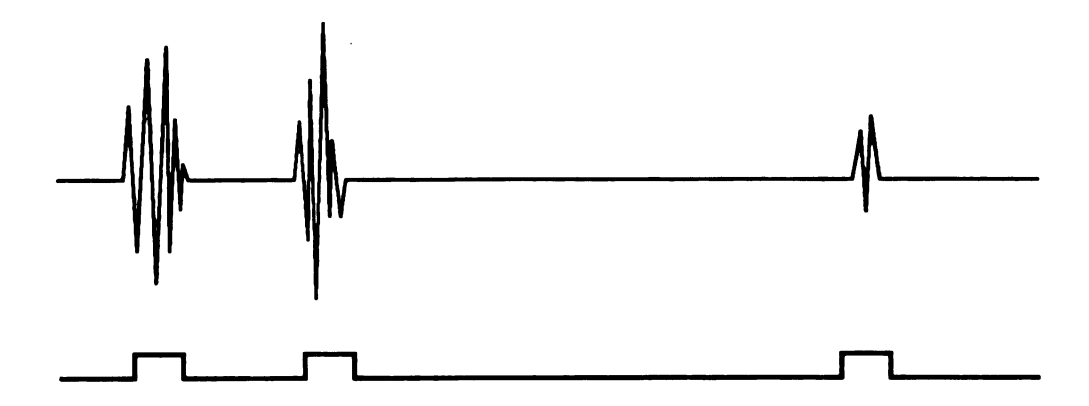


Figure 5.11 The window detector in action.

within a particular time waveform, which all will be of the form depicted in Figure 1.2. Such a waveform is shown in Figure 5.11, along with detected echoes, indicated by the presence of a logic "1" in the lower waveform. This waveform is intended to indicate the windows in time within which the echo signals are supposed to exist, and are used to partition the given total signal into regions of interest within which we will process the signal further. Regions outside of the windows are ignored from further consideration. The algorithm used to produce this result is depicted in Figure 5.12.

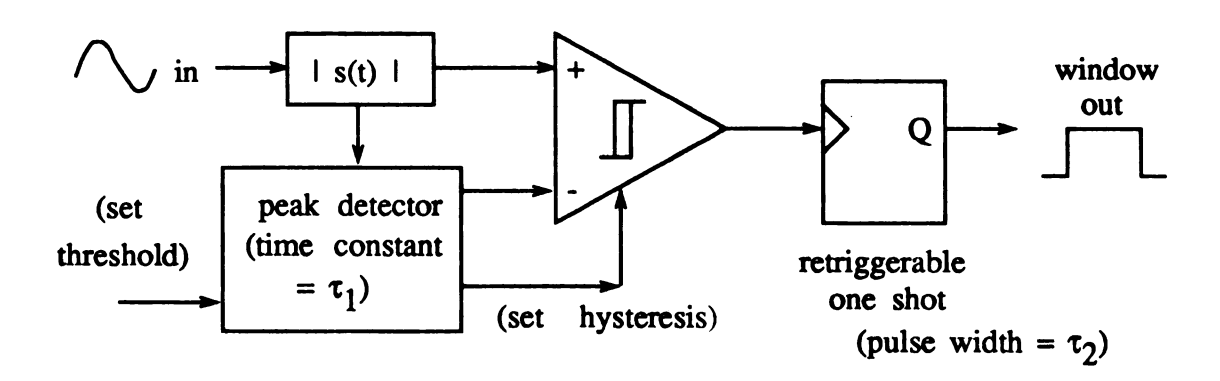


Figure 5.12 The windowing algorithm used to produce Figure 5.11.

This algorithm has been reasonably successful in detecting echo locations within the the time waveforms encountered during the laboratory experiments, but it has been seen to be susceptible to impulse noise. An obvious improvement would be the inclusion of a frequency monitor that only allows windows to occur when the signal is approximately equal to the transducer frequency; this can be done with zero crossing measurements. The latter change would help to eliminate false window generation. A disadvantage of the detector in Figure 5.12 is that pulses that are relatively close together cannot be distinguished. Methods such as deconvolution [10] of the time signal are sometimes effective in this situation, but are rather time consuming and have the tendency to introduce many false echoes into the detected pulse train.

To find the peak value of an echo pulse, we need to simply determine the largest value reached by the signal, within each time window produced by the window detector. This operation is intuitively simple, but is prone to error in cases where the A/D sampling rate is close to the Nyquist limit. Due to this situation, it is rather likely that the samples procured by the A/D unit were not acquired at the time of the exact peak of the echo pulse, instead being of lesser amplitude than the actual signal. This problem naturally is related to the ratio of transducer frequency and sampling rate, i.e.

% oversampling =
$$\frac{f_{\text{sample rate}}}{2 f_{\text{transducer}}}$$
 (5.17)

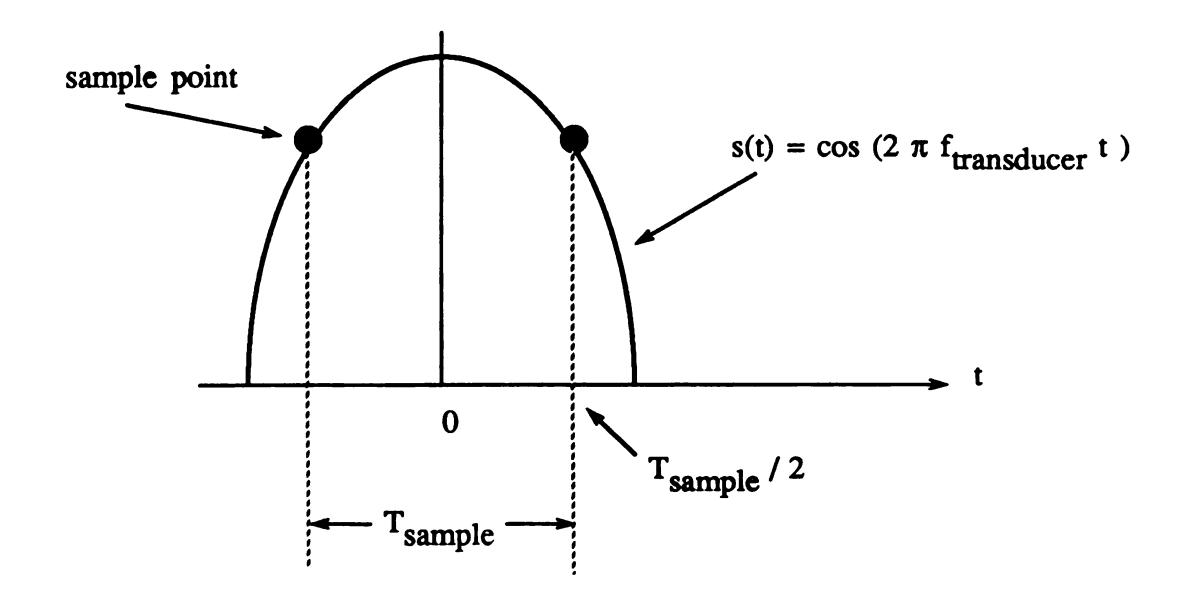


Figure 5.13 The effect of sampling nearly at the Nyquist limit on the accuracy of peak amplitude determination.

and is illustrated in Figure 5.13. The worst error that will occur is also shown in this figure, where two subsequent sample points have straddled the peak of the input sinusoid; the maximum error (neglecting quantization error) is then given by

% maximum amplitude error =
$$\cos \left(\pi \frac{f_{transducer}}{f_{sample rate}} \right) - 1$$
 (5.18)

which for the case of a 2.25 MHz transducer frequency and a 20 MSPS (20 MHz) sampling rate (approximately 8 samples taken per cycle, which is only about four times the Nyquist rate) amounts to about -6.2% error, which is rather large. In addition to this potentially severe inaccuracy in the amplitude is the equally troublesome fact that the time of occurrence of the peak amplitude is uncertain to within one sampling period width, T_{sample}. This fact can be seen by contemplation of Figure 5.13 above, if one allows the location of the depicted sampling points to vary.

A remedy for both of these problems can be found in the use of splines to curve fit a continuous function between subsequent extremum samples, such as those indicated in Figure 5.13, and approximate the actual peak echo amplitude/time by the peak value/time of the spline curve within that particular sampling period. For such an application for a function s(t), we can use cubic spline functions of the form

$$S_{1}(t) = a t^{3} + b t^{2} + c t + d \qquad \text{for } t \in [t_{0}, t_{1}]$$

$$\text{where} \qquad S_{1}(t_{0}) = s(t_{0}) = a t_{0}^{3} + b t_{0}^{2} + c t_{0} + d$$

$$S_{1}(t_{1}) = s(t_{1}) = a t_{1}^{3} + b t_{1}^{2} + c t_{1} + d$$

$$S_{1}(t_{0}) = 0 = 3 a t_{0}^{2} + 2 b t_{0} + c$$

$$S_{1}(t_{0}) = 0 = 6 a t_{0} + 2 b$$

$$(5.19)$$

is used to define S₁ on the indicated interval, and elsewhere

$$S_{i}(t) = S_{i-1}(t) + c_{i} (t - t_{i})^{3} \quad \text{for } t \in [t_{i}, t_{i+1}] \text{ and } i = 2...n$$
where
$$n = \text{the \# of sampling points in the window of interest}$$

$$t_{0} = \text{the starting time of the pulse window}$$

$$t_{i} = \text{the } i\text{-th sample point in the pulse window}$$

$$t_{i-1} = \text{sampling period} = 1 / (f_{\text{sampling rate}})$$

$$t_{n} = \text{the ending time of the pulse window}$$
and
$$c_{i} = \frac{s(t_{i+1}) - S_{i-1}(t_{i+1})}{(t_{i+1} - t_{i+1})^{3}}$$

The intricacies of applying these spline functions are best left to the references; see for example [57] for a good practical discussion of this type of spline interpolation, and a derivation of an expression for the maximum error bound for certain types of sampled

functions. For our purposes, we would use this formulation to generate a set of piecewise continuous functions within each window provided by the echo detector, and investigate these for a maximum, which we would take to be an estimate of the maximum amplitude of the original signal in the window; the time that this estimated amplitude maximum occurs at is also given as well by the spline functions, and the uncertainty error in this time is much less than one sampling period, which is an improvement over the case of such without splines. Splines will give us this amplitude and time in floating point number form which will increase the accuracy of the calculations in Chapter 4 over the use of integer numbers. Note that this will help to reduce somewhat the pessimistic error estimate we found in Equation (5.16) and shown in Figure 5.9, although it will still not completely alleviate the problem of estimating the amplitude of low level echoes. In Figure 5.14 is a plot of the errors in estimation of a sinusoid before and after spline interpolation, for the previous example we used, with $f_{transducer} = 2.25 \text{ MHz}$ and $f_{sample rate} = 20 \text{ MSPS}$; clearly the error is reduced significantly. As a final note on splines, we mention that the piecewise continuous functions S_i(t) can be used to simulate an increased sampling rate on the original function s(t), with very high rates of multiplication possible by simply choosing values of the spline curves between actual samples as virtual sample points. By selecting the virtual samples uniformly in time, higher simulated fixed sampling rates are possible, but only if the Nyquist rate for the original s(t) was exceeded by the actual sample data. Then these estimated/simulated samples will be within a reasonable error band, as can be seen in Figure 5.14. This use of splines is

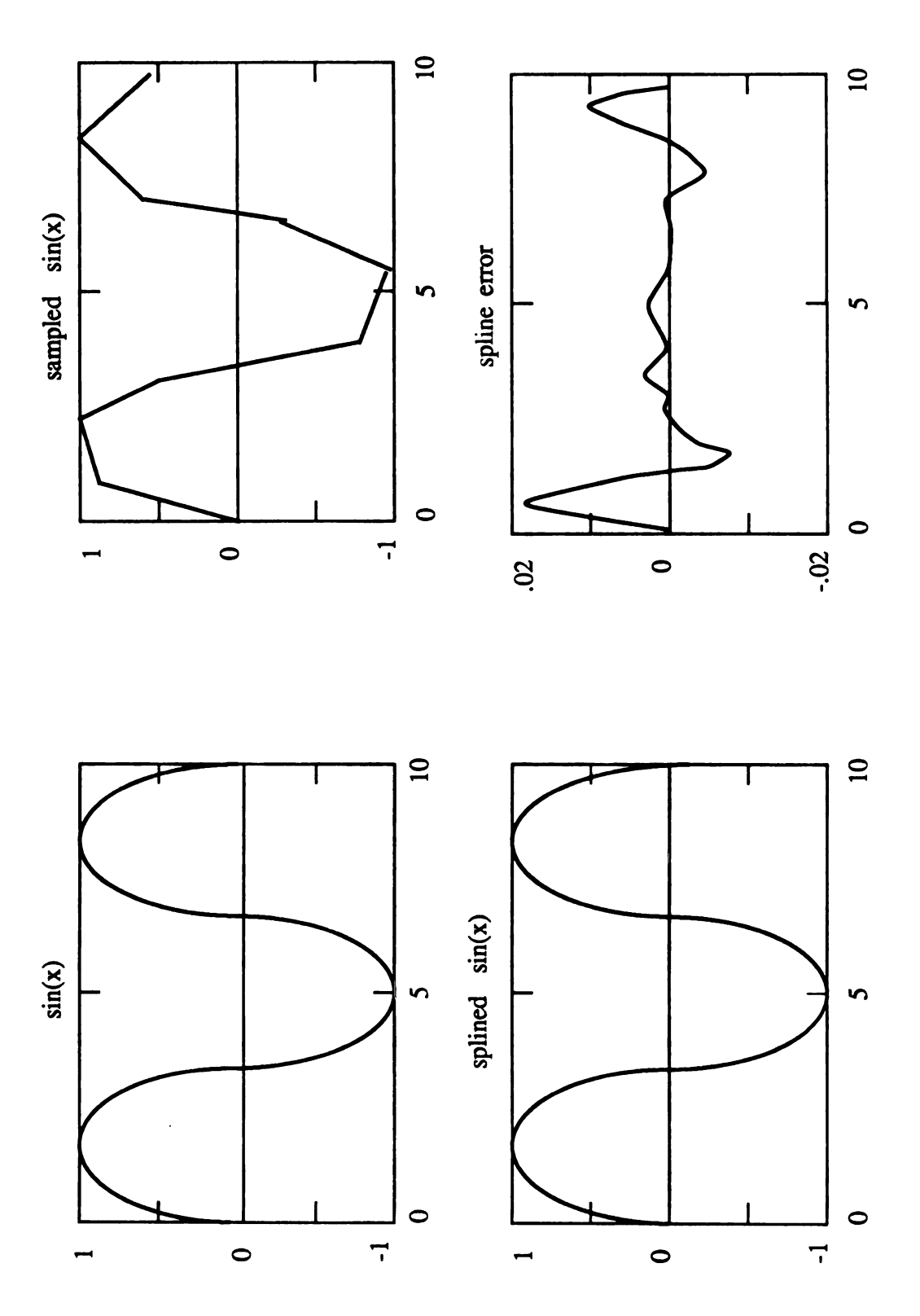


Figure 5.14 The effect of using cubic splines on the peak amplitude approximation.

handy for increasing the resolution of digital signal processing algorithms.

After applying the preprocessing software of Figure 5.10, to each of the time waveforms L, T_{LR} , R, T_{RL} we produce the data set $\{L, T_{LR}, R, T_{RL}\}_{experimental}$, which is the set of (amplitude/time) pairs for all the pulses in the time waveforms. At this point, the data is ready for processing by the algorithm of Figure 4.5, and the discussion in Chapter 4 now applies.

5.7 Sensitivity of Equations (4.20), (4.21), and (4.23) to Errors in the Amplitudes of the Primary Data

In order to investigate the effect of inaccurate values of the measured amplitudes on the calculations of Chapter 4, we will use the definition of sensitivity [58], i.e.

$$S_x^y$$
 = sensitivity of y(x) with respect to x
= fractional change in y(x) for a fractional change in x
= $\frac{\Delta y(x) / y(x)}{\Delta x / x}$
= $\frac{x}{y(x)} \frac{\Delta y(x)}{\Delta x}$ (5.20)

This quantity is a measure of how dependent y(x) is to changes in x. Note that we can interpret the differentials as a (partial) derivative of y with respect to x. If the sensitivity is less than unity (+ or -), then the function y is rather indifferent to changes (or uncertainties) in x; the opposite is true when S_x^y is greater than unity. We will now investigate Equations (4.20), (4.21), and (4.23) in this manner.

For Equation (4.20), we see that the definition of r is symmetrical with regard to both L_i and R_i , so we need only evaluate either sensitivity since $S_L^r = S_R^r$. Using the definition we gave in Equation (5.20), we find that

$$S_L^r = (1 - r^2)/2$$
 (5.21)
= S_R^r

and in a similar manner for T_{LR} and T_{RL}, by symmetry again we find that

$$S_T^r = (r^2 - 1)/2$$
 (5.22)

for both T_{LR} and T_{RL} . By inspection of Equation (2.13a), we see that $r \in [-1, 1]$, so it is apparent that Equations (5.21) and (5.22) are always less than unity in magnitude, which is desirable since this implies that the computation of r by Equation (4.20) is rather insensitive to errors in any of L, R, T_{LR} , or T_{RL} . To study the interaction of errors in these variables requires the use of higher order sensitivities, which we will not pursue here. In Figure 5.15 is plotted the sensitivity relations found in Equations (5.21) and (5.22).

For Equations (4.21a) and (4.21b), we need only investigate the sensitivities of either, since they are symmetrical and the answers will be identical again. Applying Equation (5.20) to Equation (4.21a), we find that the sensitivity of k to r_{i+1} is given

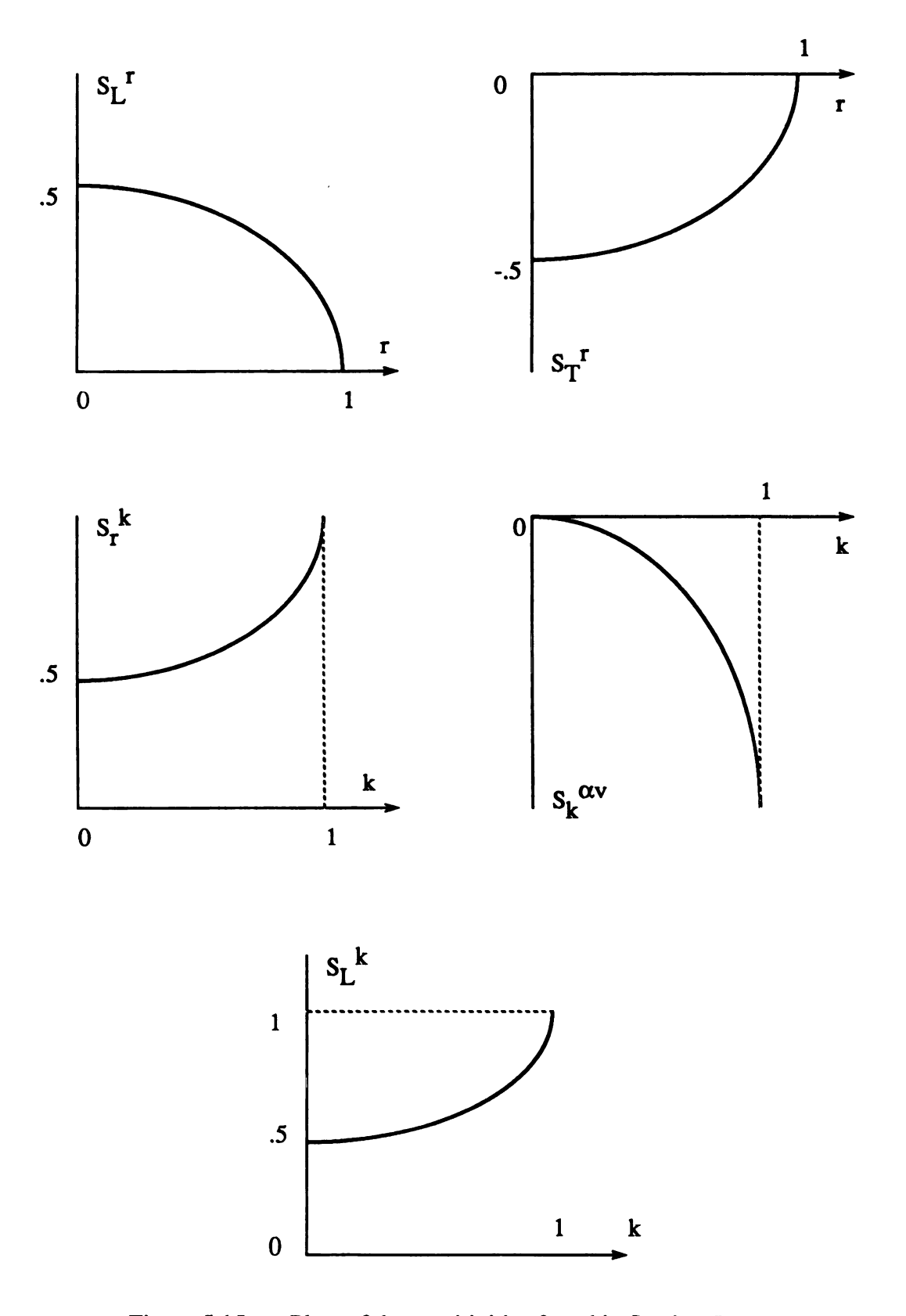


Figure 5.15. Plots of the sensitivities found in Section 5.7.

$$S_{r}^{k} = -1/2$$
 (5.23)

$$= S_{L_{i}}^{k} \qquad \text{(by symmetry with } r_{i+1}) \tag{5.24}$$

So we have in these cases low error sensitivity as well. Also

$$S_{L_{i+1}}^{k} = 1/2$$
 (5.25)

which is also pleasant. Finally, we have that

$$S_{r_{i}}^{k} = \frac{1}{2} + \frac{r_{i}^{2}}{(1 - r_{i}^{2})}$$
 (5.26)

which is not good, since k_i is very sensitive to r_i if $|r_i|$ is close to unity. Note that Equation (5.26) is also plotted in Figure 5.15.

For Equation (4.23), which is the computation to find αv given the values of k and the layer propagation times T, we determine that

$$S_k^{\alpha v} = [\ln k]^{-1} \tag{5.27}$$

and that

$$S_t^{\alpha V} = -1 \tag{5.28}$$

For Equation (5.27), the plot is also shown in Figure 5.15, and we see that the

calculation for αv is very sensitive to k when k is close to unity (by inspection of Equation(3.2), we see that $k \in [0, 1]$ since α , v, and t are always positive). The computation for k_i is not made very inaccurate by errors in t_i because this time is

usually very certain since the A/D converter is almost always driven by a crystal-controlled, high-stability oscillator for a sample frequency clock, and the frequency error of this type of oscillator is quite small, on the order of 100 parts-per-million or less.

To conclude this section, we restate that the values of r are relatively insensitive to amplitude errors, but when the magnitude of r is close to unity, the computation of k can suffer if r is not accurate. This situation is not often likely to occur, since deeper layers will be obscured by such a large value of reflection coefficient. The calculation of k is rather insensitive to errors in the amplitudes, and we can say that

$$S_{L_i}^k = S_{L_i}^r S_r^k$$

$$= (1 + r^2)/2 \qquad \text{(similarly for } R_i\text{)} \qquad (5.29)$$

(by use of the chaining property of sensitivities [57]) is always less than unity, so Equation (5.29) implies that k is insensitive to errors in the echo amplitudes, even though it is not to errors in r. Note that Equation (5.29) is plotted in Figure 5.15 also.

Finally, we can find that

$$S_L^{\alpha v} = S_k^{\alpha v} S_L^k$$

$$= (1 + r^2) / (2 \ln k) \tag{5.30}$$

which still looks like Equation (5.27) in general, so we cannot say that αv is insensitive to errors in the amplitude when k is close to unity. Fortunately, when k is near unity, the attenuation is small, so we tend to get a larger signal from that layer, which can help to alleviate this problem. For k small (close to 0), the attenuation is large, and the calculation of k is rather insensitive to errors in the echo amplitudes.

5.8 Additional System Requirements

As a final note to this chapter on system considerations, we must mention the additional hardware requirements that can be expected for an acoustic measurement system of the type discussed in this thesis. We have mentioned in the previous sections that a microcomputer (or better) is required to perform the complicated calculations necessary to implement the algorithm of Figure 4.5 and to incorporate the software outlined in this chapter. The operating speed of the computer selected will directly influence the time required for an image to be reconstructed, and this can be considerable for even a one-dimensional object problem if the number of layers is large (and there are many multiple reflections to contend with). This will tend to tip the trade-off of speed versus cost in the favor of higher hardware expense in many cases. The storage requirements, as mentioned in the previous section can be excessive, running into the tens of megabytes, for a multi-dimensional image if the entire time waveforms are saved prior to processing; this however might be the course of choice for a fast imaging system for use in e.g. clinical diagnostics. In slower

systems where processing time is not as critical, preprocessing and preconditioning of the data could be done, e.g. saving only the windowed signal fragments on disk, but naturally this will slow the system operation down by increasing the time spent between measurement cycles. This type of trade-off must be decided in light of the particular application for which the system is finally destined, weighing the target cost appropriately.

In order to effectively display attenuation-type images, some form of high resolution graphics display is desirable, either in gray scale or color. For a gray scale type of display, usually 8 bits of data per pixel is adequate, and provides near photographic quality to the average human eye, if the number of pixels per line and the number of lines per frame are sufficiently high. A color display must have a wide palette of colors available, and each color should have a large luminance range (e.g. 8 bits per color in an RGB system, meaning 24 bits per pixel). Because of the much larger memory requirements for a color system, along with the higher quality monitor (CRT) needed, the cost is much higher than the gray scale display, presently at least three times the expenditure for gray scale, and this sort of cost differential is likely to remain extant because of the added complexity of a color system. Again, the benefits and disadvantages of each display type must be considered against cost and the intended system application.

From this discussion, however, we can see that in the future the cost and ability of the hardware used in ultrasound systems is very likely to improve, and will be commensurate with like improvements in semiconductor and computer technology and manufacturing. Perhaps in the near future we will see such systems in greater proliferation than at present; the low cost and inherent safety of acoustic systems can only become more attractive to a wider variety of users, but only if the imaging quality can be equally improved.

5.9 Conclusions

In this chapter, we have considered the more esoteric needs of attenuation-type acoustic imaging systems, and have elaborated on some of the problems that face an amplitude-based measurement scheme. In the author's opinion, all of the difficulties we have covered--multiple reflections, hardware problems, operation complexity, speed, imaging quality, sophistication of processing, etc.--can all be overcome eventually if not already so, but the most severe problem is that of angular/diffuse scattering into angles outside of the receiving domain. This is really the only difference that ultimately separates ultrasound techniques from X-ray methods, for example. In Chapter 7, brief mention is made of future possibilities research in this problem; in the next chapter, we present some experimental findings of the method of attenuation-velocity product imaging.

CHAPTER VI

SIMULATIONS AND EXPERIMENTAL RESULTS

In the preceding chapters, we have developed and discussed a means for the determination of the quantity av for a medium, particularly under the conditions of a test object composed of many layers of differing media. Generally, we have constrained our considerations to a strictly one-dimensional situation; for consistency, we continue this restriction into this chapter; in Chapter 7, we discuss possible extensions to these results into higher dimensions, but here we attempt to investigate our work in Chapters 4 and 5 in a more pragmatic light.

6.1 Simulations and Results

In order to develop and investigate the results of Chapter 4, a variety of computer simulations were performed using programs developed by the author. These and the results will now be discussed.

The first requirement of the work was to develop a means for understanding the

action of waves within a layered sample, with the added need of creating simulated experimental data with which to test any algorithms developed for stability and accuracy. To meet this, a stand alone program, TWOSIDE, was written in the BASIC language and compiled for speedier use with a commercial BASIC compiler. The function of this program, which is listed in full in Appendix A, is to simulate the complete behavior of a pair of left and right input impulses to a one-dimensional userspecified object. All reflections and transmissions at the internal boundaries are followed, and any output signals are recorded and sorted in order of time of occurrence. These lists of output impulses then form a set $\{L, T_{LR}, R, T_{RL}\}$ of echoes that can include multiple output reflections and transmissions, and this set of signals can be used for testing the algorithm of Figure 4.5; in fact, the use of TWOSIDE was instrumental in the development of this method. The detailed operation of TWOSIDE was outlined in the discussion given in Section 4.7.2, where we considered the simulation of a set {N, k, r, t}_{trial} produced during the implementation of Figure 4.5; the problem is identical, and will not be repeated here.

In order to demonstrate the overall av method, we will first create a simple example using TWOSIDE. The test object we will consider is shown in Figure 6.1.

Note that it is composed of four layers, with three boundaries separating the different materials, each having the values of r, v, t, and a indicated. When TWOSIDE is run, the program first requests these values, inputted from left to right which is our convention. The program then requests a value for the smallest amplitude desired in

the simulation; as we mentioned earlier, this is necessary to terminate the simulation. The program then proceeds to simulate the left and right inputs, and eventually produces the data shown in Table 6.1; the primary signals have been indicated for the convenience of the reader. We see that is a multiple reflection in each of L and R. This set of data was then used as input information to the program ALPHA-V, which is listed in partial form in Appendix B. The results of this are depicted in Figure 6.2; we see that the algorithm has correctly selected the proper primary signals, and has found the original values of {N, k, r, t} of Figure 6.1, but not before it has tried N=5 and N=4 once, both of which involve impossible conditions for Equation (4.11), meaning that those trial choices of the primary data are self-inconsistent and therefore incorrect.

0.	•	$r_3 = r_3$ 0.4 0.	6
layer 0	layer 1 k ₁ =.90483	layer 2 k ₂ =.74082	layer 3 k ₃ =1
t ₀ =1	t ₁ =1	t ₂ =1	t ₃ =1

Figure 6.1 The example object to be considered, with N=4.

#	amplitude	time	path through boundaries
Lsimula	ited:		
L1	.300	2	0, 1, 0
L2	29801	4	0, 1, 2, 1, 0
	02928	6	0, 1, 2, 1, 2, 1, 0
L3	.20608	8	0, 1, 2, 3, 2, 1, 0
TLRsim	ulated:		
TLR	.83656	4	0, 1, 2, 3, 4
	.08219	6	0, 1, 2, 1, 2, 3, 4
	.11018	6	0, 1, 2, 3, 2, 3, 4
Rsimula	ited:		
R1	6	2	4, 3, 4
R2	.1404958	4	4, 3, 2, 3, 4
	.0185953	6	4, 3, 2, 3, 2, 3, 4
R3	0724677	6	4, 3, 2, 1, 2, 3, 4
TRLsim	ulated:		
TRL	.2627654	4	4, 3, 2, 1, 0
	.0346101	6	4, 3, 2, 3, 2, 1, 0

Table 6.1 The results of program TWOSIDE on the example of Figure 6.1.

Checking: N=5

No solution possible (signs not opposite in L(3) and R(2)).

Checking: N=4

No solution possible (signs not opposite in L(3) and R(1)).

Solution!! for:

N=4

L(1) = .3	R(1) =0724677
L(2) =2980181	R(2) = .1404958
L(3) = .2060803	R(3) =6000

TLR = .8365595TRL = .2627654

$$K(0) = 1$$
 $T(0) = 1$
 $K(1) = .904$ $R(1) = .29995$ $T(1) = 1$
 $K(2) = .7408$ $R(2) = -.410002$ $T(2) = 1$
 $K(3) = 1$ $R(3) = .6$ $T(3) = 1$

Simulating...

Checking:

Simulation = experimental!!

***** DONE *****

Figure 6.2 The results of program ALPHA-V using the data shown in Table 6.1.

6.2 Experimental Results

The attenuation-velocity method has also been tried in the laboratory, with the setup as diagrammed in Figure 6.3. To conduct the measurements, a PC-based A/D converter board (the Markenrich Corp. WAAGII) was used, providing a pair of simultaneous channels sampling at 20 MSPS with 8 bit resolution; up to 16k (16384) points may captured in each channel, providing about 820 microseconds of captured time in each single shot measurement. This unit is more than adequate for the system proposed in Chapter 5. For the receiver/transmitter function, a pair of Panametrics, Inc. 5050PR model pulser units were utilized, each providing for separate transducer matching via the front-panel controls as previously discussed in Sections 5.3 and 5.4, by means of the damping and receiver gain adjustments. A pair of Panametrics 2.25 MHz resonant frequency piezoelectric transducers, 0.5" diameter, were used to provide both the acoustic output waves and act as mechanical signal receivers; the pair selected was not initially well matched, but chosen as the best of the several combinations available in the lab, providing an opportunity to investigate the effect of transducer pair matching on the performance of the amplitude measurement system.

To facilitate the experiment, a test fixture was constructed from 1 cm plexiglass sheet, which held the transducers firmly in position to ensure stability of their alignment. The center of the test fixture was outfitted with a manually rotatable platform to allow for fine angular adjustment of the samples to be investigated. The entire test fixture, rotating platform, test sample, and pair of transducers were immersed in a

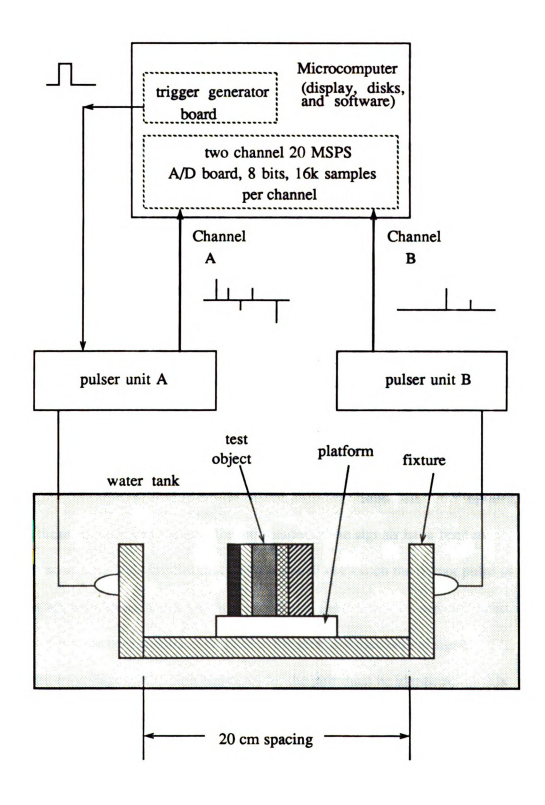


Figure 6.3 The layout of the experimental system.

plexiglass tank filled with water, which acted as a coupling medium for the acoustic waves.

The software described in Chapter 5 (i.e. the preprocessing of Figure 5.10) was implemented, and is included in Appendix C as program TWOCHANNEL. This was also written in BASIC and compiled for speed, and the execution performance is adequate for the types of measurements used in the experiments described here; a more streamlined version would be necessary for use in rotational-scanning imaging, for example.

The experimental procedure involves two main portions: (1) alignment and calibration of the transducers and test fixture, and (2) alignment and measurement of the sample object. The derivation leading up to Equations (4.20) and (4.21) show the immunity of these formulations to the difference between Ainput/left and Ainput/right; however, these equations expect that the amplitudes of the signals have been measured with accuracy. This implies that while we need not match the output pulse of the two pulser units/transducers, we must expect that the transducers are calibrated to produce the same peak electrical amplitude for identical mechanical signals--i.e., the pressure-to-voltage conversion constants for the pair must be identical. This is another shortcoming of using more than a single transducer to probe a sample, for if this calibration is not performed correctly, the numerical values of r and k will be in error, as we learned in Section 5.7. In order to perform this calibration step, a bubble of air trapped behind a stretched sheet of thin plastic film was used to approximate a

perfect reflector (at 2.25 MHz, the value of Z_{characteristic} for air is .0003 times that of water, which means that the interface between the two has a reflection coefficient close to -1, about -0.9995), and the following steps were taken to ensure calibration:

- (1) One transducer (e.g. left) was selected, and the output was adjusted to provide a moderate amplitude, low ringing signal, when the output of the pulser unit/transducer was viewed on an oscilloscope.

 To see the output signal, the planar air bubble reflector was aligned in the outgoing wave path so as to return this signal entirely to the transmitter. The amplitude of this echo was noted.
- (2) The air bubble reflector was removed, allowing the beam to pass uninhibited to encounter the far transducer (e.g. right). Using the oscilloscope to monitor the output of that transducer/pulser, the damping and receiver gain were adjusted to provide an identical signal to the one observed in (1).
- (3) The steps of (1) and (2) were repeated in the reverse order (e.g. first right, then left) to ensure accurate calibration.

It should be noted that the above procedure cannot guarantee that the transducers will remain calibrated over the long term, and therefore this procedure should be repeated often. We see then that this is a fundamental problem with all methods that employ multiple transducers, including arrays; unfortunately, it appears that unless the numerical values of the layer material constants are not of interest, the use of

an array of transducers will only aggravate this accuracy problem. The author has seen no mention of this in the literature involving array measurements, and thus the question is as yet left unanswered.

Once the setup of the test fixture has been performed, we need to concern ourselves with the test object. As we have amply mentioned, the work performed here is limited to one-dimensional structures, and the objects investigated conform to that requirement as well as the others listed in Section 4.3. For the test objects, slabs of various materials and thicknesses were used, allowing easy construction and alignment. The materials used, along with their relevant physical properties, are listed in Table 6.2. In order to align the objects so that their surfaces were normal to the acoustic beam, use of an oscilloscope was made to monitor the echoes returned from the front faces, and the orientation of the object was adjusted to maximize the amplitude of the echoes from these faces. This of course does not ensure alignment, since the beam may not always constrain itself to the line of sight between the transducers; in fact, deviation in the transmission signal intensity was noted if the sending transducer was axially rotated in place, which means that the beam is not symmetric about the line of sight. No resolution of this problem will be made, since there is little one can do to cause the acoustic beam to behave in a more controlled manner; however, the problem cannot be ignored and is certainly a major source of experimental error.

To illustrate the measurement of a simple object, we will consider the setup of Figure 6.4, where we attempt to interrogate a single layer of plexiglass. The relevant

Material	Zcharacteristic	Velocity	Reflection coefficient	***	αv
)	(m sec ⁻¹)	(w.r.t water)	(nepers m ⁻¹)	(nepers sec ⁻¹)
water	1.48	1480	ı	6950.	87.32
air	.0004	331	9995	>230	>76,130
plexiglass	3.20	2680	368	51.81	138,850.80
aluminum	18.0	6400	.848	.4663	2,984.32
** brass	28.0	3500	9668.	ŀ	ŀ
steel**	39.0	2050	.9269	1	ı
copper **	44.5	3700	.9356	ï	ì
liver	1.65	1549	.0540	24.35	37,718.2

*from Table 3.1, by α (nepers/m) = ln [10 $^{\wedge}$ (α dB/cm)(100 cm/m)(2.25 MHz / 1.00 MHz)/20] (see [2]). This extrapolates the data at 1 MHz to 2.25 MHz, but cannot be considered exact.

Table 6.2 Physical constants for some materials, at 2.25 MHz.

^{**}from [59], Appendix I.

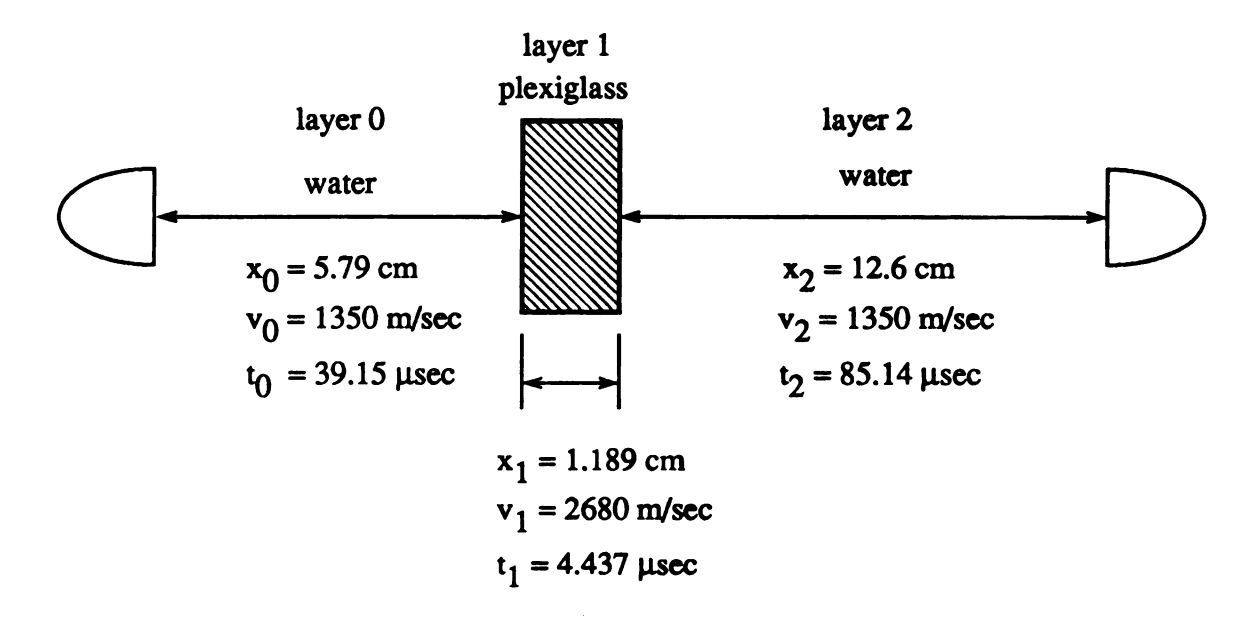
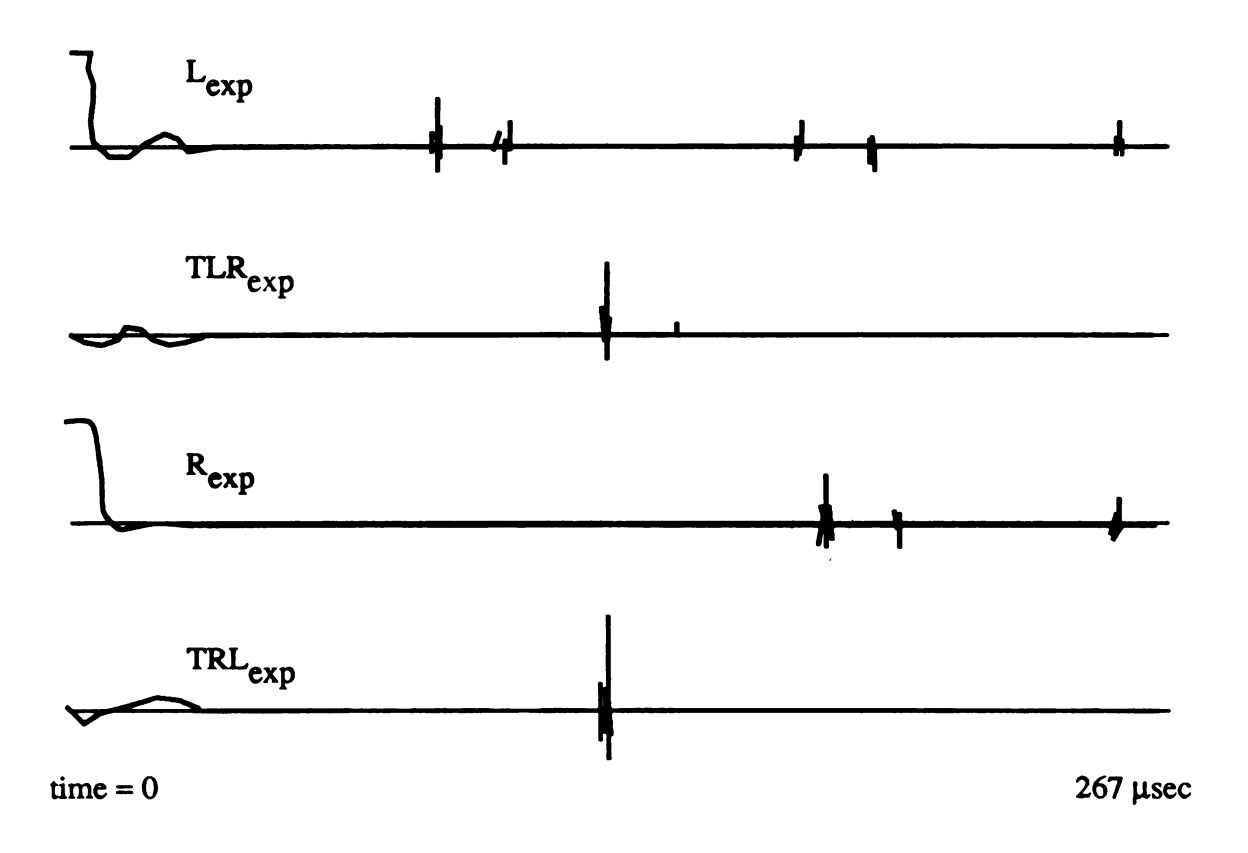


Figure 6.4 The example setup to illustrate the experimental procedure.

dimensions and ideal physical quantities are indicated. This sample was interrogated in the manner we have outlined, producing both the graphic results and the numerical values of the set {L, T_{LR}, R, T_{RL}}_{experimental}, shown in Figure 6.5, inspection of which shows the presence of multiple reflections in all these time signals. The primary echoes are also identified in Figure 6.5b, and we can use these data to compute the quantities of interest:

By Equation (4.20), we can solve for the values of r_1 and r_2 , i.e.

$$|r_1| = \sqrt{\frac{(75)(17)}{(75)(17)+(90)(94)}}$$



Lexp) :		Rexp	•	
L1 L2	75 -21 15 -24	78.9E-06 sec 87.3E-06 1.578E-04 2.566E-04	R2 R1	56 -17 14	1.6915E-04 sec 1.7755E-04 .0002562
TLR	exp:		TRLe	exp:	
TLR	90	128.3E-06 sec	TRL	94	1.2835E-04 sec

Figure 6.5 (a) The experimental time signals, and (b) the set {L, T_{LR}, R, T_{RL}}_{experimental} for Figure 6.4.

$$|r_1| = .3620$$

and

$$|r_2| = \sqrt{\frac{(21)(56)}{(21)(56) + (90)(94)}}$$

= .3490

Also, using Equation (4.21a), we find that

$$k_1 = \sqrt{\frac{21}{75}} \frac{.3620}{.3490} \frac{1}{(1 - (.3620)^2)}$$

$$= .5780$$

By means of Figure 5.6b and Equations (4.1) and (4.23), we get that, $\frac{17 \cdot 1349}{16 \cdot 936 \cdot 11 - (9.86)}$

$$\alpha_{1}v_{1} = -\left[\frac{\text{time}(L1) - \text{time}(L2)}{2}\right]^{-1} \ln(k1)$$

$$= -\left[\frac{78.9 \text{ } \mu \text{sec} - 87.3 \text{ } \mu \text{sec}}{2}\right]^{-1} \ln(.5780)$$

$$= 123,421 \text{ nepers/sec}$$

$$40 \quad \text{(1)} \quad \text{(2)} \quad \text{(2)} \quad \text{(3)} \quad \text{(4)} \quad \text{(4)} \quad \text{(5)} \quad \text{(4)} \quad \text{(4)} \quad \text{(5)} \quad \text{(4)} \quad \text{(5)} \quad \text{(4)} \quad \text{(5)} \quad \text{(5)} \quad \text{(6)} \quad$$

Additionally, from the experimental data, and knowing x_1 in Figure 6.4, we can

determine that

113 X10 40 COK

Finally, by using the above two results above, we can find

$$\alpha_1 = 46.058$$
 nepers/meter

The above information is summarized in Table 6.3 below, along with error comparison to the reference information contained in Table 6.2. The errors indicated are reasonable, in light of the difficulty of accurately calibrating the fixture and transducers and ensuring that the sample was normal to the acoustic beam. The results of this measurement serve to point out the inherent tendency of such amplitude-based techniques to be numerically imprecise, due of course to all of the problems we considered in Chapter 5, although for some applications the results would be adequate.

Quantity	experimental value	actual value	% error (in %)
Ir ₁ I	.3620	.3680	1.63 %
Ir ₂ I	.3490	.3680	5.16 %
k	.5780	.5400	7.02 %
αν (nepers/sec)	123,421	138,850	11.1 %
v (m/sec)	2679.74	2680	0.037 %
α (nepers/m)	46.058	51.81	11.07 %

Table 6.3 Summary of the experimental results for the single layer plexiglass sample.

To further illustrate the method, we will consider the similar problem of determining the same quantities for a sample of aluminum. This is actually a more difficult material to probe acoustically since it has an extremely large reflection coefficient with respect to water, about 0.848; this causes the amplitude of deeper boundaries to be very diminished, adding to the quantization inaccuracy in the manner of Equation (5.16). The experimental configuration and dimensions are shown in Figure 6.6, and the data acquired in a manner parallel to the previous discussion is shown in Figure 6.7 and Table 6.4. It is apparent that the errors are much greater in this example, and this can be attributed to the difficulty of accurately measuring very small amplitudes, such as L2 and R1; also applicable is the error given by Equation (5.26). Again, it is interesting to note that while the absolute accuracy appears to suffer, the general trend of the quantities is still to be roughly in the range of the correct answer, which may be wholly acceptable for pictorial imaging.

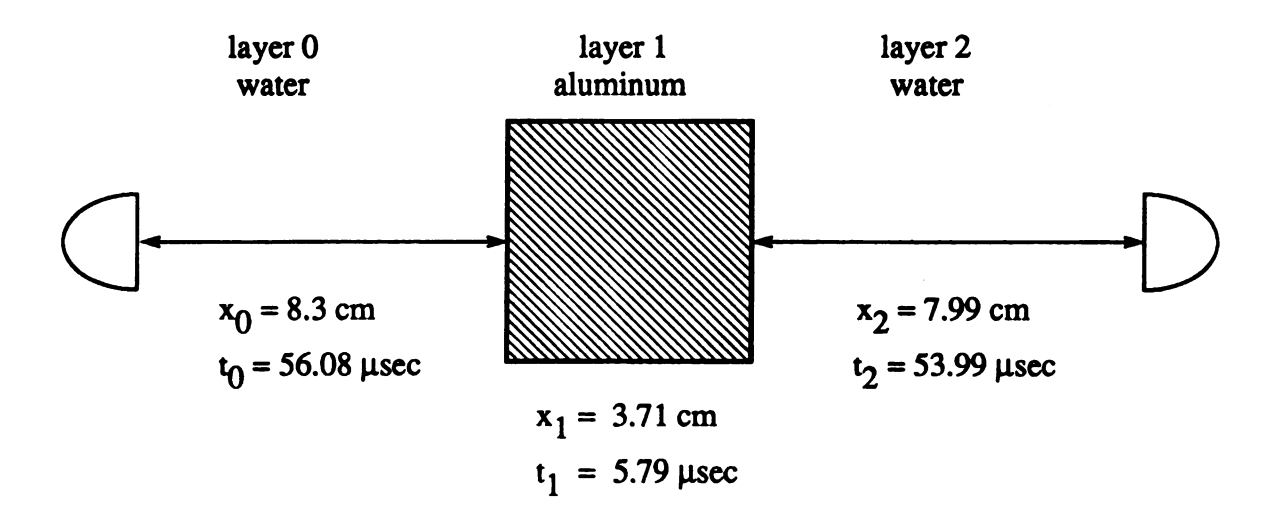


Figure 6.6 The experimental setup for the aluminum sample.

Lexp:			Rexp:		
L1	114	117.16E-06 sec	R2	85	110.98E-06 sec
L2	-16	133.74E-06	R1 -	20	120.56E-06
	7	140.71E-06		4	135.14E-06
TLRe	xp:		TRLexp	:	
TLR	24	121.97E-06 sec	TRL	28	122.15E-06 sec

Figure 6.7 The experimental data for the aluminum sample.

QV= [1] (A)

Quantity	Experimental value	Actual value	% error
Ir ₁ I	.878	.848	3.538 %
Ir ₂ I	.817	.848	3.656 %
k	.972	.983	1.12 %
αν (nepers/sec)	4880.67 a445	2984.32	63.54 %
v (meters/sec)	6238.4	6400	2.52 %
α (nepers/m)	.7820	.4663	67.8 %

Table 6.4 The experimental results for the aluminum sample.

0.99409669

In order to illustrate the additional complexity of imaging an object with a larger number of layers, we will use the case of Figure 6.8, which is comprised of two identical layers of plexiglass separated by a layer of water. In this case, all the values of the reflection coefficients should be the same, and the middle layer of water presents the opportunity to investigate the end result of interrogating low loss regions. Figure 6.9a and b depict the time signals and data, respectively, acquired for this setting. The calculations proceed in the manner of the first example, using Equations (4.20), (4.21), and (4.23). The results of this are summarized in Table 6.5; interesting to observe is that the error for most of the quantities is comparable to that of the prior examples, with the exception of the attenuation value for the middle water layer, which is rather erroneous. However, we again note that the trend of the magnitude of all these quantities is close to that of the actual values.

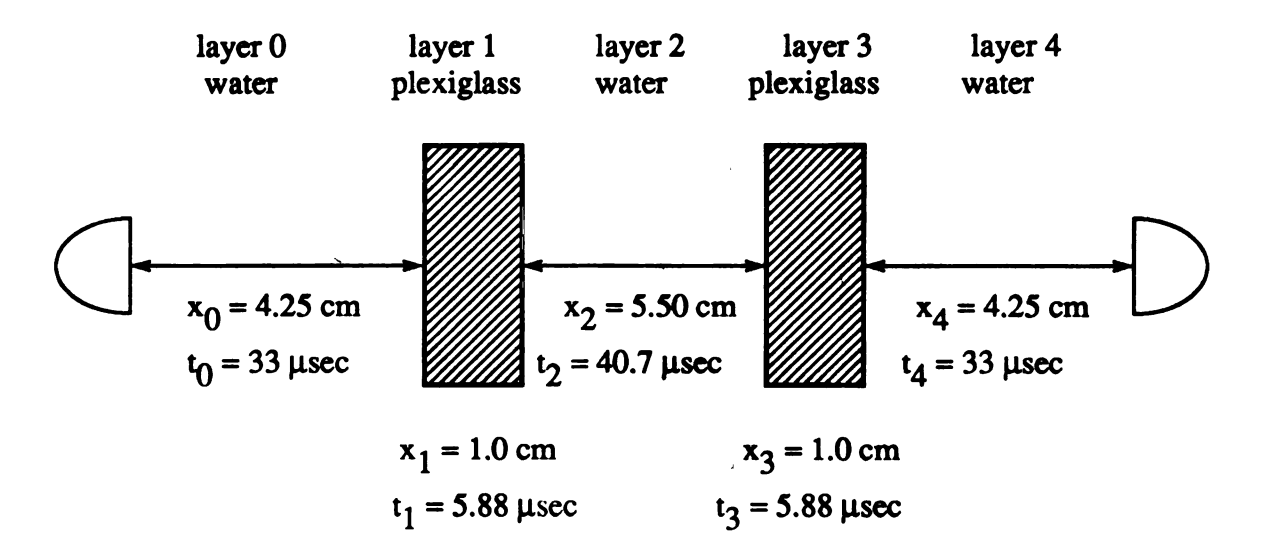
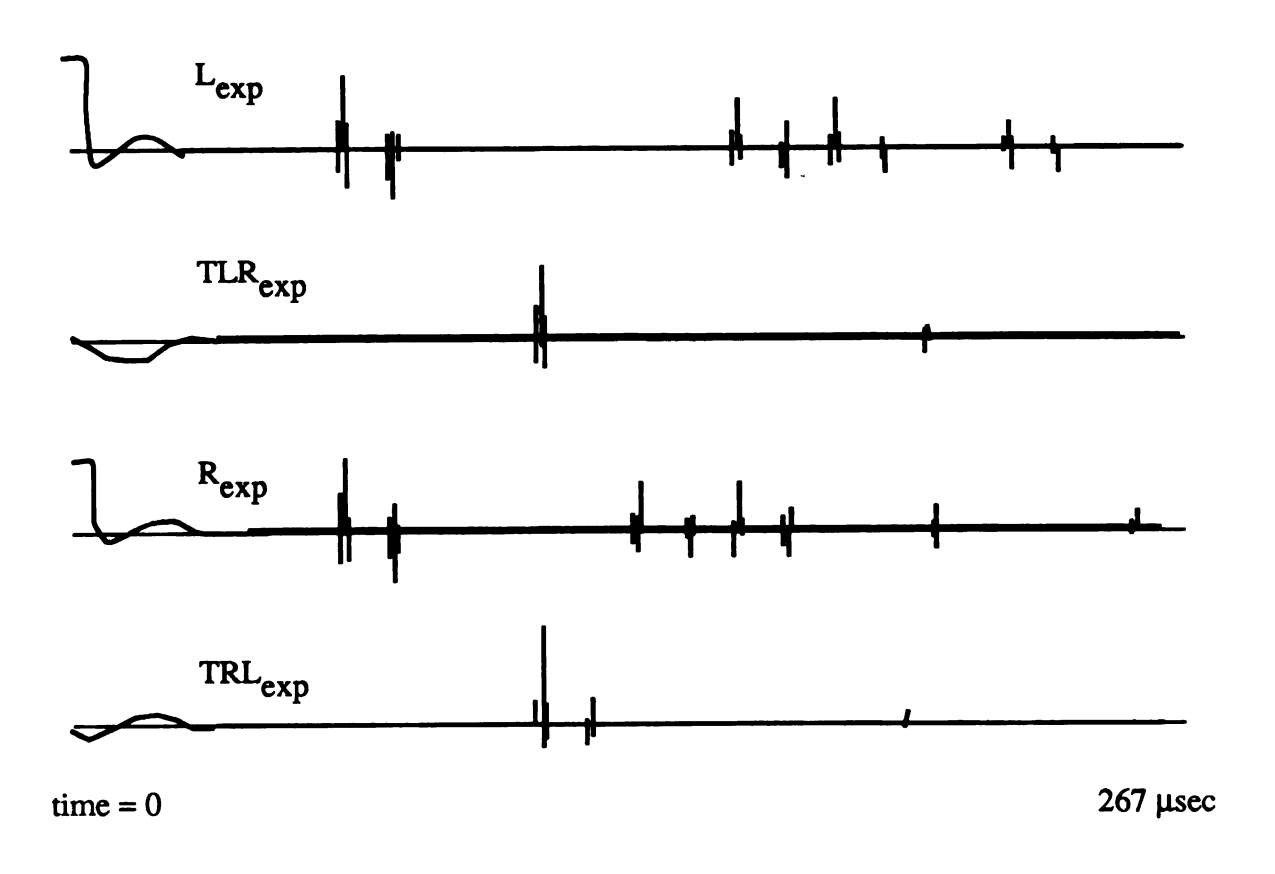


Figure 6.8 The configuration for the five layer object.



Lexp:			Rexp:			
L1	119	6.455E-05 sec	R4	106	6.375E-05 sec	
L2	-65	.0000732	R3	-41	7.245E-05	
	48	.0001311		-14	.0001269	
	32	1.3955E-04		9	1.3615E-04	
L3	40	.0001484	R2	18	.0001476	
L4	-9	1.5715E-04	R1	-4	.0001539	
	11	.0001972		-16	1.9535E-04	
	9	.0002061		10	.0002224	
	14	.000215				
TLRex	xp:		TRLex	кр:		
TLR	46 12	.0001095 sec 1.7585E-06	TRL	109 12	.0001113 sec 1.1995E-04	

Figure 6.9 (a) The experimental time signals and (b) the echo data for the five layer object of Figure 6.8.

Quantity	Experimental value	Actual value	% error
lr ₁	.2945	.368	18.66 %
lr ₂ l	.4350	.368	20.17 %
lr ₃ l	.4965	.368	37.15 %
Ir ₄ I	.3998	.368	10.4 %
\mathbf{k}_1	.6363	.596	6.762 %
k ₂	.8155	.997	18.21 %
k ₃	.6090	.596	2.181 %
$\alpha_1 v_1$ (nepers/sec)	104,517.8	138,850.8	24.73 %
$\alpha_2 v_2$ (nepers/sec)	5424	87.32	6,116 %
α ₃ v ₃ (nepers/sec)	114,008.5	138,850.8	17.89 %
v ₁ (m/sec)	2312	2680	13.75 %
v ₂ (m/sec)	1396.3	1480	5.68 %
v ₃ (m/sec)	2298.9	2680	14.22 %
α_1 (nepers/m)	45.207	51.81	12.70 %
α_2 (nepers/m)	3.885	.0569	26,911 %
α_3 (nepers/m)	49.594	51.81	4.26 %

Table 6.5 Summary of the results for the five layer object.

As a final example of the possibilities in choosing materials with which to experiment, a section of common beef liver was suspended in the fixture/tank, thus forming a three layer object, as shown in Figure 6.10. The sample was interrogated as before, with the experimental data resulting shown in Table 6.6a; in Table 6.6b the computations and corresponding errors are shown as before. The reflection coefficient of the liver-water interface is extremely small, about 0.051 in magnitude, and this accounts for the difficulty in measuring the echo amplitudes from these boundaries. An additional difficulty is manifested in the surface of the liver which is somewhat rough, as is characteristic of biological samples; this surface acts as a diffuse scattering source and this action too adds to the error present in the data. Nevertheless, the percentages of error in this measurement are not much different than for the previous experiments.

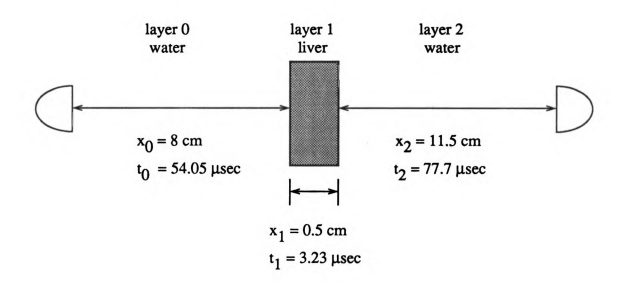


Figure 6.10 The experimental setup for the liver sample.

Lexp:				Rexp):	
L1	20	115.35E-06	sec	R1	22	165.3E-06 sec
L2	-9	121.4E-06		R2	-8	171.8E-06

TLRexp: TRLexp:

TLR 74 138.75 E-06 sec TRL 126 130.55E-06 sec

Quantity	Experimental value	Actual value	Percentage error
lr ₁ I	.130	.0540	140.7 %
Ir ₂ I	.143	.0540	164.8 %
k ₁	.6520	.7839	16.83 %
$\alpha_1 v_1$ (nepers/sec)	66,829.8	37,718.2	77.18 %
v ₁ (m/sec)	1607.3	1549	3.764 %
α_1 (nepers/m)	41.58	24.35	70.76 %

Table 6.6 (a) The experimental data, and (b) the computed results for the liver sample.

CHAPTER VII

RECOMMENDATIONS AND CONCLUSIONS

In the preceding chapters, we have, from basic principles, built up to a detailed understanding of the possibilities and problems that confront attenuation imaging, both at present and in the future. Such an acoustic measurement technique must rely on amplitude processing of the experimental data acquired during a measurement situation, and this aggravates certain deficiencies in ultrasonic techniques that are currently unsolved, such as angular (non-collinear with the direction of propagation) scattering. In fact, based on the reported work in the literature and the results reported here in this thesis, the author is of the opinion that almost all of the discussed difficulties may in fact be surmounted eventually, at least with sufficiency to permit useful imaging in many circumstances, with the possible exception of the aforementioned angular scattering problem, which appears to be the most severe limitation. It appears that this difficulty may also yield to a scanning/array technique, such as that pursued by Clement et al. in [56], which shows very promising results. It is in this spirit that the recommendations of Section 7.1 are made, that future work should center on investigation of higher dimensional models, interrogated by means of a scanned set of transducers.

7.1 Recommendations For Future Investigation

The work reported in this thesis has centered on a one-dimensional model for the test object, which is not usually realistic except in certain cases, such as when imaging composite materials. We now briefly consider the possibility of extension to other cases of interest.

7.1.1 Extension to Higher Dimensional Objects

In order to reconstruct the internal makeup of a test object with spatial dimensions higher than one, the space curves (or surfaces) that define the boundaries of the different regions must be specified. In practice, due to the discrete number of scanning angles/positions available when performing the requisite measurements, it will not be feasible to exactly measure the shape of these boundaries, so an approximation to these shapes must be made, perhaps by means of spline fitting of either curves or surfaces to the data. This method will be satisfactory only if sufficient data points are available to accurately determine the first two spatial derivatives of the boundary, in the case of cubic splines, implying that a rather large number of separate measurements are necessary, as mentioned before in Chapter 5. However, the main difficulty with this concept is that it is difficult to decide which data points belong to which boundary, since the number of regions can change with measurement position and boundaries may even intersect. Once the boundaries are known, then steps can be taken to correct for the effect of angular scattering on the calculation of the reflection coefficients, as mentioned in Chapters 4 and 5, and calculations similar to that of Chapter 4 may be possible. In two dimensional slice measurements of a three

dimensional test object, there will be perhaps significant error introduced from assuming that all the acoustic energy is confined to a region coplanar with the measurement plane, in a similar vein to that discussed in Chapter 5 for the onedimensional test object model. Investigation of these higher-order objects must answer the questions of uniqueness of the solution, whether multiple reflections can be removed, and what form of experimental data is needed, all of which will directly influence the system hardware complexity, computation time of the measurement, and accuracy. A good starting place for such research would be to confine the study to a two-dimensional object, i.e. one that does not scatter acoustic energy into the third dimension and out of the measurement plane, and reconsider the information necessary to uniquely describe the object internal structure, forming an object set much like the set {N, k, r, t} used in this thesis. For example, internal ray tracing may be helpful in accomplishing this goal, and a good assumption to make is that all of the scattered energy is received and acknowledged by measurement system. Intuitively, it appears to the author that this two-dimensional situation will respond in kind as has the one-dimensional case, albeit in a more restricted or complex manner; normally, we expect to see elements of simpler system behavior within the total response of a more complex object, which can be useful in attacking the more complex situation. It is evident that the measurement needs of this two-dimensional object would entail some sort of array/scanning procedure to ensure recapture of all the outputted acoustic energy, and much investigation into various schemes to do this is possible, with many performance/complexity trade-offs permissible.

7.1.2 Extension of the Alpha-V Method to Transmission Tomography

More specifically, we shall briefly consider the potential of upgrading the method of transmission tomography forwarded by Greenleaf et al. in [43]. As we have discussed previously, this latter work is intuitively appealing in its similarity to X-ray tomographic methodology, but suffers in accuracy from ignoring angular scattering effects, which includes reflective backscattering if one assumes one-dimensional energy propagation. We have shown that this mechanism is indistinguishable from loss if only transmission data is used (see Section 4.5.2), and this will result in poor accuracy in cases of large impedance discontinuities.

The alpha-v method can be used to help rectify this problem, and in order to show how this might be accomplished, we will assume that the measurement situation is likewise the same in Greenleaf et al.; here we have a two dimensional psuedocircular object to image, composed of a single region with a continuous spatial variation of acoustic attenuation. For our purposes, we can extend this model to the more general case of such a test object, but one composed of various regions with continuous spatial variation of attenuation, bounded by impedance discontinuities, such as that shown in Figure 7.1. It is readily apparent that this type of object is a superset of the type discussed in Greenleaf et al. and is the most general two-dimensional test object that is worthy of imaging consideration. In the cited work, the measurement is performed by modeling the object as a set of one-dimensional diametric slices, with the experimental data acquired by rotating a pair of transducers about a common

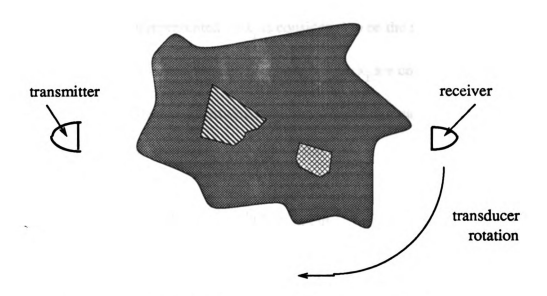


Figure 7.1 The type of object proposed in Section 7.1.2.

center, about which the test object is located. Each one-dimensional slice is treated as a transmission imaging problem, like that described in Section 4.5.2 of Chapter 4. As we mentioned, the main assumption in [43] is that the reflection coefficients of any boundaries present are negligibly small, so Equation (4.5) reduces to

$$T_{LR}(\mathbf{k},\mathbf{r}) = A_{\text{input}} k_1 k_2 \dots k_n$$

$$= A_{\text{input}} \exp \left[-(\alpha_1 x_1 + \alpha_2 x_2 + \dots + \alpha_n x_n) \right]$$
(7.1)

where n is taken to be a large integer (note that n is *not* the number of layers, since it has been assumed that there are no discontinuities in the acoustic properties of the object internal structure), and x; are a fixed small distance which is given by

$$x_i = \frac{\text{overall object length}}{n}$$
 (7.2)

for i = 1 to n. The length represented by x_i is considered to be the same as the length of one pixel of the output screen display; therefore, all the x_i are considered identical. Thus, given a particular measurement direction, we proceed to measure the transmitted amplitude T_{LR} (experimental) and then can write that

$$\alpha_1 + \alpha_2 + \ldots + \alpha_n = -\ln \left[T_{LR} / A_{input} \right] / x \tag{7.3}$$

If this is repeated from a sufficiently large number of angles, say n such distinct positions, then we will have a set of n linear equations to solve for the n values of α_i , giving us a discrete pixel map approximation of the variation of the attenuation within the object. Implicit in this is that n is very large so as to allow adequate resolution, and to furnish sufficient data pertaining to each pixel to permit complete specification of the linear system.

As we stated, the premise of this method is to ignore the reflection information as irrelevant; we have seen that in fact the reflected energy contains much more information than the transmitted. Our proposal is to incorporate our knowledge of the results of Chapter 4 into the above discourse. This may be done simply by following the bidirectional interrogation scheme described therein, and performing the calculations of Equations (4.20) to find the reflection coefficients of each boundary. Then we can use the full form of Equation (4.5) and rewrite Equation (7.3) more formally

$$\alpha_1 + \alpha_2 + \ldots + \alpha_n = \frac{-\ln [T_{LR} / A_{input}]}{x (1 + r_1) (1 + r_2) \ldots (1 + r_N)}$$
 (7.4)

where N represents the number of apparent layers in the particular measurement direction. Following the lead from this point, it should be possible to image internal regions of an object bounded by impedance discontinuities even if these areas have a continuous variation in acoustic properties. This would be a most valuable accomplishment, but it should be noted that the angular scattering problem must be addressed as well before congratulations are in order; in effect, we must also solve the proposed problem given in Section 7.1.1 as well. This topic, taken in its entirety, appears to be most lucrative for further research, with the rewards of success being inestimable.

7.1.3 Extension to the Electromagnetic (and General Wave) Situations

The results of Chapter 4 are by no means limited to acoustic probing; in fact, many systems can be described by the formulations forwarded therein. For example, uniform transmission lines with characteristic impedance discontinuities fit this type of behavior, and the results of Equations (4.20) and (4.21) apply directly. Additionally, the case of a single such transmission line is the epitome of the one-dimensional situation, since the electrical energy has only an axial component (assuming no radiation, unless one wishes to model this as a loss per unit length)! These equations could be used to probe long electrical lines to find the position and perhaps type of fault that exist at some remote but unknown location; perhaps the results of Chapter 4 could be expanded to include lines with distribution branches as well. Unfortunately, the practical application of these equations to radar and underground remote sensing

seems limited, since only one side of the test "object" is available to the investigator.

7.2 Conclusions

In this thesis, we have investigated a one-dimensional coplanar N-layered homogeneous test object being probed by acoustic means. On the way, we discovered the following:

- (1) The only experimental data that permits unique solution of the problem is the bidirectional (two-sided) four-signal interrogation employed in Chapter 4. This suggests that in order to uniquely solve an n-th order spatial dimension object problem of this type, it may in fact be necessary to investigate it remotely from a space with at least 2n degrees of freedom, and perhaps viewing this object from a space of higher order than 2n would not permit a unique solution to be found either, due to overspecification. For a three-dimensional object, this would mean that the reflected and transmitted data at/from each spherical angle must be recorded, possibly a vary large quantity of information to process in practice.
- (2) The one-dimensional N-layer problem can be decoupled into first a solution for **r**, then secondly a solution for **k**, implying that the uniqueness of then problem is not governed by the losses of the layers.
- (3) The solution we found in Chapter 4 always exists, for any combination of

- data even with experimental errors.
- (4) An algorithm was developed that demonstrates the possibility that the solution of the N-layer one-dimensional object is unique even in the presence of multiple reflections in the experimental data. Unfortunately, this immensely important result remains to be rigorously proved at present.
- (5) The algorithm also finds N, the number of object layers, uniquely, given experimental data that may or may not be corrupted with multiple reflections, as long as the primary signals are present in this data.
- (6) The above strongly suggests that the solution is unique even with multiple reflections and prior unknown N. It appears possible that this condition may be true for the similar classes of two- and three-dimensional objects if the necessary and sufficient experimental data can be acquired. The solution of such problems will by no means be computationally simpler than the already involved one-dimensional situation. Further research should be directed at this topic.
- (7) The system analysis of Chapter 5 has indicated the benefits and difficulties of an amplitude measurement system. This study has shown that the solution equations derived in Chapter 4 for the N-layer case are rather insensitive to experimental error, if certain system features and

corrections are incorporated prior to commencing the calculations indicated. The major source of error was clearly shown to be scattering of energy into non-measurement directions, which can only be corrected by some form of array/scanning method to allow complete recapture of the output energy, and treating the test object as a two- or three-dimensional entity.

- (8) Experimental work has been performed to verify the correctness of the derived solution, and to investigate the practical feasibility of amplitudebased measurements. The results show reasonable agreement with published values. Interestingly, the αν product appears to be extremely varied for different materials, which supports the notion of using this product as an index for imaging and/or material identification. Unfortunately, it has been found that the use of multiple transducers is very difficult, since pressure-to-voltage calibration (matching) is necessary. This fact tends to reduce the attractiveness of transducer arrays, which is decidedly unfortunate since mechanical scanning of a pair of transducers will always remain the slower alternative. Additionally, target angle has been found to be a strong influence on the accuracy of reflected amplitudes, not having as large an influence on the transmitted pulses, even for slight misalignment. This will definitely be a topic of ardorous contention, even with array/scanning advancements.
- (9) Suggestions have been forwarded for further research areas related to the

work pursued here, centering primarily on expanding the results to objects of higher spatial dimension. It is not crucial that all work performed in this be of practical value, since much can be learned about what is or is not possible by formulating a somewhat abstract situation an investigating it in a reasonable manner. This is perhaps the author's greatest criticism of the literature in this field, but this lack has left a wide range of theoretical investigation open to nascent researchers.

APPENDICES

APPENDIX A

Program: TWOSIDE

```
1 Rem **** TWOSIDE: a bidirectional simulator for N-layer test objects
2 Rem
                        J. Nodar
                                       1989
                                                     MSU
3 Rem
                 BY:
4 Rem
8 Rem --- initialize-----
9 Rem
10 Dim S(500,4),S$(500),Lout(30,2),Lout$(30),Rout(30,2),Rout$(30)
20 Dim K(10),R(10),T(10)
30 Dim Lsim(30,2),Rsim(30,2),TLRsim(30,2),TRLsim(30,2)
40 Dim Lsim$(30),Rsim$(30),TLRsim$(30),TRLsim$(30)
45 Ain=1: Tol=.02*Ain
48 Rem
49 Rem --- read input data file to get {N, k, r, t} -----
51 Input "Input file"; A$: Open A$ for input as #1
54 Input #1,N
55 For I=0 to N-1: Input #1,K(I): Next I
56 For I=1 to N-1: Input #1,R(I): Next I
57 For I=0 to N-1: Input #1,T(I): Next I
70 Close 1
90 Rem
92 Rem --- simulate {N, k, r, t} using TWOSIDE algorithm ----
95 Gosub 1000: Rem -- now have {LTRT}simulated
99 Rem
100 Rem ---- print results of simulation -----
101 Rem
200 Print: Print"Lsim:": Print
210 For I=1 to Lsim(0,0): Print Lsim(I,1),Lsim(I,2),Lsim(I): Next I
211 Print: Print"TLRsim:": Print
212 For I=1 to TLRsim(0,0): Print TLRsim(I,1), TLRsim(I,2), TLRsim$(I): Next I
220 Print: Print"Rsim:": Print
221 For I=1 to Rsim(0,0): Print Rsim(I,1),Rsim(I,2),Rsim(I): Next I
```

```
230 Print: Print"TRLsim:": Print
235 For I=1 to TRLsim(0,0): Print TRLsim(I,1),TRLsim(I,2),TRLsim$(I): Next I
240 Rem
250 Rem ---- print to line printer
255 Rem
260 Rem ---- save to disk file
800 Rem
850 Rem ---- done -----
900 Rem
999 End
1000 Rem -----
1010 Rem --- TWOSIDE simulation subroutine -----
1030 Rem
1040 Rem ---- input variables:
                           N = number of layers in model
                         K() = loss of each layer
                         R() = reflection coefficient of each boundary
                         T() = time delay in each layer
                         Ain = input pulse amplitude
                         tol = minimum amplitude to use in simulation
1100 Rem ---- output variables:
                  Lsim(),Lsim$() = simulated left echoes, paths
             TLRsim(), TLRsim$() = simulated left to right transmissions, paths
                  Rsim(),Rsim$() = simulated right echoes,paths
             TRLsim(), TRLsim$() = simulated right to left transmissions, paths
                NOTE: Lsim(0,0) = number of echoes in Lsim(), etc.
1200 Rem ---- internal variables:
                         S() = stack of internal waves
                        S$() = stack of internal wave paths
                           P = stack pointer
                          I,J = loop counters
                       Side$ = indicator for input pulse side
              Lout(),Lout$() = left output wave list, paths
```

```
Rout(),Rout$() = right output wave list,paths
                      Temp, Temp$ = scratch variables for sorting
                            S(P,1) = wave amplitude
                  NOTE:
                            S(P,2) = wave time delay
                            S(P,3) = wave direction (0=left, 1=right)
                            S(P,4) = current boundary location (i.e. 0...N)
1250 Rem ---- initialize the simulation -----
     Ain = Ain : Tol = Tol
1300 Rem --- Input on the left side -----
     Side$="left": Gosub 1500
     For I=1 to Lout(0.0): For J=1 to 2: Lsim(I,J)=Lout(I,J): Next J
        Lsim$(I)=Lout$(I) : Next I : Lsim(0,0)=Lout(0,0)
    For I=1 to Rout(0,0): For J=1 to 2: TLRsim(I,J)=Rout(I,J): Next J
        TLRsim$(I)=Rout$(I): Next I: TLRsim(0,0)=Rout(0,0)
1400 Rem ---- Then input on the right side -----
     Side$="right" : Gosub 1500
     For I=1 to Lout(0,0): For J=1 to 2: TRLsim(I,J)=Lout(I,J): Next J
        TRLsim(I)=Lout(I): Next I: TRLsim(0,0)=Lout(0,0)
    For I=1 to Rout(0,0): For J=1 to 2: Rsim(I,J)=Rout(I,J): Next J
        Rsim$(I)=Rout$(I): Next I: Rsim(0,0)=Rout(0,0)
1450 Rem ---- Done with both sides, so leave -----
    Return: Rem -- goes back to calling routine
1500 Rem ---- Simulate the model from the specified side -----
    Rem -- init this part
    P=0: Lout(0,0)=0: Rout(0,0)=0: S(P,1)=Ain: S(P,2)=0
    if side\$="left" then S(P,3)=1:S(P,4)=0:S\$(P)=STR\$(0)
                  else S(P,3)=0: S(P,4)=N: S(P)=STR(N)
```

```
1580 Rem ---- start the simulation -----
     If P=-1 then 2000: Rem -- stack is empty, so done!
     If abs(S(P,1)) < tol then P=P-1 : Goto 1580
1630 Rem -- left output wave?
     if S(P,4) <> 0 or S(P,2) = 0 then 1700
     Lout(0,0)=Lout(0,0)+1
     Lout(Lout(0,0),1)=S(P,1): Lout(Lout(0,0),2)=S(P,2): Lout(Lout(0,0))=S(P)
     P=P-1: Goto 1580
1700 Rem -- right output wave?
     If S(P,4) \Leftrightarrow N or S(P,2)=0 then 1800
     Rout(0,0)=Rout(0,0)+1
     Rout(Rout(0,0),1)=S(P,1): Rout(Rout(0,0),2)=S(P,2)
     Rout(0,0)=S(P)
     P=P-1: Goto 1580
1800 Rem -- left going wave?
     If S(P,3) < 0 then 1900
     S(P,4)=S(P,4)-1
     S(P,1)=S(P,1)*K(S(P,4))
     S(P,2)=S(P,2)+T(S(P,4))
     S(P)=S(P)+","+STR(S(P,4))
     If S(P,4)=0 then 1580 else S(P+1,1)=S(P,1)*(1-R(S(P,4))
                               S(P+1,2)=S(P,2)
                               S(P+1,3)=0
                               S(P+1,4)=S(P,4)
                               S$(P+1)=S$(P)
                               S(P,1)=S(P,1)*(-R(S(P,4))
                               S(P,3)=1
                               P=P+1: Goto 1580
1900 Rem -- right going wave?
     S(P,1)=S(P,1)*K(S(P,4))
     S(P,2)=S(P,2)+T(S(P,4))
     S(P,4)=S(P,4)+1
     S(P)=S(P)+","+STR(S(P,4))
     If S(P,4)=N then 1580 else S(P+1,1)=S(P,1)*(1+R(S(P,4)))
                               S(P+1,2)=S(P,2)
                               S(P+1,3)=1
                               S(P+1,4)=S(P,4)
```

```
S(P+1)=S(P)
                                          S(P,1)=S(P,1)*(+R(S(P,4)))
                                          S(P,3)=0
                                          P=P+1: Goto 1580
2000 Rem --- sort the output wave lists in increasing time order -----
     For I=1 to Lout(0,0): For J=1 to Lout(0,0)-I
     If Lout(J,2)>Lout(J+1,2) then temp=Lout(J,1):Lout(J,1)=Lout(J+1,1):
                                 Lout(J+1,1)=temp
                                 temp=Lout(J,2):Lout(J,2)=Lout(J+1,2):
                                 Lout(J+1,2)=temp
                                 temp\=Lout\(J)C : Lout\(J)=Lout\(J+1) :
                                 Lout(J+1)=temp
     Next J,I
     For I=1 to Rout(0,0): For J=1 to Rout(0,0)-I
     If Rout(J,2)>Rout(J+1,2) then temp=Rout(J,1): Rout(J,1)=Rout(J+1,1):
                                 Rout(J+1,1)=temp
                                 temp=Rout(J,2): Rout(J,2)=Rout(J+1,2):
                                 Rout(J+1,2)=temp
                                 temp\$=Rout\$(J) : Rout\$(J)=Rout\$(J+1) :
                                 Rout(J+1)=temp$
     Next J,I
2200 Rem ---- all done with this side -----
```

return: Rem -- goes back to either 1300+ or 1400+

APPENDIX B

Program: ALPHA-V

100	Rem **** Elimination of multiple reflections in {LTRT}experimental
105	Rem
106	Rem BY: J. Nodar 1989 MSU
110	Rem
	Rem initialize
	Rem
	Rem Lexp(30,2),Rexp(30,2),TLRexp(30,2),TRLexp(30,2)
	Dim Lsim(30,2),Rsim(30,2),TLRsim(30,2),TRLsim(30,2)
135	Dim Lsim\$(30),Rsim\$(30),TLRsim\$(30),TRLsim\$(30)
140	Dim Lpri(30,2),Rpri(30,2),TLRpri(2),TRLpri(2)
	Dim $K(30),R(30),T(30)$
160	Dim \$(500,4),\$\$(500),Lout(30,2),Lout\$(30),Rout(30,2),Rout\$(30)
180	Rem
185	amptol=.1: timetol=.1
199	Rem
	Rem read data file into {LTRT} experimental arrays
	Rem
206	Input "input file: "; A\$: Open A\$ For Input As #1
	Input #1, $Lexp(0,0)$
	For $I=1$ to $Lexp(0,0)$: For $J=1$ to 2: Input #1, $Lexp(I,J)$: Next J,I
215	Input #1, TLRexp(0,0)
218	For $I=1$ to $TLRexp(0,0)$: For $J=1$ to 2: Input #1, $TLRexp(I,J)$: Next I,J
	Input #1, $Rexp(0,0)$
225	For I=1 to $Rexp(0,0)$: For J=1 to 2: Input #1, $Rexp(I,J)$: Next I,J
230	Input #1, TRLexp(0,0
235	For I=1 to TRLexp(0,0): For J=1 to 2: Input #1, TRLexp(I,J): Next I,J
250	Close 1
	Rem
300	Rem begin processing
	Rem
302	Rem see if transmission data is present and get it
303	If TLRexp(0,0)=0 or TRLexp(0,0)=0 then Print"error!!" : Stop

```
304 Tsample=(TLRexp(1,2) + TRLexp(1,2))/2
305 TLRpri(1)=TLRexp(1,1) : TLRpri(2)=TLRexp(1,2)
306 TRLpri(1)=TRLexp(1,1) : TRLpri(2)=TRLexp(1,2)
307 Rem
308 Rem -- find upper bound on the number of layers in object
309 Rem
310 If Lexp(0,0)<Rexp(0,0) Then N=Lexp(0,0)+1 Else N=Rexp(0,0)+1
312 Rem --- main loop on N -----
313 Rem
320 While N>0 : Print "N=":N : Print
325 Rem
326 Rem --- choose a combination of N-1 left echoes as Lpri() ----
327 Rem
330 For I=1 to Lexp(0,0): If I>N-1 Then Lexp(1,0)=0 Else Lexp(1,0)=1 : Next I
331 Rem
335 Rem -- test to see if it has N-1 echoes in it
340 Count=0: For I=1 to Lexp(0,0): Count=Count+Lexp(I,0): Next I
342 If Count=N-1 then Goto 400: Rem -- has sufficient # of echoes in it
345 Rem
350 Rem -- get next left echo combination and test if N<1 (DONE?)
352 Carry=1: For I=2 to Lexp(0,0): Lexp(I,0)=Lexp(I,0)+Carry: Carry=0
354 If Lexp(I,0)=2 then Lexp(I,0)=0 : Carry=1
356 Next I
357 If Carry=1 then N=N-1: WEND: Print"no combinations work!?": Stop
358 Goto 335
399 Rem
400 Rem -- put the left echo combination into Lprimary
410 J=1: For I=1 to Lexp(0,0)
415 If Lexp(I,0)=0 then 420
417 Lpri(J,I)=Lexp(I,1) : Lpri(J,2)=Lexp(I,2) : J=J+1
420 Next I: If J>N-1 then Print"error!!!": Stop
499 Rem
500 Rem --- choose a combination of right echoes ----
510 Rem
530 For I=1 to Rexp(0,0): If I>N-1 then Rexp(I,0)=0 else Rexp(I,0)=1: Next I
532 Rem
535 Rem -- test to see if right combination has N-1 echoes in it
540 Count=0: For I=1 to Rexp(0,0): Count=Count+Rexp(I,0): Next I
542 If Count=N-1 then 600 : Rem -- i.e. has sufficient # of echoes
549 Rem
550 Rem -- get next right echo combination
552 Carry=1: For I=2 to Rexp(0,0): Rexp(I,0)=Rexp(I,0)+Carry: Carry=0
554 If Rexp(I,0)=2 then Rexp(I,0)=0 : Carry=1
```

```
556 Next I: If Carry=1 then 350: Rem -- no right combinations left to try
558 Goto 535
599 Rem
600 Rem -- put the right combinations into Rprimary
610 J=1: For I=1 to Rexp(0,0)
615 If Rexp(I,0)=0 then 620
617 Rpri(J,1)=Rexp(I,1): Rpri(J,2)=Rexp(I,2): J=J+1
620 Next I: If J>N-1 then Print"Error!": Stop
649 Rem
650 Rem ---- test if left and right combinations are compatible -----
655 Rem
660 Rem -- check for opposite signs on echo amplitudes
665 For I=1 to N-1: If Lpri(I,1)*Rpri(N-I,1)>0 then 550: Rem -- i.e. not OK
667 Next I
668 Rem
669 Rem -- check the time delays
670 For I=1 to N-1: If Abs((Lpri(I,2)+Rpri(N-I,2))/2/Tsample -1)>Timetol then 550
671 Next I
679 Rem
680 Rem ---- print echo combination found -----
681 Rem
682 For I=1 to N-1 : Print "L(";I;")=";Lpri(I,1),"R(";I;")=";Rpri(I,1) : Next I
683 Print: Print
685 Print"TLR=";TLRpri(1)
686 Print"TRL=";TRLpri(1)
689 Rem
690 Rem --- Do alpha-v computations to find {N, k, r, t}trial -----
695 Rem
699 Rem -- find the reflection coefficients
700 For I=1 to N-1
710 R(I)=Sgn(Lpri(I,1)*Sqr(Lpri(I,1)*Rpri(N-I,1)/(Lpri(I,1)*Rpri(N-I,1)-Ipri(I,1)*Rpri(I,1)*Rpri(I,1)*Rpri(I,1)*Rpri(I,1)*Rpri(I,1)*Rpri(I,1)*Rpri(I,1)*Rpri(I,1)*Rpri(I,1)*Rpri(I,1)*Rpri(I,1)*Rpri(I,1)*Rpri(I,1)*Rpri(I,1)*Rpri(I,1)*Rpri(I,1)*Rpri(I,1)*Rpri(I,1)*Rpri(I,1)*Rpri(I,1)*Rpri(I,1)*Rpri(I,1)*Rpri(I,1)*Rpri(I,1)*Rpri(I,1)*Rpri(I,1)*Rpri(I,1)*Rpri(I,1)*Rpri(I,1)*Rpri(I,1)*Rpri(I,1)*Rpri(I,1)*Rpri(I,1)*Rpri(I,1)*Rpri(I,1)*Rpri(I,1)*Rpri(I,1)*Rpri(I,1)*Rpri(I,1)*Rpri(I,1)*Rpri(I,1)*Rpri(I,1)*Rpri(I,1)*Rpri(I,1)*Rpri(I,1)*Rpri(I,1)*Rpri(I,1)*Rpri(I,1)*Rpri(I,1)*Rpri(I,1)*Rpri(I,1)*Rpri(I,1)*Rpri(I,1)*Rpri(I,1)*Rpri(I,1)*Rpri(I,1)*Rpri(I,1)*Rpri(I,1)*Rpri(I,1)*Rpri(I,1)*Rpri(I,1)*Rpri(I,1)*Rpri(I,1)*Rpri(I,1)*Rpri(I,1)*Rpri(I,1)*Rpri(I,1)*Rpri(I,1)*Rpri(I,1)*Rpri(I,1)*Rpri(I,1)*Rpri(I,1)*Rpri(I,1)*Rpri(I,1)*Rpri(I,1)*Rpri(I,1)*Rpri(I,1)*Rpri(I,1)*Rpri(I,1)*Rpri(I,1)*Rpri(I,1)*Rpri(I,1)*Rpri(I,1)*Rpri(I,1)*Rpri(I,1)*Rpri(I,1)*Rpri(I,1)*Rpri(I,1)*Rpri(I,1)*Rpri(I,1)*Rpri(I,1)*Rpri(I,1)*Rpri(I,1)*Rpri(I,1)*Rpri(I,1)*Rpri(I,1)*Rpri(I,1)*Rpri(I,1)*Rpri(I,1)*Rpri(I,1)*Rpri(I,1)*Rpri(I,1)*Rpri(I,1)*Rpri(I,1)*Rpri(I,1)*Rpri(I,1)*Rpri(I,1)*Rpri(I,1)*Rpri(I,1)*Rpri(I,1)*Rpri(I,1)*Rpri(I,1)*Rpri(I,1)*Rpri(I,1)*Rpri(I,1)*Rpri(I,1)*Rpri(I,1)*Rpri(I,1)*Rpri(I,1)*Rpri(I,1)*Rpri(I,1)*Rpri(I,1)*Rpri(I,1)*Rpri(I,1)*Rpri(I,1)*Rpri(I,1)*Rpri(I,1)*Rpri(I,1)*Rpri(I,1)*Rpri(I,1)*Rpri(I,1)*Rpri(I,1)*Rpri(I,1)*Rpri(I,1)*Rpri(I,1)*Rpri(I,1)*Rpri(I,1)*Rpri(I,1)*Rpri(I,1)*Rpri(I,1)*Rpri(I,1)*Rpri(I,1)*Rpri(I,1)*Rpri(I,1)*Rpri(I,1)*Rpri(I,1)*Rpri(I,1)*Rpri(I,1)*Rpri(I,1)*Rpri(I,1)*Rpri(I,1)*Rpri(I,1)*Rpri(I,1)*Rpri(I,1)*Rpri(I,1)*Rpri(I,1)*Rpri(I,1)*Rpri(I,1)*Rpri(I,1)*Rpri(I,1)*Rpri(I,1)*Rpri(I,1)*Rpri(I,1)*Rpri(I,1)*Rpri(I,1)*Rpri(I,1)*Rpri(I,1)*Rpri(I,1)*Rpri(I,1)*Rpri(I,1)*Rpri(I,1)*Rpri(I,1)*Rpri(I,1)*Rpri(I,1)*Rpri(I,1)*Rpri(I,1)*Rpri(I,1)*Rpri(I,1)*Rpri(I,1)*Rpri(I,1)*Rpri(I,1)*Rpri(I,1)*Rpri(I,1)*Rpri(I,1)*Rpri(I,1)*Rpri(I,1)*Rpri(I,1)*Rpri(I,1)*Rpri(I,1)*Rpri(I,1)*Rpri(I,1)*Rpri(I,1)*Rpri(I,1)*Rpri(I,1)*Rpri(I,1)*Rpri(I,1)*Rp
                     TLRpri(1)*TRLpri(1)))
712 Next I
715 Rem -- find the loss parameters
720 K(0)=1: K(N-1)=1: For I=1 to N-2
725 K(I)=Sqr(R(I)/R(I+1)/(1-R(I)^2)*Lpri(I+1,1)/Lpri(I,1))
727 Next I
730 Rem -- find the layer time delays
735 If N=1 then T(0)=Tsample else T(0)=Lpri(1,2)/2
737 For I=1 to N-2: T(I)=(Lpri(I+1,2)-Lpri(I,2))/2: Next I: T(N-1)=Rpri(1,2)/2
750 Rem
760 Rem ---- print the set {N, k, r, t}trial -----
770 For i=0 to N-1 : Print "N=";N : Print
772 Print"k(";I;")=";K(I); : If I=0 then Print ;; : goto 774
```

```
773 Print, "r(";I;")=";R(I);
774 Print ,"t(";I;")=";T(I) : Next I
799 Rem
800 Rem ---- simulate the set {N, k, r, t}trial using TWOSIDE algorithm -----
810 Gosub 1000: Rem -- now have the set {LTRT} simulated
880 Rem
881 Rem ---- rescale the set {LTRT} simulated so that Ain(sim)=Ain(exp) -----
882 Rem
883 Print"Rescaling the simulated data set..."
884 If N>1 then Scale=Lexp(1,1)/Lsim(1,1) Else Scale=1
886 For I=1 to Lsim(0,0): Lsim(I,1)=Lsim(I,1)*scale: Next I
887 For I=1 to TLRsim(0,0): TLRsim(I,1)=TLRsim(I,1)*scale: Next I
888 If N>1 then Scale=Rexp(1,1)/Rsim(1,1)
890 For I=1 to Rsim(0,0): Rsim(I,1)=Rsim(I,1)*scale: Next I
895 For I=1 to TRLsim(0,0): TRLsim(I,1)=TRLsim(I,1)*scale: Next I
899 Rem
900 Rem --- check if simulation and experimental data sets agree -----
910 Rem
911 Print"Checking if exp is in sim..."
915 Rem
920 For I=1 to Lexp(0,0): For J=1 to Lsim(0,0)
922 If abs(Lexp(i,1)/Lsim(J,1)-1))<amptol and abs(Lexp(I,2)/Lsim(J,2)-1)<timetol
      then 924
923 Next J: goto 950: Rem -- not OK
924 Next I: goto 963: Rem -- is OK!
926 For I=1 to Rexp(0,0): For J=1 to Rsim(0,0)
928 If abs(Rexp(I,1)/Rsim(J,1)-1)<amptol and abs(Rexp(I,2)/Rsim(J,2)-1)<timetol
      then 930
929 Next J: Goto 950: Rem -- not OK
930 Next I: Goto 963: Rem -- is OK!
940 Rem
950 Print"Checking if sim is in exp..."
952 For I=1 to Lsim(0,0): For J=1 to Lexp(0,0)
954 If abs(Lsim(I,1)/Lexp(J,1)-1)<amptol and Abs(Lsim(I,2)/Lexp(J,2)-1)<timetol
      then 956
955 Next J: Print"sim <> exp???" : Goto 550
956 Next I
958 For I=1 to Rsim(0,0): For J=1 to Rexp(0,0)
960 if abs(Rsim(I,1)/Rexp(I,1)-1) < amptol and <math>abs(Rsim(I,2)/Rexp(I,2)-1) < timetol
      then 962
961 Next J: Print"Sim<>exp???": goto 550
962 Next I: Print"SIM=EXP!!!!": END
1000 Rem ---- insert TWOSIDE (lines 1000-) of Appendix A here -----
```

APPENDIX C

Program: TWOCHANNEL

```
100 Rem **** TWOCHANNEL: Controls WAAGII board and gets {LTRL}exp.
110 Rem
120 Rem
                     By: J. Nodar 1989
                                                     MSU
130 Rem
140 Rem ---- initialize -----
150 Rem
170 '
175 Def FNLOBT(x) = x and &HFF
176 Def FNHIBT(x) = &HFF and ((x and &HFF00) \setminus 256)
177 '
180 RAM = \&H0 : REG = \&H178 : REG0 = REG+0 : REG1 = REG+1
    REG2=REG+2: REG3=REG+3: SEGMENT=&HD000
185 '
190 N=5333: '--- number of sample points to take
                  based on a sample rate of 20 MHz
                  and a 20 cm span test fixture.
195'
199 DEFINT C.X
200 DIM oldflag(2),max(2),tmax(2),flag(2),peak(2),shot(2),
         ch(1,5333),x(1,5333),
         impulse(1,20,2),
         Lexp(20,2),TLRexp(20,2),Rexp(20,2),TRLexp(20,2)
215 '
220 A=0: B=1: '---- channel marker flags
222 '
1000 '--- main routine -----
1005'
1010 '---- init
1011'
1020 Lexp(0,0)=0: TLRexp(0,0)=0: Rexp(0,0)=0: TRLexp(0,0)=0
1030 '
1100 '---- loop for input on left, then right sides
1110'
```

```
1115 Cls: Locate 5,10: Print "Two Channel for {L,TLR,R,TRL}exp.": Print: Print
1116 Input "Number of times to average: "; avnum: Print: Print
1120 Input "Theta: "; theta: Print: Print
1125'
1126 '---- left input
1127 '
1128 Print "Left input <CR>?": input A$: Gosub 13000: Gosub 11000: Gosub 12000
1129 '
1130 For I=1 to impulse(A,0,0): For J=1 to 2
     Lexp(I,J)=impulse(A,I,J): Next J: Next I
     Lexp(0,0)=impulse(A,0,0)
1135 '
1140 For I=1 to impulse(B,0.0): For J=1 to 2
      TLRexp(I,J)=impulse(B,I,J): Next J: Next I
      TLRexp(0.0)=impulse(B.0.0)
1145 '
1200 ' ---- right input
1210 '
1220 Print "Right input <CR>?": Input A$: Gosub13000: Gosub 11000:
      Gosub 12000
1225 '
1230 For I=1 to impulse(A,0,0): For J=1 to 2
      TRLexp(I,J)=impulse(B,I,J): Next J: Next I
      TRLexp(0,0)=impulse(A,0,0)
1235 '
1240 For I=1 to impulse(B,0,0): For J=1 to 2
      Rexp(I,J)=impulse(B,I,J): Next J: Next I
      Rexp(0,0)=impulse(B,0,0)
1245 '
1300 '---- save data to a file
1310'
1320 Input "file to save "; A$ : if A$="" then 9999
1330 open A$ for output as #1
1335 '
1340 Print #1,theta
1350 Print #1, Lexp(0,0)
      For I=1 to Lexp(0,0): Print #1,Lexp(I,1),Lexp(I,2): Next I
1360 Print #1,TLRexp(0,0)
      For I=1 to TLRexp(0,0): Print #1,TLRexp(I,1),TLRexp(I,2): Next I
1370 Print #1, Rexp(0,0)
      For I=1 to Rexp(0,0): Print #1, Rexp(I,1), Rexp(I,2): Next I
1380 Print #1,TRLexp(0,0)
      For I=1 to TRLexp(0,0): Print #1,TRLexp(I,1),TRLexp(I,2): Next I
1390 Close 1
9999 CLS: END
```

```
10000 ---- Subroutine to get two channels of WAAGII data -----
10010 '
10020 '---- init control registers
10030 '
10040 Def SEG=SEGMENT
10045 OUT REG3, &HC0: OUT REG2, &H6F: '-- load trigger offset of 140.
10050 Poke 0,140
10055 OUT REG3, &H80: OUT REG2, &H6F: '-- reset the control values
10060 DEF SEG
10070 '
10100 '---- enable sampling
10150 '
10170 Print: Print "Sampling....";
10180 OUT REG3, &H80: OUT REG2, &H6F: '-- init the control register
10190 OUT REG1, &HFF: OUT REG0, &HFF: '-- clear the byte counter
10200 OUT REG1, &HFF: OUT REG0, &HFF
10210 NUM=-(N+&HFF): '-- compute the correct byte count
10215 OUT REG1, FNHIBT(NUM): OUT REG0, FNLOBT(NUM)
10220 OUT REG1, FNHIBT(NUM): OUT REG0, FNLOBT(NUM)
10230 CONTROL=&HBFFC and &H800C: '-- engage the trigger mechanism
10250 OUT REG3, FNHIBT(CONTROL): OUT REG2, FNLOBT(CONTROL)
10260 '
10270 OUT &H3E4, 0: '--- trigger the one shot on the motor control board
10275 '
10290 WAIT REG2,1: '---- wait until all data is read into sample memory
10300 '
10310 '--- read back the data into the array called ch()
10330 OUT REG3, &H80: OUT REG2, &H6F: '-- enable the ram for read
10340 VTA=2*(INP(REG0)+(INP(REG1)) and &H3F) * 256)
10360 '--- read the data into ch(A<sub>1</sub>) and ch(B<sub>1</sub>)
10365 '
10370 Print "Loading data...."
10390 DEF SEG=SEGMENT
10400 I=0
10410 \text{ ch}(A,I) = PEEK(VTA) : \text{ch}(B,I) = PEEK(VTA+1)
      if VTA=&H7FFF then VTA=0 else VTA=VTA+2
      I=I+1: If I<=N then goto 10410 else DEF SEG
10450 '
10460 '---- all done with this side
10470 '
10480 return
10490 '
```

```
11000 '---- plot the results on the PC graphics screen -----
11010 '
11015 CLS: Screen 2: Key off
11020 Locate 1,1 : Print CHA:" : Locate 15,1 : Print "CHB:"
11040 Pset(0,35-35*(ch(A,0)/128-1)): Pset(0,135-35*ch(B,0)/128-1))
11050'
11060 For I=1 to N
      Line((I-1)/N*640, 35-35*(ch(A,I-1)/128-1)) -
           (I/N*640, 35-35*(ch(A,I)/128-1))
       Line((I-1)/N*640,35-35*(ch(B,I-1)/128-1)) -
           (I/N*640, 35-35*(ch(B,I)/128-1))
       Next I: Beep: Locate 24,1
11090 Return
12000 '--- use the delta detector to find the amplitude and time of each echo ----
12010 '
12020 average=128: threshold=3: samperiod=1/2e+7: cutoff=7: decay =8/9
12023 '
12025 For I=A to B
       flag(I)=0 : shot(I)=0 : peak(I)=0 : impulse(I,0,0)=0 :
       Next I
12030 '
12040 For T=1 to N
       For chan= A to B
       oldflag(chan)=flag(chan)
       if abs(ch(chan,t)-average)-peak(chan) < threshold then 12080
                                      else peak(chan)=abs(ch(chan,T)-average):
                                          flag(chan)=1;
12080 peak(chan)=peak(chan)*decay
       if peak(chan) < cutoff then peak=cutoff:
                                 flag(chan)=0:
       if flag(chan)=1 then shot(chan)=8
                                                        : '-- trigger the one shot
       if shot(chan) > 0 then flag(chan)=1
      shot(chan)=shot(chan)-1: if shot(chan)<0 then shot(chan)=0
12100 if oldflag(chan)=flag(chan) then 12120
       if flag(chan)=0 then 12110
      max(chan)=0: goto 12120
12110 impulse(chan,0,0)=impulse(chan,0,0)+1
       impulse(chan,impulse(chan,0,0),1)=max(chan)*sgn(max(chan)-average)
       impulse(chan,impulse(chan,0,0),2)=tmax(chan)*samperiod
      goto 12200
```

```
12120 if flag(chan)=0 then 12200
            if abs(max(chan)) < abs(ch(chan,T)-average) then max(chan)=ch(chan,t)-average)
                                                          average):
                                                          tmax(chan)=T
12200 Next chan
12205 '-- plot the square wave output of the detector to shown echoes
      pset (T/N*640, 80-5*flag(A))
      pset (T/n*640,180-5*flag(B))
12210 Next T
      Beep: Input A$: return : '---- done with this side's plot
13000 '---- averaging subroutine -----
13025 Print "Averaging ";avnum; "time(s)..." : Print
      if avnum=1 then gosub 10000:
                      return
      Gosub 10000
      For chan=A to B: For T=1 to N:
      x(chan,T)=ch(chan,t)
      Next T: Next chan
      for Z=2 to avnum
      Gosub 10000: Print"Averaging..."
      For chan=A to B: For T=1 to N
         x(chan,T)=(x(chan,T)*(Z-1)+ch(chan,T))/Z
         ch(chan,T)=x(chan,T)
     Next T, chan, Z
     return
```

BIBLIOGRAPHY

BIBLIOGRAPHY

- [1] Blitz, Jack. <u>Fundamentals of Ultrasonics</u>. Second Edition, Plenum Press, 1967.
- [2] Wells, P. N. T. <u>Physical Principles of Ultrasonic Diagnosis</u>. Academic Press, 1969.
- [3] Haykin, Simon. <u>Communication Systems</u>. Second Edition, John Wiley & Sons, 1983.
- [4] Nilsson, James W. <u>Electric Circuits</u>. Second Edition, Addison Wessely Publishing Company, 1987.
- [5] Acoustical Imaging. Volume 10, Plenum Press, 1980.
- [6] Mason, Warren P. <u>Piezoelectric Crystals and Their Application to Ultrasonics.</u> Van Nostrand Company Inc., 1950.
- [7] Glover, G. H., and J. C. Sharp. "Reconstruction of Ultrasound Propagation Speed Distributions in Soft Tissue by Time-of-Flight Tomography" IEEE Transactions on Sonics and Ultrasonics, Volume SU-24, pp 229-234, 1977.
- [8] Carson, P. L., T.V. Oughton, W.R. Hendee. "Ultrasonic Transaxial Tomography by Reconstruction" in <u>Ultrasonics in Medicine</u> Volume 2 pp 314-350, 1976.
- [9] Carson, P. L., T.V. Oughton, W.R. Hendee, A.S. Ahuja. "Imaging Soft Tissue Through Bone with Ultrasound Transmission Tomography by Reconstruction" in Medical Physics, Volume 4, pp 302-309, 1977.
- [10] Kak, A.C., and K.A. Dines. "Signal Processing for the Measurement of Attenuation of Soft Tissue" in NSF Symposium on Tissue Characterization. Volume 11, 1977.

[11]	Liang, Kenneth K. "Accuracy of Acoustic Impedance Determination Using a Focussed Beam" 1987 IEEE Ultrasonics Symposium Proceedings. pp 1141-1146.
[12]	Composite Materials: Testing and Design. Proceedings of The American Society for Testing and Materials. February 1986.

- [13] Stumpf, F. B. Analytical Acoustics. Ann Arbor Science Publishers Inc., 1980.
- [14] Herzfeld, Karl F., and T. A. Litovitz. <u>Absorption and Dispersion of Ultrasonic Waves</u>. Academic Press, 1959.
- [15] Crawford, Alan E. <u>Ultrasonic Engineering, With Particular Reference to</u>
 <u>High Power Applications</u>. Butterworth Scientific Publications, 1955.
- [16] Kishoni, Doron. "Removal of Dominant Reverberations from Ultrasonic Time-Record of Layered Material By Digital Predictive Deconvolution" 1987 IEEE Ultrasonics Symposium Proceedings, pp 1075-1078.
- [17] Kremkav, Fredrick W. "Molecular Absorption of Ultrasound in Biological Materials". ibid., pp 979-988.
- [18] Botros, N., W.K. Chu, J.Y. Cheung. "In-Vivo Ultrasound Tissue Differentiation Through the Acoustic Attenuation Coefficient". IEEE Ultrasonics Symposium Proceedings, 1987. pp 927-930.
- [19] Kim, W.W., D.T. Borup, S.A. Johnson, M.J. Bergrev, and Y. Zhou.

 "Accelerated Inverse Scattering Algorithms for Higher Contrast
 Objects". ibid. pp 903-906.
- [20] Zhou, Y., S.A. Johnson, M.J. Bergrev, B.L. Carruth, and W.W. Kim.

 "Constrained Reconstruction of Object Acoustic Parameters from
 Noisy Ultrasound Scattering Data" IEEE Ultrasonics Symposium
 Proceedings, 1987. pp 897-902.
- [21] Schwarz, H.P. "Development of a Divided Ring Array for Three-Dimensional Beam Steering in Ultrasonic Nondestructive Testing" in 1987 IEEE Ultrasonics Symposium Proceedings, pp 859-861.

- [22] Dick, Donald E., P. Carson, E. Bayly, T. Oughton, J. Kubicheck, and F. Kitson. "Technical Evaluation of an Ultrasonic CT Scanner" 1977 IEEE Ultrasonics Symposium Proceedings, pp 176-181.
- [23] Klepper, John R., G. Brandenburger, L. Busse, and J.G. Miller. "Phase Cancellation, Reflection, and Refraction Effects in Quantitative Ultrasonic Attenuation Tomography". ibid., pp 182-188.
- [24] Greenleaf, J.F., S.A. Johnson, S.L. Lee, G.T. Herman, and E.H. Wood.

 "Algebraic Reconstruction of Spatial Distributions of Acoustic
 Absorption Within Tissue from Their Two-Dimensional Acoustic
 Projections" in <u>Acoustic Holography</u>. P.S. Green, ed. Volume 5,
 Plenum Press, 1974. pp 591-603.
- [25] Greenleaf, J.F., S.A. Johnson, W.F. Samoyon, F.A. Duck. "Algebraic Reconstruction of Spatial Distributions of Acoustic Velocity in Tissue From Their Time-of-Flight Profile". in <u>Acoustic Holography</u> Volume 6 Plenum Press, 1975.
- [26] Greenleaf, James F., J. Ylitalo, and John J. Gisvold. "Ultrasonic Computed Tomography for Breast Examination" in IEEE Engineering in Medicine and Biology, December 1987, pp 27-32.
- [27] Driller, Jack, and F. L. Lizzi. "Therapeutic Applications of Ultrasound: A Review" ibid. pp 33-40.
- [28] Klepper, John R., G.H. Brandenburger, J.W. Mimbs, B. E. Sobel, and J.G. Miller. "Application of Phase-Insensitive Detection and Frequency-Dependent Measurements to Computed Ultrasonic Attenuation Tomography". IEEE Transactions on Biomedical Engineering, Volume BME-28, No. 2, February 1981. pp 186-201.
- [29] Greenleaf, J.F., and S.A. Johnson. "Algebraic Reconstruction of Spatial Distributions of Refractive Index and Attenuation in Tissues from Time-of-Flight and Amplitude Profiles". in <u>Ultrasonic Tissue Characterization</u>, National Bureau of Standards, Washington, D.C., Special Publication 453, pp 109-119, 1976.
- [30] Greenleaf, J.F., S.A. Johnson, R.C. Bahn, and B. Rajagopalan. "Quantitative Cross-Sectional Imaging of Ultrasound Parameters" in Proceedings of The IEEE Ultrasonics Symposium, 1977, pp 989-995.

- [31] Kak, A.C., and K.A. Dines. "Signal Processing of Broadband Ultrasound: Measurement of Attenuation in Soft Tissue" in IEEE Transactions in Biomedical Engineering, Volume BME-25, pp.321-344, 1978.
- [32] Kuc, Ramon, M. Schwarz, and L. VonMicsky. "Parametric Estimation of the Acoustic Attenuation Coefficient Slope for Soft Tissue" in Proceedings of the IEEE Ultrasonics Symposium, 1976, pp 44-47.
- [33] Verhoef, W.A., M.J.T.M Cloostermans, and J.M. Thijssen. "Diffraction and Dispersion Effects on the Estimation of Ultrasound Attenuation and Velocity in Biological Tissues" in IEEE Transactions on Biomedical Engineering, Volume BME-32, No. 7, July 1985. pp 521-529.
- [34] Fink, M., F. Hottier, and J.F. Cardozo. "Ultrasonic Signal Processing for invivo Attenuation Measurement: Short Time Fourier Analysis" in Ultrasonic Imaging Volume 5, pp 117-135, 1983.
- [35] Ophir, J., N.F. Maklad, and R.F. Bigelow. "Ultrasonic Attenuation Measurements of in-vivo Human Muscle" in <u>Ultrasonic Imaging</u> Volume 4, pp 290-295, 1982.
- [36] Cloostermans, M.J.T.M., and J.M. Thijssen. "A Beam Corrected Estimation of the Frequency Dependent Attenuation of Biological Tissue From Backscattered Ultrasound" in <u>Ultrasonic Imaging</u> Volume 5, pp 137-147, 1983.
- [37] O'Donnell, M. "Effects of Diffraction on Measurements of the Frequency-Dependent Ultrasonic Attenuation" in IEEE Transactions on Biomedical Engineering, Volume BME-30, pp 320-326, June 1983.
- [38] Kaya, Azmi, A. Sokollu, E. Holasek. "Mathematical Modeling of Tissues by Ultrasonic Signals" in 1975 IEEE Proceedings of the Ultrasonics Symposium, pp 37-40.
- [39] Bamber, J.C., and C.R. Hill. "Ultrasonic Attenuation and Propagation Speed in Mammalian Tissues as a Function of Temperature" in <u>Ultrasound in Medicine and Biology</u>, Volume 5, Plenum Press, pp 149-157, 1979.
- [40] Dameron, D.H. "Determination of the Acoustic Velocity in Tissues Using an Inhomogeneous Media Model" IEEE Transactions on Sonics and Ultrasonics, Volume SU-26, No.2, March 1979, pp 69-74.

- [41] Jones, J.P. "Ultrasonic Impediography and its Applications to Tissue Characterization" in <u>Recent Advances in Ultrasound in Biomedicine</u>
 Volume 1, D.H. White, ed., Research Studies Press, 1977. pp 131-156.
- [42] Parker, K., and R.C. Waag. "Measurement of Ultrasonic Attenuation Within Regions Selected from B-Scan Images" in IEEE Transactions on Biomedical Engineering, Volume BME-30, No. 8, August 1983, pp 431-437.
- [43] Greenleaf, J. F., and R.C. Bahn. "Clinical Imaging With Transmissive Ultrasonic Computed Tomography" in IEEE Transactions on Sonics and Ultrasonics, Vol. SU-28, pp 177-185, 1981.
- [44] Kuc, R.C. "Clinical Application of an Attenuation Coefficient Estimation Technique for Liver Pathology Characterization" IEEE Transactions on Biomedical Engineering, Vol. BME-27, No. 6, pp 313-319, 1980.
- [45] Ho, B., A. Jayasumana, and C.G. Fang. "Ultrasonic Attenuation Tomography by Dual Reflection Technique" 1983 IEEE Ultrasonics Symposium, pp 770-772.
- [46] Fry, W.J. "Mechanism of Acoustic Absorption in Tissue" Journal of the Acoustical Society of America, Volume 24, Number 4, July 1952, pp 412-415.
- [47] Ilic, D.B., G.S. Kino, A.R. Selfridge, and F.E. Stanke. "Computer-Controlled System for Measuring Two-Dimensional Acoustic Velocity Fields" 1979 IEEE Ultrasonics Symposium Proceedings, pp 269-272.
- [48] Farrell, E.J. "Backscatter and Attenuation Imaging from Ultrasonic Scanning in Medicine" IBM Journal of Research and Development, Vol 26, No.6, November 1982, pp 746-758.
- [49] Bjorno, L., and P.A. Lewin. "Nonlinear Focussing Effects in Ultrasonic Imaging" in 1982 IEEE Ultrasonics Symposium Proceedings, pp 659-662.
- [50] Lindsay, R.B. "Relaxation Processes in Sound Propagation in Fluids: A Historical Perspective" in <u>Physical Acoustics</u> Volume 16, W.P.Mason and R.N. Thurston eds., Academic Press, 1982, pp 1-37.
- [51] Flax, L., G.C. Gaunaurd, and H. Uberall. "Theory of Resonance Scattering" in <u>Physical Acoustics</u> Volume 15, W.P. Mason and R.N. Thurston, eds., Academic Press, 1981, pp 191-294.

- [52] Pao, Y., and R.R. Gajewski. "The Generalized Ray Theory and Transient Responses of Layered Elastic Solids" in <u>Physical Acoustics</u> Volume 13, W.P. Mason and R.N.Thurston, eds., Academic Press, 1980, pp 184-266.
- [53] Liebermann, L.N. "Resonance Absorption" in <u>Physical Acoustics</u> Volume 4A, W.P. Mason, ed., Academic Press, 1966, pp 183-194.
- [54] Lamb, John. "Thermal Relaxation in Solids" in <u>Physical Acoustics</u> Volume 2A, W.P. Mason, ed., Academic Press, 1965, pp 203-280.
- [55] Addison, R.C., L.J. Graham, R.S. Linebarger, and B.R. Tittmann. "Synthesis of an Ultrasonic Array using Laser-Based Techniques" in 1987 IEEE Ultrasonic Symposium Proceedings, pp 1109-1114.
- [56] Clement, M., P. Alais, J.C. Roucayrol, and J. Perrin. "Computerized Ultrasonic Tomography by Electronic Scanning and Steering of a Ring Array" in <u>Acoustical Imaging</u> Volume 10, P. Alais and A. F. Metherell, eds., Plenum Press, 1982, pp 397-414,
- [57] Curtis, A. R. "The Approximation of a Function of One Variable by Cubic Splines" in Numerical Approximation to Functions and Data

 J.G. Hayes, ed. The Athlone Press, 1970, pp 28-42.
- [58] Choma, J. <u>Electrical Networks: Theory and Analysis</u> John Wiley & Sons, 1985.
- [59] Kinsler, L., and A. R. Frey. <u>Fundamentals of Acoustics</u> Second Edition, John Wiley and Sons, 1962.

1				
1				
1				
1				
į				
/				
į				
1				
:				
1				
1				
1	l 1			
- 1	l			
į				
!			,	
1			, ,	
i				
1				
i				
		•		
٠				

MICHIGAN STATE UNIV. LIBRARIES
31293006096659